ISSN 1580-2949
UDK 669+666+678+53 MTAEC9, 42(6)235–309(2008)

MATER. TEHNOL.	LETNIK VOLUME 42	ŠTEV. NO. 6	STR. P. 235–309	LJUBLJANA SLOVENIJA	NOV.–DEC. 2008

VSEBINA – CONTENTS

PREGLEDNI ČLANKI – REVIEW ARTICLES

IZVIRNI ZNANSTVENI ČLANKI – ORIGINAL SCIENTIFIC ARTICLES

STROKOVNI ČLANKI – PROFESSIONAL ARTICLES

UDK 539.3:519.61
Review article/Pregledni članek

ISSN 1580-2949
MTAEC9, 42(6)237(2008)

ON THE DETERMINATION OF SAFETY FACTORS FOR MACHINES USING FINITE ELEMENT COMPUTATIONS

O DOLOČITVI FAKTORJEV VARNOSTI ZA NAPRAVE PRI IZRAČUNU Z METODO KONČNIH ELEMENTOV

Leonid B. Getsov, B. Z. Margolin, D. G. Fedorchenko

SPbSPU (St.Petersburg), CRISM "Prometey" (St.Petersburg), SNTK (Samara), Russia
getsov@online.ru

Prejem rokopisa – received: 2007-04-06; sprejem za objavo – accepted for publication: 2008-03-25

Principles for the selection of modern methods for the determination of local strength safety factors in design computations of GTE parts for static and cyclic loading are suggested. It is shown that the selection of methods for the evaluation of local strength safety factors should be carried out applying special criteria and computations including adequate models of visco-elasto-plasticity. On the basis of the analysis of computational practice the minimum values of local strength safety factors for static and cyclic loading, which may be recommended for FEM computations, have been proposed.

Key words: safety factor, finite element computation, creep, loading, cycle, fatigue

Predloženi so principi za izbiro metod za določitev lokalnih faktorjev varnosti za GTE-dele in za statično ter ciklično obremenitev. Izbira metod za oceno lokalnega faktorja varnosti za trdnost je mogoča z uporabo primernih meril in primernih modelov visko-elasto-plastičnosti. Na podlagi analize prakse izračunavanja so predložene najnižje vrednosti za faktorje varnosti za lokalno trdnost za statično in ciklično obremenitev pri FEM-izračunih.

Ključne besede: faktor varnosti, izračuni z metodo končnih elementov, lezenje, obremenitev, cikel

1 INTRODUCTION

The wide and universal propagation of commercial finite element packages (**ANSYS, ABAQUS, MARC, LS DYNA, NASTRAN** etc) for computations in design of machines and civil structures made possible to define more accurately the stress-strain state (SSS) and opened the way to solve some problems connected with the normalization of safety factors. One of these problems is the determination of the possibility of defining more reliable values for safety factors values based on the more accurate knowledge of the SSS of the construction. The more reliable reduction of safety factors would allow to decrease the weight of material for the construction, however, it may also increase the risk of flaws arising during the exploitation. The application of the finite element methods (FEM) for computing SSS in the locations of stress concentration makes it possible to design more accurately the configuration of these details of components, to obtain minimal stresses, increase the life time of parts supporting static stresses, and, more importantly, also the lifetime of parts submitted to cyclic loading. FEM is indispensable for prognosticating the crack propagation rate in parts with geometry, temperature and stress gradients where conventional computation schemes cannot be applied with sufficient reliability.

In the process of normalization of strength values for parts, it should be provided for the introduction of safety factors, both for material properties and for loading parameters of a construction. In both cases the risk may arise of use of non verified data.

It is known that some cases damages of parts during the turbine exploitation were caused by the improper evaluation of local strength in the stage of design. As examples of such events may be mentioned in particular cracks networks revealed at the inspection of gas turbine rotors after a determined operational time; cracks on gas turbine disk rims; thermal fatigue cracks on the border and the back of cooled working and regulation blades and cracks on components of combustion chambers of gas turbine engines (GTE).

The basic principles for the normalizing of safety factors considering the local static and low-cycle fatigue strength in this paper were experimentally verified in an independent report. The experience of normalizing safety factors, both in gas turbine and reactor design is widely used [1,2,3].

The application of FEM requires a high qualification designer skilled in computational mechanics, inasmuch as the computation results depend significantly on the methods of partitioning an analyzed part with a finite element (FE) network and the selection of FE types. With the aim to describe the material properties in determining the SSS of constructions applying FEM, the method of "average values minus two or three average quadratic deviations" is used. In some cases, for example, for creep strain, it is necessary to apply "average values plus two or three average quadratic deviations". However, the insufficient quantity of experimental data for new materials, insufficient information's on the dependence of properties on operating conditions as well

as data accounting for the influence of environment, restricts the application of this method. In this situation, to make easier the proper application of available experimental data, is expedient to use a sufficiently widespread concept of the "upper and lower envelop curves"[4].

Generally, the process of rupture at static loading may be of three types:

a) exhaustion of short-time plasticity,
b) creep,
c) brittle.

It is evident that the differentiation of safety factors depends on the type of rupture and should be considered in the normalization of local stresses. It is clear that the greatest safety factor value should be considered in the case of brittle fracture that may occur in the range of maximal scatter of material parameters.

2 STATIC STRENGTH

2.1 Static strength of deformable materials

The presence of stress concentration does not lead to a decrease of the bearing capacity of deformable materials in case of short-time or long-time static loading. From here on, the term "bearing capacity of plastic materials" should be understood as the conditions in which the ultimate load causing the rupture of a construction is determined with the loss of bearing capacity according to the "plastic hinge mechanism". If the value of long-time plasticity of a deformed material exceeds 4–5 %, it is not sensitive to the notch effect in long-time strength tests. Also heterogeneous cast alloys are not notch-sensitive. The temperature dependence of the plasticity of materials is not monotonous. Thus, analyzing a material state with consideration of the exploitation parameters, it is necessary to have on disposal the data of material deformability as function of the temperature and the strain rate (creep rate).

The analysis of experimental and calculated data indicates that the value of the ratio $K^{\sigma} = \sigma_B{}^n/\sigma_B{}^s$ may be taken as a criterion for the material plasticity ($\sigma_B{}^n$ and $\sigma_B{}^s$ are ultimate strength values determined by testing notched and smooth specimens). Alloys with $K^{\sigma} \geq 1.3$ obtained at appropriate temperatures for specimens with $\alpha_{\sigma} = 3.5$–4.5 (α_{σ} is coefficient concentration of stress), submitted to short and long-time tensile tests, are not propensive to brittle rupture. The use of alloys with $K^{\sigma} < 1.3$ is permitted only on the base of results of appropriate tests that include the statistical evaluation of results of tests of specimens with initial cracks (Sharpy impact tests) and low-cycle fatigue characteristics obtained from tests with notched specimens. We may assert, for this reason, that the introduction of FEM-computations for parts from plastic materials and the more precise determination of SSS at stress concentration locations should not be the base for the correction of safety factors related to the bearing capacity of constructions. At the same time, if the bearing capacity of constructions is ensured, the assumption of the needlessness of evaluation of safety factors related to the static strength and based on local stress values, is justified.

The analysis of the criteria defined in the strength standards [1,2], as well as the suggested approaches to the evaluation of the static strength and the experience of exploitation of various parts show that all attempts to restrict the value of yield strength are senseless. On the other hand, it became generally accepted that in case of appropriate ultimate strain exceeding 4–6 %, it is not necessary to take into account the residual stresses in the computations of static strength. The same is valid also for the thermal stress σ_T, if $\sigma_T = 2\alpha\Delta T < 2E$ % (α – coefficient of linear expansion; E – Young elastic modulus; ΔT – range of temperature variation).

In such approach to the normalization of the static strength of constructions, it is necessary to verify the respect of the condition that the value of J-integral is below its critical value J_c. Thus, for example, according to [1], in this case the maximal nominal static stresses (without accounting for concentrators) for pressure vessels are permitted to be below of 1/1.5 for yield strength and below of 1/2.6 for tensile strength.

The following approaches are expedient to apply for the evaluation of safety factors related to local stresses:

1. The application of the proper model of kinematical hardening is justified for solving many practical problems. However, the optimal is the SSS computation and the choice of a plasticity model depend on the material analyzed and of the loading in accordance with the conception of multimodel approach[8].
2. The static strength of deformable materials should be evaluated on the base of exhaustion of the ultimate material plasticity ε^*, which, in turn, depends on the loading rate or time. Incidentally, one should differ ultimate states for intragranular and intergranular rupture. Intragranular rupture is characterized by the absence of dependence of ultimate strains on loading rate, at the same time, for intragranular rupture, the ultimate strain diminishes with the decrease of loading rate.
3. If the local strength is evaluated with respect to the short-time plastic strain, the safety factor on strains $\varepsilon^*/\varepsilon_p$ (ε_p – plastic strain) should not be lower than 2.0, with ε^* defined with regard to the stress state triaxility by the following equations

$$\varepsilon^* = \varepsilon_p{}^{ult}\, 1.7\exp(-1.5\overline{\sigma}/\sigma_i) \qquad (1a)$$

$$\varepsilon^* = \varepsilon_p{}^{np}\, K_e\sigma_i^2/3(\sigma_i\sigma_{cp}) \qquad (1b)$$

which give a conservative estimation of the plasticity. Here

$\varepsilon_p{}^{ult}$ – ultimate strain (deformability) at short time tension;

K_e – characteristic of material state (at brittle state – $K_e = 1$, at plastic state – $K_e = 1.2$);

$\overline{\sigma}$ – mean stress.

The value of ε_p is defined with elastoplastic computation using an appropriate plasticity model and the lower strain envelop curve. In this case safety factor on stresses shall not be lower than 1.2–1.4.

It should be noted also, that the problem of normalizing of the static strength needs further development on the base of comprehensive investigations of material properties aimed to the improve the plasticity models for computing three-dimensional SSS and to further develop the rupture criteria. It should be noted that it is necessary to adapt effectively, after comprehensive testing, new plasticity models to commercial FE packages.

2.2 Safety factors for local strength for creep loading

By considering the safety factors for local strength, it is expedient to proceed from the following considerations:

1. The evaluation of rupture situation of parts operating at creep deformation can be implemented with applying the ultimate strain value, which depends on temperature, time and of the stress state rigidity. Therefore, as in the case of normalizing, the safety factors for static strength of parts from deformable materials, the use of FEM computations and the more exact knowledge of SSS for stress concentration locations cannot be the base for correcting the values of creep safety factors. In this case, there is no need to use of modern methods for stress computation. The safety factors for creep should be defined with applying the crack initiation criteria.
2. Correction of modern safety factors for creep should be based on the improvement of creep models, especially applied to parts operating in three-dimensional stress state and submitted to multifactor and nonstationary loading, as well as on the results of the analysis of creep characteristics and long-time strength of materials.
3. For the description of the influence of material properties and stress complexity in a part on its deformability, it is expedient to apply the following equations that are analogous to (1a) and (1b)

$$p^* = 1.7\ \varepsilon_c \exp(-1.5\bar{\sigma}/\sigma_i) \tag{2a}$$

$$p^* = \varepsilon_n K_e \sigma_i^2/3(\sigma_i \sigma_{cp}) \tag{2b}$$

where:

ε_c – critical creep strain at uniaxial loading;

p^* – ultimate creep strain (deformability) at the complex stress state;

K_e – characteristic of material state (K_e = 1 – for brittle state and K_e = 1.2 – for plastic state).

These, as well as equations (1a) and (1b), give a conservative evaluation of the ultimate strain. In this case and considering the values of accumulated creep strains along the upper envelop curve, the minimal strain safety factor value should not be below 2. For the determination of the safety factors on life time ($K_{\tau,N}$) and on stresses (K_σ), it is recommended to use the life-time lower envelop curves obtained with the probability of 99 %. It is expedient to apply safety factor values not lower than K_σ = 1.2 and $K_{\tau,N}$ = 1.5. In this range the minimal value of the safety factor should be selected. In some situations the values of safety factor may be determined with the use of the average curves and depending on the scatter of material properties, the safety factors should be not less than K_σ = 2 and $K_{\tau,N}$ = 10.

4. It has been shown in several investigations (STP ASTM No 165, 1954 [11]) that for the accounting of a nonstationary situation in computations using the formulas of linear summation of damages (in deformation or time interpretation), a conservative estimation is obtained on condition that the sum of damages is taken equal to 0.87. For the constructions submitted to a large number of launchings and stops it is necessary to take into account the effect of cyclic loading on the parameters of creep and life-time strength.

2.3 Safety factors in conditions of brittle fracture

The criterion characterizing the brittle fracture is the value of plain strain stress intensity factor K_1. For constructions with flaws, the computed values of stress intensity factor K_1 should be compared with its critical K_{1c} value. The brittle strength is assumed to be ensuring if the following condition is observed:

$$K_1 \leq K_{1c} \tag{3}$$

It is recommended to calculate the value of K_1 according the following equation (1):

$$K_1 = \eta \cdot \frac{(\sigma_p M_p + \sigma_q M_q) \cdot (\pi a/10^3)^{0.5}}{\left[1 + 4.6(a/2c)^{1.65}\right]^{0.5}} \tag{4}$$

where:

η – coefficient accounting for the influence of stress concentrations;

σ_p – tension component of stress intensity;

σ_q – bending component of stress intensity;

$M_p = 1 + 0.12(1 - a/c)$; $M_q = 1 - 0.64\ a/h$;

a – crack depth, generally assumed to be elliptical;

c – crack half length;

h – area within which bending stress component remains positive (the value of h for the formula (4) is permitted to be taken equal to half wall thickness).

For constructions with non detected flaws, the value of K_1 (according[1]) should be computed assuming the presence of defects of size comparable with the sensitivity of the inspection apparatus. Here, it is also necessary to account for the dimensions of a "shaded" zone where it is impossible to check up the presence of flaws in exploitation. In design, it is generally assumed that the construction should ensure the safety for the crack of size equal to 1/4 thickness of the part bearing

section (wall), that is considered as defect size in the computation[3]. In case of sufficiently careful inspection during the exploitation, the crack size may be taken as equal to the sensitivity parameter of the inspection apparatus, or in case of detected crack, to the size of the crack. As a rule, it is assumed that the safety factor on K_{1c} shall be not less than 2 and a lower safety factor may be adopted in case of availability of sufficient statistical data.

3 CYCLIC STRENGTH

In the case of evaluation of cyclic strength, various methods have been suggested for determining the local strength safety factors. These may be conditionally divided in five groups: computational for a rigid cycle, computational for a general situation, computational-experimental, based on the theory of adaptability and based on deformation criteriia.

2.1 *For cyclic loading and rigid cycle* (case of uniaxial loading with cycle asymmetry coefficient $r \approx -1$), it is expedient to use the values of amplitude intensity of conditionally elastic full strains as parameters of loading:

$$\Delta\varepsilon = \sqrt{2/3\Delta\varepsilon_{ij}\varepsilon_{ij}} \tag{5}$$

The resistance to fatigue for elastic cyclic deformation is evaluated applying the Goodman's equation:

$$\sigma_{\max} = \sigma_{-1}(1 - \overline{\sigma}/\sigma_B) \tag{6}$$

with:

$\sigma_{\max}$ – maximum cycle local stress with account of stress concentration;

$\overline{\sigma}$ – average cycle stress;

σ_{-1} – endurance limit of a material for symmetrical cycle with account of stress concentration.

The determination of the resistance to elasto-plastic deformation at cyclic loading is possible using of cyclic strain curves. In this case the conditions for the rupture at elasto-plastic cyclic deformation is obtained applying the Coffin's deformation criterion:

$$\sum (\Delta\varepsilon_p^{(k)}/\varepsilon^*)^m \, \mathrm{d}N = 1 \tag{7}$$

where:

$\Delta\varepsilon_p^{(k)}$ – plastic strain amplitude in K-cycle;

m – constant;

ε^* – ultimate strain deduced applying the equations (1a) and (1b).

In connection with the generally insufficiency of experimental data for the statistical analysis, as in case of creep static loading, it is expedient to evaluate the value of local strength safety factor with the use of the average curve and assuming the value of 2 in case of evaluation based on stress (or strain) amplitude, or equal to 10 if the evaluation is based on life time parameters. However, if the quantity of experimental data is sufficient and the lower envelop curve is reliable, the values of safety factors defined by stresses and by life time parameters may be taken equal to 1.2 and 1.5, correspondingly. It should be noted that the values of deformability ε^* and coefficient m in equation (6) should be determined experimentally for every material. In the case of using the universal value of coefficient m in Coffin's equation (7), the values of safety factors should be increased.

2.2 *For cyclic loading in a general case*, when the unilateral accumulation of strain (characteristic for a mild cycle and generally called "ratcheting") and stress variation (characteristic for a rigid cycle) takes place, different approaches to the evaluation of cyclic strength safety factors may be applied. Among all the known strength characteristics of a material, the life time under cyclic loading is depends mostly on the influence of factors related to the construction, technology, metallurgy and operation. Therefore, the evaluation of the life time under cyclic loading for constructions is possible considering the results of test specimens and construction components with accounting of all above mentioned factors. The main operational factors affecting the life time of a part under cyclic loading, are temperature and holding time at maximal loads and temperature, cyclic asymmetry, superposition of high-frequency component upon the low-frequency variation of loading. The realization of tests within all the range of operational loading is a rather labor consuming task. Therefore, is quite urgent to develope methods based on conventional tests of specimens for the evaluation of life time of constructions submitted in operation to complex loading.

For low-cyclic loading, material damages may be computed applying the deformation or energy criteria of rupture. Here, for computing the kinetics of stress-strain state, both for complex noncyclic loading and for cyclic loading with altering loading parameters, instead of a number of cycles n (or number of semi cycles k) it is expedient to use the relations of Odquist's type as parameters of of the actual state of the material. These relations are expressed by the following formulas [12,13]:

$$\lambda_1 = \int \mathrm{d}\varepsilon_{\mathrm{p}} - \varepsilon_{\mathrm{p}};\ \mathrm{d}\varepsilon_{\mathrm{p}} = (2/3\mathrm{d}\varepsilon_{\mathrm{p}ij}\mathrm{d}\varepsilon_{\mathrm{p}ij})^{0.5};$$
$$\varepsilon_{\mathrm{p}} = (2/3\mathrm{d}\varepsilon_{\mathrm{p}ij}\mathrm{d}\varepsilon_{\mathrm{p}ij})^{0.5} \tag{8a}$$

$$\lambda_2 = \int \mathrm{d}p - p;\ \mathrm{d}p = (2/3p_{ij}p_{ij})^{0.5};$$
$$p = (2/3p_{\mathrm{p}ij}p_{\mathrm{p}ij})^{0.5} \tag{8b}$$

$$\Delta\lambda_1 = \lambda^{(k)} - \lambda^{(k-1)} \geq 0$$

k – the ordinal number of a semi cycle.

The increment of nonelastic strains ($\mathrm{d}\varepsilon^{\mathrm{ne}}$) and the value of nonelastic strain intensity ($\varepsilon^{\mathrm{ne}}$) are defined with the equations:

$$\mathrm{d}\varepsilon_{ij}^{\mathrm{ne}} = \mathrm{d}\varepsilon_{\mathrm{p}ij}\mathrm{d}p_{\mathrm{p}ij}$$
$$\varepsilon^{\mathrm{ne}} = (2/3\mathrm{d}\varepsilon_{ij}^{\mathrm{ne}}\,\mathrm{d}\varepsilon^{\mathrm{ne}})^{0.5} \tag{9}$$

For the case of creep for known stress, the accumulated creep strains should be distinguished from the nonelastic strains.

In the particular cases of cyclic loading, instead of the mentioned parameters, by simple transformation the

computation of damages is replaced with the traditional applying the values of cycles and semi cycles. Then, for the evaluation of the life time under cyclic loading, Coffin's type formulas may be used:

$$(\Delta\varepsilon_{\mathrm{p}})^2 N = C_1;\ \sum \Delta\varepsilon_{pi}^2 = C_1 \qquad (10a)$$

$$(\Delta p)^n N = C_2;\ \sum (\Delta p_i)^n = C_2 \qquad (10b)$$

For the evaluation of the static component of life time, the value of ε_{p} (or Odquist's parameter) is compared with the ultimate strain ε^* of a material.

The described approach probably has one only deficiency, it is unsuitable for characterizing damages in conditions of neutral loading ways (neutral load path). This deficiency in the describing of the nonstationary cyclic loading can be avoided by applying the Coffin's formula (10a) and V. V. Novozhilov's suggestion[16] on the dependence of the accumulation rate of micro damages p:

$$D = k\int \rho \mathrm{d}\lambda = A;\ p = G\varepsilon_{\mathrm{p}} \qquad (11)$$

where $G = \mathrm{d}\sigma/\mathrm{d}\varepsilon_{\mathrm{p}}$ is deformation hardening parameter.

2.3 *The methods of adaptability computation* allow to determine the cyclic strength safety factors for the general case for sign-variable flow and increasing deformation[10,11]. The ultimate material characteristics for the sign-variable flow are:

σ_{s} – half value of the cyclic yield strength $S_{0.4}$ in a stable cycle with the tolerance of plastic strain amplitude within the cycle of 0.4 %.

In the case of presence of stress concentrators:

$\sigma_{\mathrm{s}} = \sqrt{E\varepsilon(N)\sigma_{(\varepsilon N)}}$, with $\varepsilon(N)$ – semi amplitude of the full strain corresponding to the appearance of low-cycle fatigue macro crack in N cycles and

$\sigma_{\varepsilon(N)}$ – in accordance with $\varepsilon(N)$ on the isochronous cyclic strain curve.

For creep in one semi cycles: $\sigma_{\mathrm{s}} = S_{0.4}^{\mathrm{c}} - 0.5S_{0.4}$, with $S_{0.4}^{\mathrm{c}}$ – cyclic yield strength by presence of creep.

For the progressing deformation, as ultimate characteristics $\sigma_{\mathrm{s}} = \sigma_{\mathrm{B}}$ – for transitional modes and $\sigma_{\mathrm{s}} = \sigma_{\mathrm{LTS}}$ $(t,\Sigma\Delta\tau)$ – for stationary modes are taken with σ_{LTS} – long-time strength in accordance with the all life time length of loading.

In [16,17,18] the results of the analyses of stress-strain state and strength of the disks and rims of regulating apparatus (two- and three-dimensional computations) are discussed. The following values of safety factors may be recommended for the strength computations of GTE disks : K_{SVF} = 1.2–1.5 – for sign-variable flow and K_{PD} = 1.9–2.2 – for progressing deformation. For the central part of disks is preferable to specify higher values of safety factor K_{SVF} and lower K_{SVF} values for not central stress concentrators.

4 CONCLUSIONS

1. Principles for the selection of methods for the determination of local strength safety factors in design computations of GTE parts for static and cyclic loading have been proposed. The methods are to be used in solutions of edge problems applying digital-analytical methods, e.g. FEM.
2. It has been shown that the selection of methods for the evaluation of local strength safety factors should be carried out applying special criteria and computations including adequate models of visco-elasto- plasticity.
3. It has been shown that the attempts to limit the values of local static stresses by the value of yield strength are without sense.
4. On the basis of the analysis of computational practice the minimum values of local strength safety factors for static and cyclic loading, which may be recommended for FEM computations, have been defined.

5 REFERENCES

[1] Standards for the calculation of durability of the equipment and pipelines nuclear power installations ПНАЭ Г-7-002-86; Energy-atomizdat, 1989, 524

[2] Rules for designing and manufacturing of mechanical components of atomic power stations with reactors with pressurised water; (EDF). Translation from English, 1995, November

[3] ASME Boiler and Pressure Vessel Code. Section III, Rules for Construction of Nuclear Power Plant Components, 1992, New York

[4] G. P. Karzov, B. Z. Margolin, V. A. Shvezova: A physicomechanical modelling of processes of destruction. S.Peterburg: Polytechnics, 1993, 388

[5] V. P. Kogaev, N. A. Machutov, A. P. Gusenkov: Calculation on strength and durability of machines details and designs. Handbook, Mechanical engineering (**1985**), 223

[6] A. P.Gusenkov: Strength at isothermical and non-isothermical low cyclic loading; Nauka, 1979, 295

[7] N. A. Machutov, M. M. Gadenin, M. I. Burak: Mechanics of low cyclic fracture; Nauka, 1986, 264

[8] B. E. Melnikov, L. B. Getsov, A. S. Semenov: A method of the automated selection of thermo-elasto-visko-plasticity models, ensuring adequate definition of stress - strain state at the arbitrary programs of loading; Transactions of 4-th International Conference Technological problem of reliability prediction for durability of designs and methods of their solution S.Petersburg, 2001, 213–215

[9] A. P. Gusenkov, P. I. Kotov: Long and non- isothermal low cyclic strength of elements of constructions. M: Mechanical engineering, 1988, 261

[10] D. A Gokhfeld, O. F. Cherniavsky: Limit analysis of structures at thermal cycling; The Netherlands – Rockville, USA, 1980, 577

[11] L. B. Getsov: Materials and strength of gas turbine parts; M: Nedra, 1996, 591

[12] L. B. Getsov: Problems of creation of the "universal" fracture theory of materials; Journal of machinery manufacture under realibility problem, (**2001**) 5, 49–55

[13] L. B. Getsov, M. G. Kabelevskiy: The questions of theories of plasticity and creep at cyclic nonisothermal loading; Strength of materials, (**1978**) 6, 660–665

[14] V. V. Novozilov, Yu. I. Kadashevitch: Microstresses in engeneering materials. L: Mechanical Engineering, 1990, 223

[15] V. I. Tsejtlin, D. G. Fedorchenko: Estimation of safety factors at multicomponent loading in view of scatter of materials properties; Strength of materials (**1979**) 9, 31–33

[16] A. R. Beljakov, L. B. Getsov, A. E. Ginzburg et al: Strength of guide vane components of gas turbines. Strength of materials (**1989**) 11, 119–129

[17] Beljakov, L. B. Getsov, V. K. Dondoshanskiy, J. B. Shneerson in A. R. Beljakov, L. B. Getsov, V. K. Dondoshanskiy, J. B. Shneerson: Use of the adaptability theory in calculation for the strength of gas turbine discs, Strength of materials (**1988**) 11, 100–106

[18] L. B. Getsov, A. A. Nigin, M. G. Kabelevskiy. Use of finite-element method for numerical evaluation of thermal cycling endurance of disks, Strength of materials (**1979**) 4, 69–72

UDK 620.1/.2:678:66.017
Pregledni članek/Review article

ISSN 1580-2949
MTAEC9, 42(6)243(2008)

POLIMERI V BELI TEHNIKI

POLYMER MATERIALS IN WHITE GOODS INDUSTRY

Vasilije Vasić

Razvoj PPA, Gorenje, d. d., Partizanska 12, 3503 Velenje, Slovenija
vaso.vasic@gorenje.si

Prejem rokopisa – received: 2007-10-04; sprejem za objavo – accepted for publication: 2008-06-16

Velik prispevek k tehnično-tehnološkem razvoju izdelkov bele tehnike so prispevali prav polimerni materiali in njim pripadajoče tehnologije. Razvoj je opazen ne samo pri izboljšanju primarnih funkcionalnih lastnosti, temveč je tudi vse bolj uveljavljen okoljevarstveni vidik razvoja izdelka (t. i. "eco design"). Za izbrane primere so prikazane tehnična in ekonomska upravičenost rabe polimernih materialov in pripadajočih tehnologij ter specifičnost snovanja takšnih izdelkov. Prikazane so tudi nekatere usmeritve v sedanji rabi polimernih materialov in v bližnji prihodnosti ob uporabi nanotehnologije.

Ključne besede: polimerni materiali, bela tehnika, "eko-design", nanotehnologija

Significant contribution to technical and technological development of white goods products is due to polymers and related technologies. Development reflects not only the improvement of primary functional features, but also the ecology aspect of product design (eco-design) and pleasurable industrial design. The shown examples demonstrate the technical and economical feasibility of polymer application and related technologies as well as the design particularity of such products. The polymer application is growing and in the near future we could expect even bigger presence of nanotechnology.

Key words: polymer materials, white goods, eco design, nanotechnology

1 UVOD

Industrija bele tehnike je zrela industrijska panoga, ki sledi usmeritvam tehnološkega razvoja na različnih področjih in socio-ekonomskim zahtevam trga. Med najpomembnejša področja tehnološkega razvoja bele tehnike se uvrščata razvoj novih materialov in elektronika, s katerimi se dosegajo nove ali izboljšane funkcionalne lastnosti in ergonomsko všečne oblike.

Med izdelke bele tehnike prištevamo velike in majhne gospodinjske aparate – npr. hladilnike, zamrzovalnike, pralne stroje, sušilnike perila, mešalnike itd. Zaradi velikih svetovnih kulturoloških in socio-ekonomskih razlik velja tudi različen način pri potrebah ter s tem tudi pri snovanju gospodinjskih aparatov.

Na evropskem trgu bele tehnike so najuspešnejši proizvajalci izdelkov bele tehnike iz Švedske, Nemčije in Italije ter iz nekaterih drugih dežel – npr. Španije, Turčije in Francije. Različna podjetja si na različne načine ustvarjajo konkurenčno prednost, ki temelji bodisi na tehnološki prednosti (superiornosti), všečnosti izdelkov (industrijsko oblikovanje) ali pa na prepoznavnosti in ugledu lastne blagovne znamke.

Pri razvoju vsake naslednje generacije izdelkov bele tehnike prevladujejo ključne tržne usmeritve – povečana konkurenčnost na trgu, občutljivost cen, nenehne zahteve kupcev po povečani funkcionalnosti in všečnosti ter ergonomija.

Osnovni razlogi za uvedbo polimernih materialov in zamenjavo kovinskih elementov so predvsem manjša masa polimernega izdelka, velika korozijska in okoljska odpornost ter velika fleksibilnost pri izdelkih zapletenih oblik. Razen ekonomike in tehničnih razlogov je v ospredju vse bolj stroga okoljevarstvena zakonodaja (npr. WEEE, RoHS, IEC 60335), ki jo predpisujejo posamezne države ali pa posamezna svetovna (panožna ali strokovna) združenja (npr. CECED – Evropsko združenje proizvajalcev bele tehnike) – npr. obveznost za reciklažo lastnih izdelkov in okolju prijazna proizvodnja.

V podjetju Gorenje, d. d., namenjamo veliko pozornost razvoju polimernih materialov in pripadajočih tehnologij. V zadnjih letih se je opravilo kar nekaj raziskav na področju polimernih materialov in tehnologij, ter ocenil potencial uvedbe nanotehnologij v industriji bele tehnike.[1,2,3,4] Preliminarne študije izvedljivosti uporabe so bile del razvojno-raziskovalnih aktivnosti v okviru tehnološke mreže Inteligentni polimerni materiali in tehnologije, kjer smo strokovno utemeljili in dokazali pomen investicije za modernizacijo razvoja polimernih produktov na primeru polimerne pralne kadi pralnega stroja.[5]

V prispevku bodo prikazane specifičnosti in praktične projektne izkušnje v Gorenje, d. d., pri razvoju plastične kadi za sodobne pralne stroje in antibakterijske zaščite pri hladilno-zamrzovalnih aparatih.

2 PREGLED UPORABE POLIMERNIH MATERIALOV IN PRIPADAJOČIH TEHNOLOGIJ V INDUSTRIJI BELE TEHNIKE

Polimerni materiali so multifunkcijski, saj lahko nasprotno od drugih materialov (npr. kovine) izkazujejo hkrati več dobrih, a med seboj fizikalno različnih lastnosti. Vzporedno z razvojem polimernih materialov in

pripadajočih tehnologij se veča tudi masni delež polimernih materialov v izdelkih bele tehnike. Od leta 1960 pa do 2000 se je namreč utežni delež polimernih materialov v produktih bele tehnike povečal na 30% [6].

Razloge za uporabo polimernih materialov v industriji bele tehnike in nadomeščanje kovinskih elementov lahko strnemo v naslednjih točkah:[7]

- doseganje novih in uporabniku prilagojenih specifičnih lastnosti izdelka (npr.dušenje vibracij, hrupa);
- izboljšanje sedanjih lastnosti izdelka, kar lahko pomeni zmanjšano porabo energije do 30 %,
- enostavno doseganje kompleksnih oblik izdelka s konvencionalnimi postopki predelave (npr. injekcijsko stiskanje);
- znatno zmanjšanje proizvodnih stroškov (tudi do 20 %);
- zmanjšanje nujnih investicij v proizvodno linijo (tudi do 50 %);
- odprava problemov s korozijo;
- povečanje možnosti reciklabilnosti izdelka in njegovih komponent ter
- nižja cena aparatov z uporabo polimernih materialov (vsaj 25 %).

V beli tehniki so prevladujoči polimeri plastomeri: PS, ABS in PP ter duromer PUR, kot je razvidno iz diagrama o porabi polimernih materialov v izdelkih bele tehnike (**Slika 1** [8]).

Vendar se danes polimerni materiali zelo redko uporabljajo v končnih izdelkih brez dodatka aditivov ali polnil, s katerimi skušamo izboljšati sedanje, želene lastnosti končnega izdelka (npr. zmanjšanje skrčkov – dimenzijska stabilnost, udarna žilavost, togost, moč) in hkrati predelovalnost polimernega materiala. To sicer pogosto pomeni pozitiven finančni učinek, vendar pa moramo le najti kompromis med želenimi lastnostmi in predelovalnostjo polimernega materiala.

Z dinamičnim razvojem aditivov in polnil so postali polimerni materiali v industriji bele tehnike še bolj konkurenčni kovinam, kar nam tudi prikazujejo lastnosti nekaterih materialov, podane na **sliki 2**.[9]

Zelo podoben primer koristnosti uporabe polimernih materialov v evoluciji izdelka bele tehnike se lahko pokaže pri sorodnem gospodinjskem aparatu, sesalnika za prah (**Tabela 1**,[10] **Slika 3**[10]).

Za čas iznajdbe sesalnika se smatra leto 1908 in od takrat do danes se je njegova masa zmanjšala skoraj na pol, istočasno pa se je moč povečala za 40-krat. Uvedba polimernih materialov je omogočila razen všečnejše oblike tudi manj sestavnih delov. Današnje ohišje sesalnika je sestavljeno iz 4 delov, ki so združeni z enim samim veznim elementom, v primerjavi z ohišjem iz leta 1950 iz 11 delov in 8 veznimi elementi. Možne so tudi izboljšave materiala in njegove vrste (npr. kompozit ali nano-polnila), vendar niso tržno konkurenčna s sedanjimi tehničnimi rešitvami pri sesalnikih.[10]

Nasprotno od kovin velja za polimerne materiale, da imajo zelo dobre lastnosti dušenja in da so njihove materialne lastnosti časovno spremenljive ter zelo odvisne od vpliva temperature in/ali vlage. Prav zato je treba pri konstruiranju izdelkov iz polimernih materialov upoštevati fizikalni pojav lezenja (sprememba dimenzij) polimernega izdelka pod vplivom (konstantne) obremenitve ali relaksacije (sprememba obremenitve, npr. nosilnosti) pod vplivom (konstantne) deformacije.[9]

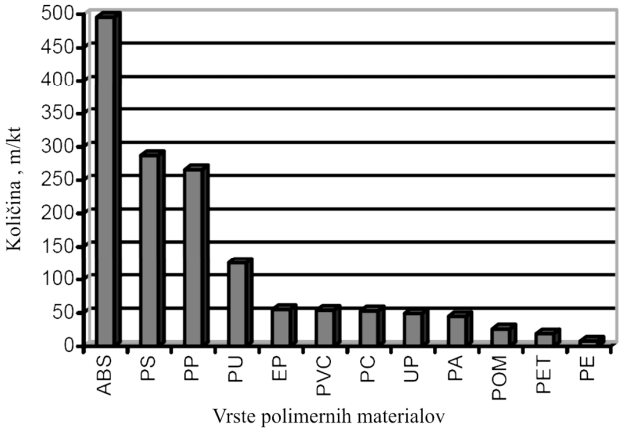

Slika 1: Poraba polimernih materialov v industriji bele tehnike v Evropi v letu 2000

Figure 1: Consumption of polymer materials in white goods industry for year 2000

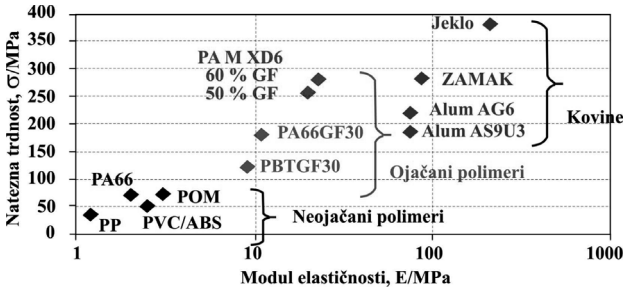

Slika 2: Primerjava natezne trdnosti in nateznih modulov za kovine in polimere

Figure 2: Strenght and flexural modulus for different polymer materials and metals

Tabela 1: Prikaz evolucije sesalnika za prah od iznajdbe do danes

Table 1: Evolution of vacuum cleaner from the invention to the present moment

Sesalnik *Pogon/Proizvajalec*	Leto	Prevladujoči material	Moč (W)	Masa (kg)	Cena
Ročni pogon	1900	les, jadrovina, usnje	50	10	£ 240 / $ 380 / 304 €
Elektromotor/Cylinder	1950	lahko jeklo	300	6	£ 96 / $ 150 / 120 €
Elektromotor/Cylinder	1985	brizgan ABS in PP	800	4	£ 60 / $ 95 / 76 €
Elektromotor/Dyson	1995	PP, PC in ABS	1200	6,3	£ 193 / $ 300 / 240 €

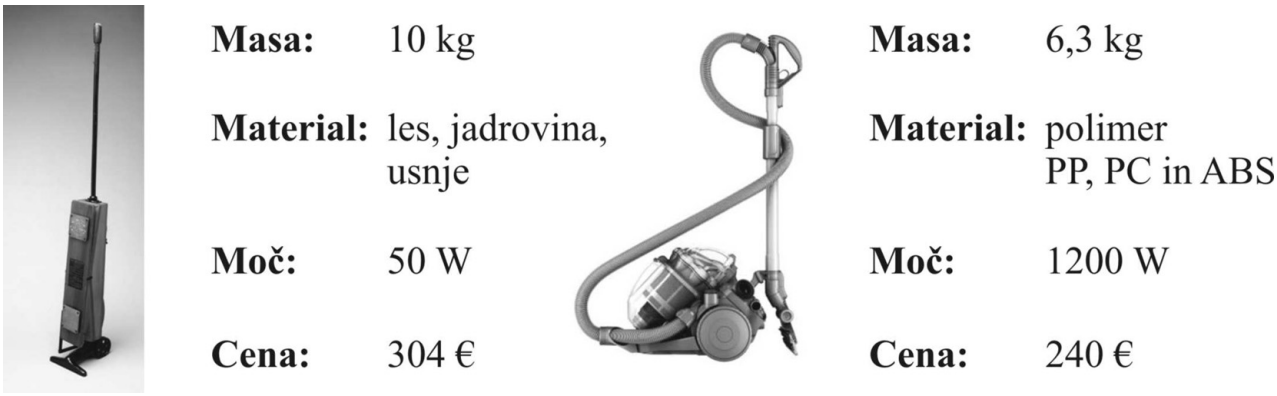

Slika 3: Prvi ročni sesalnik za prah (1908) in sodobna izvedba (2005)
Figure 3: First vacuum cleaner (1908) and contemporary vacuum cleaner (2005)

Kot primer razvoja navajamo multifunkcionalni polimerni material za potrebe hladilno-zamrzovalne tehnike (MABS – BASF Terlur). Razen navadnih lastnosti material omogoča boljšo prozornost, odpornost proti razpokam, povzročenim s čistili in olji, visoko udarno žilavost in dobre mehanske lastnosti. Prav tako ima izboljšano zvočno izolativnost v primerjavi s sedanjim SAN materialom, in s tem se lahko bistveno prispeva k zmanjšanju hrupnosti hladilno-zamrzovalnega aparata.[11]

V primerjavi z drugimi materiali, npr. kovinami, je toplotna prevodnost polimerov 100- do 1000-krat manjša, z nekaterimi polnili pa se prevodnost lahko poveča za 3- do 4-krat. Ta lastnost se izkaže za zelo uporabno pri hladilno-zamrzovalnih aparatih (izolacija) in pri pralnih strojih (plastična kad pralnega stroja). Vendar pa so prav zaradi dobre toplotne izolativnosti (slabe toplotne prevodnosti) polimerni materiali zelo zahtevni za predelavo (Op.a. Slaba toplotna prevodnost upočasnjuje cikel predelave zaradi potrebe po enakomernem ohlajanju produkta) in zato za lažjo predelavo potrebujejo dodatek aditivov ali polnil.[12]

Zato moramo za doseganje končnih funkcionalnih lastnosti upoštevati tudi značilnosti postopkov predelave. V industriji bele tehnike so najpogosteje zastopane enostavnejše oblike polimernih tehnologij:

- **injekcijsko stiskanje** – notranje komponente hladilno-zamrzovalnih aparatov (police- ABS) in pralni stroj (pralna kad – PP);
- **ekstrudiranje** – celice in protivrata hladilno-zamrzovalnih aparatov (PS);
- **toplotno preoblikovanje (vakuumiranje)** – celice in protivrata hladilno-zamrzovalnih aparatov (PS);
- **tehnologija formiranja poliuretanskih pen** – toplotna izolacija hladilno-zamrzovalnih aparatov.

Pri snovanju polimernih komponent v beli tehniki si med drugim pomagamo tudi z računalniškimi orodji za modeliranje predelovalnih procesov – npr. MoldFlow©, UGS NASTRAN, kjer skušamo predvideti vedenje polimernega materiala med predelovanjem in pri kasnejši rabi izdelka pri predvidenih pogojih delovanja.

3 VLOGA NAPREDNIH POLIMERNIH MATERIALOV PRI RAZVOJU INDUSTRIJSKIH IZDELKOV

Osnovni namen uvedbe naprednih materialov je doseči izboljšavo sedanjih in dodatnih funkcionalnosti izdelka, ki jih sicer z navadnimi materiali in postopki ne bi bilo mogoče doseči.

Pri navadnih polimernih mešanicah (blendih) in polimerih s polnili moramo namreč za doseganje želene multifunkcionalnosti narediti kompromis med izboljšavo želene lastnosti in drugimi lastnostmi materiala ter stroški in procesibilnostjo (predelovalnostjo). Omenjene omejitve brez težav premagujemo s polimeri na osnovi mikro- in nanokompozitov.

V nadaljevanju so predstavljeni trije zgledi sedanje in možne uporabe naprednih materialov v industriji bele tehnike, in sicer:

- preprečevanje prask na površini aparatov;
- antibakterijska/antimikrobna zaščita;
- odpravljanje razpok v materialu in
- uvajanje mikro- in nanopolnil v polimerne materiale.

Preprečevanje prask na površini aparatov je lahko zgled, značilen za avtomobilsko industrijo. Na avtomobilih se zaradi vse pogostejšega pranja v avtopralnicah uničuje lak, ker se na ščetkah avtopralnic nahajajo majhni delčki. Preprečevanje abrazije laka so se pri Mercedes Benzu lotili z uporabo nanodelcev pri novem laku. Za premaz uporabljajo nanokeramične polimerne kompozite, ki tvorijo zelo gosto mrežo v strukturi premaza. Le-ta preprečuje mikropraske, ki sčasoma nastanejo in so pogosto posledica abrazije. Proizvajalci zagotavljajo, da nano-premaz omogoča trojno povečanje odpornosti proti praskam v primerjavi z navadnim premazom.[1,2]

V svetu velja vse večja zdravstvena ozaveščenost kupcev in mednje spada tudi nevarnost okužb, ki so posledica človeku nevarnih mikroorganizmov. Znano je namreč, da so določeni tipi plastike ali s plastiko prevlečeni materiali zelo ugodni za rast mikroorganizmov. Kontaminacija se lahko pokaže v obliki vidne rasti

mikroorganizmov na površini materiala, razbarvanja ali smradu, v najslabšem primeru pa lahko celo pripelje do poslabšanja vizualnih in funkcionalnih lastnosti plastike. Med zadnje prištevamo moč in upogljivost, električno izolativnost in prozornost. Na Japonskem so se zaradi gostote populacije in specifične klime kar nekajkrat soočili z množičnimi zastrupitvami s hrano, ki je prihajala v stik s polimernimi izdelki.

Zaradi tega se je v industriji bele tehnike že pred leti pričela intenzivno uporabljati antibakterijska/antimikrobna zaščita, ki se navadno izvede s t. i. antimikrobno (antibakterijska) plastjo, naneseno na osnovni (nosilni) material (**Slika 4a**). Takšen pristop je možen tako pri polimernih materialih (npr. koekstruzija vrhnje plasti na nosilni (polimerni) material) ali pa pri drugih materialih (npr. kovinah, keramiki, lesu). Obstaja pestra ponudba antibakterijskih sredstev, ki so najpogosteje anorganskega izvora (srebrovi nanodelci) in se med seboj razlikujejo po stopnji delovanja, učinkovitosti glede na določen mikroorganizem, zahtevano stopnjo

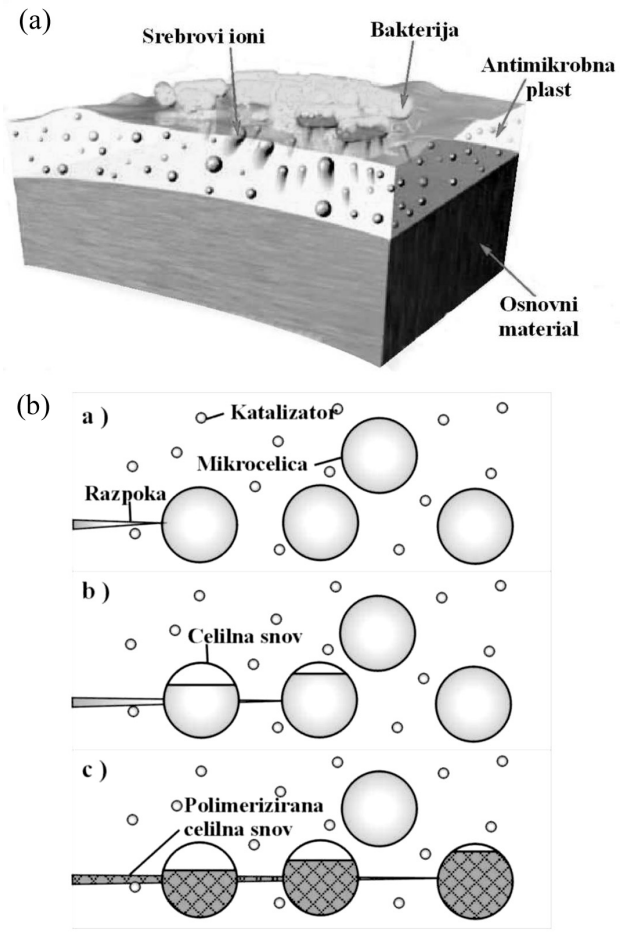

Slika 4: Prikaz delovanja antibakterijske zaščite in odprave razpok v polimernem materialu: **a)** Antibakterijska površinska zaščita polimera, **b)** Princip celjenja razpoke v polimernem materialu

Figure 4: Demonstration of antimicrobial protection and crack healing in the polymer materials: **a)** antimicrobial surface of polymer materials, **b)** principle of crakc healing in the polymer material

dodajanja, termično stabilnost in obstojnost proti spiranju.

Princip delovanja temelji na kovinskih ionih, ki so tako stabilizirani v vrhnji (koekstrudirani) površini, da se aktivirajo v stiku z drugim agentom, kot je npr. maščoba (**Slika 4b**). Kovinski ioni v vsakem primeru vzajemno delujejo s celičnimi membranami mikrobov, predvsem pa na osnovi delovanja encimov, in preprečujejo njihovo rast. Celice bakterij absorbirajo srebrove ione, ki preprečijo delitev RNA/DNA in tako zavirajo rast (t. i. biostatično delovanje).[4,13]

Polimer, namenjen za strukturne elemente, je izpostavljen poškodbam v obliki razpok, ki se lahko razširijo globoko v strukturo, kar je zelo težko zaznati ter skoraj nemogoče popraviti. Razpoke povzročijo mehansko degradacijo, v elektronskih komponentah pa so vzrok za kasnejše funkcionalne napake. Nastanek (mikro)razpok je posledica termičnega in mehanskega staranja, kar je dolgoročen problem pri polimernih materialih. Rešitev omenjenega problema nam lahko ponudijo polimeri z vgrajenimi mikrokapsulami t. i. celilnega sredstva, ki se sprosti ob pojavu razpoke. Polimerizacija celilnega sredstva se sproži v stiku z vgrajenim katalizatorjem kateri obkroža robove razpoke (**Slika 4b** [13]). Na osnovi eksperimentalnih rezultatov nam ponujena tehnična rešitev lahko povrne po razpoki kar 75 % togosti materiala.

V redno industrijsko uporabo v beli tehniki so prišli tudi polimerni materiali z mikropolnili. Zgled takšnega materiala je mikropolnila v PP (Borealis-Borcom), ki je omogočil med 8 % in 24 % manj uporabljenega materiala ob istočasnem povečanju udarne žilavosti za 30 %.[14]

Zaradi zelo podobnih dimenzijskih sprememb (skrčkov) izdelka po obdelavi ob zamenjavi obstoječega materiala z mikrokopozitom ni potrebna draga sprememba orodja. Zelo važno pa je vedeti, da se zaradi zmanjšanja mase izdelka in na splošno manj uporabljenega materiala zmanjšajo logistični stroški. Za enako količino uporabljenega polipropilena z vsebnostjo talka (20 %) ali kalcijevega karbonata ($CaCO_3$; 40 %) se lahko dosežejo tudi do 15 % prihranki na materialu.[14]

Mikrokompoziti so dejansko osnova za razvoj nanostrukturnih materialov in nanokompozitov, ki kljub obetajočim napovedim še niso popolnoma zaživeli v vsakdanji industrijski praksi in izdelkih bele tehnike.

4 EKOTEHNOLOŠKO SNOVANJE IZDELKA BELE TEHNIKE

Med prvine trajnostnega razvoja se uvršča način snovanja izdelka, ki upošteva vse faze razvoja – načrtovanje izdelka, proizvodnjo, uporabo in recikliranje. Takšen način snovanja se imenuje angleško Life Cycle Management (LCM) in obravnava celoten trajnostni cikel produkta kot celoto ter optimizira interakcijo med načrtovanjem izdelka, proizvodnjo ter aktivnostmi v in po eksploataciji (uporabi).

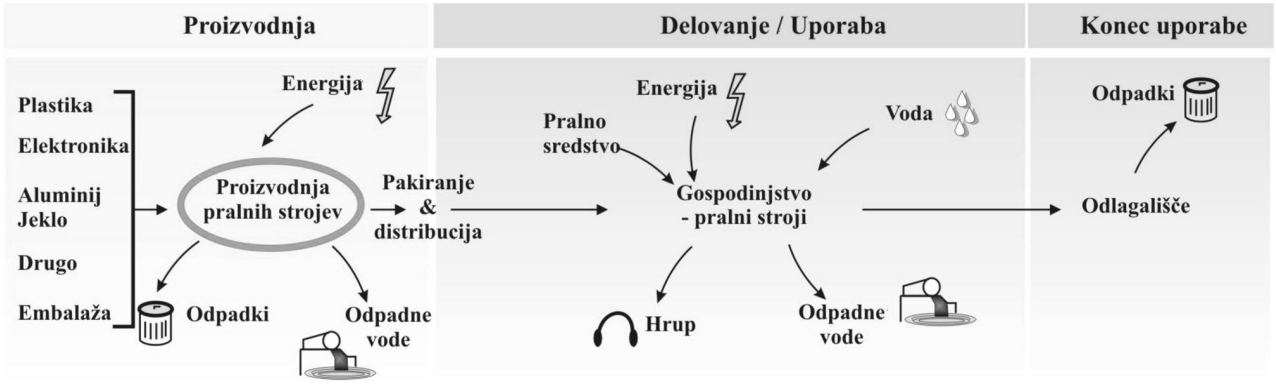

Slika 5: Primer trajnostne dobe gospodinjskega aparata – pralnega stroja
Figure 5: Appliance life cycle – washing machine

Osnovni cilj je racionalna raba razpoložljivih virov in maksimalna učinkovitost trajnostnega cikla, upravljanja s podatki o izdelku, tehnični podpori in seveda s celotnimi stroški (**Slika 5** [15,16]).

V mnogih industrijskih državah, vštevši Evropsko unijo, se je predlagalo ali celo že uveljavilo kar nekaj okoljevarstvenih zahtev za produkte, s katerimi želijo zmanjšati vpliv na okolje z različnimi ukrepi:

– eko-oznake ali okoljske deklaracije – s katerimi se označuje ta okoljsko ovrednoten izdelek in njegov možen vpliv na okolje;
– okoljsko ozaveščanje javnosti in nakup okoljsko prijaznejših izdelkov;
– razvrščanje izdelkov glede na njihov okoljski vpliv in na razpoložljive (naravne) vire ter
– obvezujoče recikliranje lastnih izdelkov po koncu uporabe (eksploatacije).

Za vsak izdelek veljajo različne faze trajnostnega cikla, ki jih lahko povzamemo kot inženiring in proizvodnjo na eni strani ter čas uporabe na drugi. Vsak proizvajalec mora zagotoviti zanesljiv in predvsem neškodljiv nastanek (proizvodnjo) in delovanje izdelka ter možnost kasnejše ponovne uporabe ali okolju prijazne razgraditve.

Za primer pralnega stroja in v primerjavi z ostalimi produkti je pokazan primer trajanja posameznih trajnostnih faz (**Slika 6** [16]).

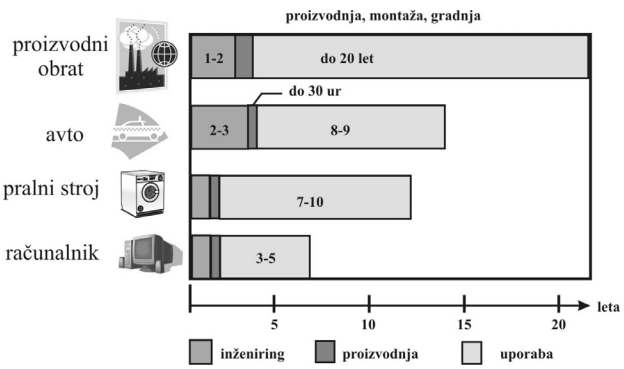

Slika 6: Prikaz posameznih faz trajnostnega cikla za nekatere izdelke
Figure 6: Phases of life cycle of some typical products

Proizvajalci polimernih materialov in pripadajočih tehnologij v beli tehniki imajo zato s stališča omenjene okoljske regulative zelo točno predpisane mejne vrednosti za uporabo v sodobnem gospodinjskem aparatu (npr. toplotna izolativnost, reciklabilnost, hrupnost), ki so iz leta v leto vse bolj stroga in zahtevna.

5 PRIMER IZ PRAKSE – RAZVOJ POLIMERNEGA MATERIALA ZA BELO TEHNIKO V GORENJU

V podjetju Gorenje, d. d., je že dolgo poznan in uveljevljen najzahtevnejši sistem okoljskega (ekološkega) menedžmenta po prvinah standarda ISO 14001, WEEE direktive (2002/96/EC), RoHS-direktive (2002/95/EC). V letu 2003 se je sistem okoljskega menedžmenta poenotil in nadgradil s sistemom EMAS – Energy Management and Audit Scheme (EC/761/2001). Podjetje tako pri izbiri ne samo polimernih materialov, temveč vseh komponent upošteva Evropsko direktivo o okoljskem načrtovanju izdelkov, ki porabljajo energijo (EuP – Eco-design Requirements for Energy-Using Products).[17,18]

Najbolj izrazita zgleda uporabe polimernega materiala v proizvodnem programu bele tehnike skupine Gorenje, d. d., sta plastična kad pralnega stroja (kompozit PP×40 CaCO3) in antibakterijska zaščita hladilno zamrzovalnega aparata (PS).[4,5]

Uporaba polimerne pralne kadi v proizvodnji ima pred podobno iz nerjaveče pločevine kar nekaj prednosti:[5,18,20]

– manjše število sestavnih delov in s tem posledično tudi pralnega stroja;
– izboljšanje nekaterih funkcionalnih lastnosti pralnega stroja (npr. energijska učinkovitost, hrup, vibracije…);
– avtomatiziranost in poenostavljenost proizvodnega procesa, kar posledično pomeni hitro, ceneno in fleksibilno proizvodnjo z racionalnejšim številom delavcev;

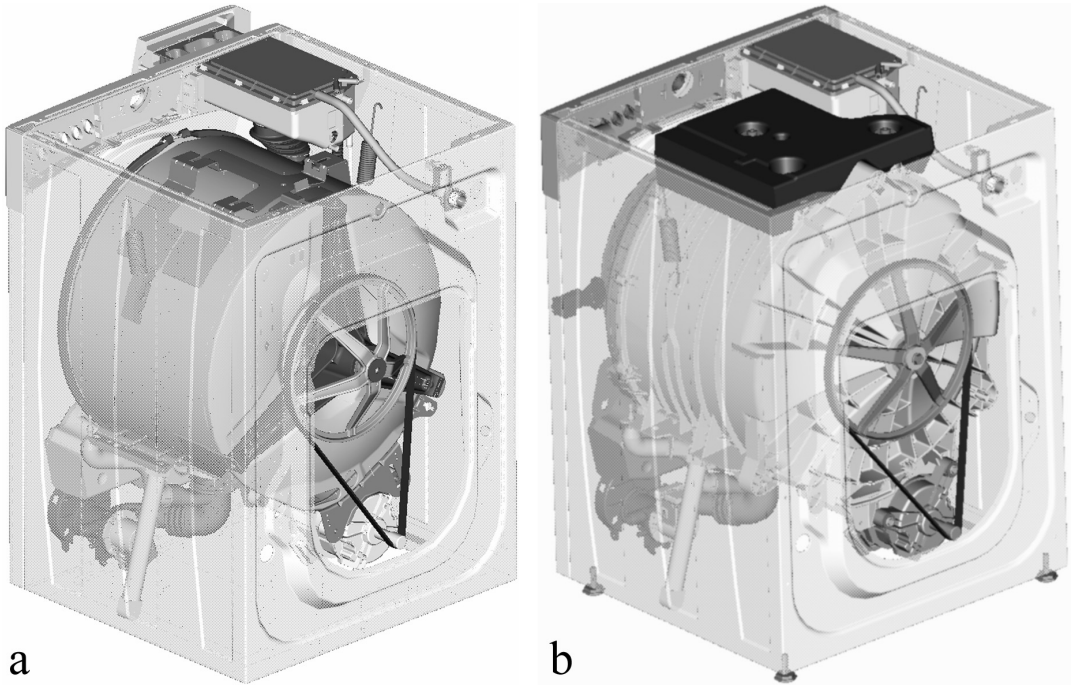

Slika 7: Shematski prikaz sestave pralnega stroja s kovinsko in polimerno pralno kadjo; **a)** Pralni stroj s kovinsko kadjo, **b)** Pralni stroj s polimerno kadjo
Figure 7: Description of washing machine with metal and polymer tub; **a)** washing machinme with metal tub, **b)** washing machine with polymer tub

– manjše število delavcev, potrebnih za sestavo pralne skupine in posledično večja produktivnost;
– zaradi nižjih stroškov proizvodnje in manj komponent pralnega stroja se s tem veča konkurenčnost podjetja na trgu.

Primerjava pralnega stroja s polimerno pralno kadjo in pralnim strojem s kovinsko kadjo nam nazorno prikazuje spodnja shema (**Slika 7** [20]).

Pri pralnih strojih so nas predvsem zanimale termo-mehanske lastnosti polimerne kadi na dinamične obremenitve (npr. vibracije, hladna in topla voda) in zagotavljanje lastnosti v trajnostni dobi izdelka (t. i. časovna odvisnost materialnih lastnosti). Zamenjava kovinske s polimerno kadjo je zahtevala precejšnjo spremembo sestavnih komponent (tudi do 30 komponent [18]) in uvedbo novih programskih orodij za snovanje izdelka (MoldFlow©) ter upoštevanje zakonitosti mehanike polimerov in kompozitov.[20,21]

Razvoj hladilno-zamrzovalnih aparatov se je usmeril v povečanje toplotne izolativnosti polimernih materialov ter hkrati v dušenje vibracij in hrupa celotnega sistema. Pri teh aparatih smo se srečali tudi s tržno zahtevo za povečanje stopnje zadravstvene in higienske zaščite uporabnikov, ki smo jo dosegli z antimikrobno (antibakterijsko) zaščito.[4,22] Projekt je zajemal uvedbo izboljšanega tehnološkega postopka (koekstruzije) in poznavanje zakonitosti delovanja aditivov ter postopkov preizkušanja učinka aditivov polimera.

Antimikrobna zaščita je bila uvedena pri veliki večini hladilno-zamrzovalnih aparatov, in s tem se je potrdila skrb podjetja za končnega kupca gospodinjskih aparatov Gorenje.

Razen izboljšanja funkcionalnih lastnosti izdelka je uporaba polimernih materialov znatno povečala všečnost izdelka in s tem t. i. emocionalno komponento, ki jo lahko dosegajo oblikovalci z drznimi oblikami in barvnimi odtenki.[23]

6 SKLEPI

V beli tehniki imajo polimerni materiali in njim pripadajoče tehnologije velik pomen pri razvoju za okolje in uporabnika racionalnega izdelka. Razen znatne izboljšave ključnih funkcionalnih lastnosti (npr. energijska učinkovitost, zdravstvena zaščita, manjši čas pranja, manj vibracij in hrupa) so polimerni materiali izdelkom bele tehnike povečali vščenost in ergonomičost.

Zaradi velike vsebnosti polimernih komponent v industriji bele tehnike se je tudi bistveno spremenil koncept snovanja izdelkov, spodbudile pa so tudi aktivnosti na za to vejo industrije pomembnih raziskovalnih področjih v Sloveniji (npr. mehanika polimerov in kompozitov, brizganje polimerov, orodja za simulacijo). V bližnji prihodnosti tako lahko pričakujemo večjo vsebnost mikro- in nanopolnil v polimernih materialih oz. večjo vsebnost mikro- in nanokompozitov na osnovi polimernih materialov.

7 LITERATURA

[1] Heath, D., Vasić, V.: Advanced polymer and smart polymer materials in major domestic appliance design, Ljubljana: Institut "Jožef Stefan" – International Centre for Sustainable Development, 2004, 49

[2] Heath, D., Vasić, V.: Nanotehnologija, Gorenje, Informacijski bilten – GiB, Velenje – Gorenje, 1 (**2004**), 1–9

[3] Vasić, V., Umek, P.: Potencials of nanomaterials and nanotechnology in the white goods industry, SLONANO 2004 / 3rd Slovenian workshop on nanoscience and nanotechnology, Ljubljana, 21–22 October, 2004. – Ljubljana: Institut "Jožef Stefan", 2004, 20

[4] Vasić, V, Meža, M., Dovšak, T.: NGC 600 ABP – Uvajanje in analiza antibakterijske zaščite v hladilno zamrzovalnih aparatih nove generacije, project documentation, Velenje: Gorenje, 2005, 200

[5] Vasić, V., Dimitrievski, I., Cvelbar, R., Emri, I.: Intelegentni polimerni materiali in pripadajoče tehnologije, ocena tehnološkega potenciala Slovenije na področju okoljskih tehnologij in materialov, elaborat, Center za eksperimentalno mehaniko, Katedra za mehaniko polimerov in kompozitov, Univerza v Ljubljani, Fakulteta za strojništvo, april 2003

[6] Posch, W.: Plastics for improved major appliances, International Appliance Technology Conference 2005, 9

[7] Hagan, R. S., Keelan, W. R.: Plastics – Key materials for innovation and producitivity in major appliances, American Plastics Council, 1994, 21

[8] Posch, W.: Borealis polypropylene – helping to shape the future of the white goods industry, International Appliance Manufacturing (**2002**), 184–187

[9] Desai, K. C.: Structural plastics – better performance and low cost, International Appliance Conference, 2005

[10] Ashby, M: Material selection in material design, Butterworth-Heinemann, 2nd ed, 1999

[11] BASF – Terlur MABS: Transparent, stress cracking resistant and sound dampening material, 2005

[12] Van der Vegt, A. K.: From polymers to plastics, Delft University Press, 2002, 149

[13] White, S. R., co: Autonomic healing of polymer composites, Nature, 409 (**2001**), 794–817

[14] Gubo, R.: Slim down for best performance – Borcom Microcomposites: A new product generation to minimize weight and costs, International Appliance Manufacturing, (**2005**), 124–128

[15] The European Eco-label: The European ecological label for washing machine – product fact sheet, Comission Decission 2000/45/EC, [ec.europa.eu/environment/ecolabel/pdf/infokit/washmach_en.pdf], 2

[16] Westkämper, E., Alting, L., Arndt, G.: Life cycle management and assessment: approaches and visions towards sustainable manufacturing, Proceedings of the Institution of Mechanical Engineers. Part B. Journal of engineering manufacture, 215 (**2001**) B, 599–626

[17] Gorenje – Corporate Social Responsibility Report and EMAS – Environmental Statement, Velenje: Gorenje, 2006

[18] Vasić, V., Vaupot, J.: Necessary energy regulations for achieving rational energy consumption – Gorenje case, Klimatizacija, grejanje i hlađenje / zbornik radova pisanih za 35. kongres o grejanju, hlađenju i klimatizaciji. – Beograd: Savez mašinskih in elektrotehničkih inženjera i tehničara Srbije (SMEITS), 2004, 120–129

[19] Sovič, B.: Polimerna pralna kad prinaša številne prednosti, Pika na G, Velenje – Gorenje, 1 (**2007**), 20–21

[20] Vasić, V.: Vloga polimerov in pripadajočih tehnologij v industriji bele tehnike, TM IPMT Življenjski cikel polimernega produkta, Vseživljensko izobraževanje : življenski cikel polimernega produkta, Ljubljana, 21 junij 2006, Gospodarska zbornica Slovenije

[21] Fržović, M.: Gorenje razvija materiale za pralne stroje in hladilnike, Finance 52 (**2006**), 2

[22] Heath, D., Vasić, V.: Antimikrobna zaščita pri gospodinjskih aparatih. GiB, Velenje – Gorenje, 9 (**2005**), 12–22

[23] DuPont: Elegant design details, DuPont Engineering Design 1–2 (**2005**), 1–2

KRATICE

ABS – Akrilonitril-butadien-stiren kopolimer
ALUM – Aluminij
CECED – Conseil Européen de la Construction d'appareils Domestiques – Združenje proizvajalcev aparatov bele tehnike
EMAS – ECO – Management and Audit Scheme / Evropska uredba o orodju za sistematizirano ravnanje z okoljem
EuP – Eco-design Requirements for Energy-Using Products
GF – Glass Fibres – Steklena vlakna
LCM – Life Cycle Management / Menadžment trajnostnega cikla produkta
MABS – Metilmetakrilat-akrilonitril-butadien-stiren kopolimer
PA – Poliamid
POM – Polioksimetilen
PS – Polistiren
PUR – Poliuretan
PVC – Polivinilklorid
RNA/DNA – Ribonucleic acid / Deoxyribonucleic acid – Ribonukleinska kislina / Deoksinukleinska kislina
RoHS – Restriction of the use of certain hazardous substances in electrical and electronic equipment / Omejitev uporabe nevarnih materialov v električnih in elektronskih napravah
SAN – Stiren-akrilonitril
WEEE – Waste Electrical and Electronic Equipment Directive / Direktiva o odpadnem materialu električnih in elektronskih naprav
ZAMAK – Cinkova zlitina (Zink – Aluminium – Magnesium – Kupfer), New_Jersey_Zinc_Company

UDK 669.14.018.252:542.428.2
Original scientific article/Izvirni znanstveni članek

ISSN 1580-2949
MTAEC9, 42(6)251(2008)

CHARACTERIZATION OF MULTILAYER PACVD TiN/Ti(B-N)/TiB_2 COATINGS FOR HOT-WORKED TOOL STEELS USING ELECTRON SPECTROSCOPY TECHNIQUES

KARAKTERIZACIJA VEČPLASTNE PACVD TiN/Ti(B-N)/TiB2 PREVLEKE ZA ORODNA JEKLA ZA DELO V VROČEM S TEHNIKAMI ELEKTRONSKE SPEKTROSKOPIJE

Monika Jenko[1], Djordje Mandrino[1], Matjaž Godec[1], John T. Grant[2], Vojteh Leskovšek[1]

[1]Institute of Metals and Technology, Lepi pot 11, Ljubljana, Slovenia
[2]University of Dayton, 300 College Park, Dayton, OH 45469, USA
monika.jenko@imt.si

Prejem rokopisa – received: 2008-10-13; sprejem za objavo – accepted for publication: 2008-11-18

Multilayer Ti(B-N) layers have been sandwiched between a TiN coating on treated AISI H11 steel and an outermost TiB_2 coating. The films were deposited with plasma-assisted chemical vapour deposition (PACVD) and have been characterized using electron spectroscopy techniques. The thickness of the total coating is 1.6 μm and comprised 21 layers. Earlier studies of such coatings using X-ray diffraction (XRD), energy dispersive spectroscopy (EDS), and wavelength dispersive spectroscopy (WDS) suffer from their relatively large analysis depths. In this work, Field-emission Auger electron spectroscopy (FE-AES) was used to examine the composition of the multilayered films since it has a smaller analysis depth. AES line-scans across cross-sectioned samples and AES depth profiling were used and are shown to be well suited for characterizing these multilayered coatings. These results are compared with combined Field-emission scanning electron microscopy (FE-SEM) and wavelength dispersive spectroscopy (WDS) measurements of the cross-sectioned samples.

Key words: plasma-assisted chemical vapour deposition (PACVD), hard TiN/Ti(B-N) coating, AISI H11 tool steel, Auger electron spectroscopy (AES), Field-emission SEM, wavelength-dispersive spectroscopy (WDS)

Večplastne Ti(B-N) plasti so vrinjene med TiN prevleko jekla AISI H11 in zunanjo TiB_2 plast. Plasti so bile nanesene po postopku kemijske parne faze ob pomoči plazme (PACVD), raziskali smo jih z različnimi tehnikami osnovanimi na elektronski spektroskopiji. Debelina celotne prevleke iz 21 plasti je 1.6 μm. Prejšnje raziskave tovrstnih prevlek z rentgensko difrakcijo (XRD), energijsko disperzijsko spektroskopijo (EDS), valovno disperzijsko spektroskopijo (WDS) niso dovolj natančne zaradi relativno velike analizne globine. V članku predstavljamo uporabo Augerjeve elektronske spektroskopije s FEG izvorom elektronov (FE-AES) za raziskavo sestave posameznih plasti v večplastni prevleki. AES linijska analiza preko preseka vzorca in AES globinski profil se je pokazala za zelo primerno za karakterizacijo tovrstnih večplastnih prevlek. Rezultate smo primerjali z meritvami z vrstično elektronsko mikroskopijo s FEG izvorom elektronov (FE-SEM) in valovno disperzijsko spektroskopijo (WDS) na prečno prerezanih vzorcih

Ključne besede: s plazmo podprt nanos preko kemijske parne faze (PACVD), trde TiN/Ti(B-N) prevleke, AISI H11 orodno jeklo, Augerjeva elektronska spektroskopija (AES) vrstično elektronska mikroskopija s FEG izvorom elektronov (FE-SEM), valovno disperzijska spektroskopija (WDS)

1 INTRODUCTION

Hard thin films, such as Ti(B-N), are well known for providing surfaces with a high hardness, and good corrosion and wear resistance, giving them a wide range of industrial applications [1–15]. Duplex treatments consisting of plasma nitriding the steel surface first and then using plasma-assisted chemical vapour deposition (PACVD) to deposit the hard coating has proven successful in improving the wear, fatigue and corrosion resistance, as well as the load-carrying capability, of steel substrates [16–21]. The increasing industrial demand for improved hard coatings with tailored properties for die casting and forging tools requires the development of multi-element and/or multi-phase hard films, as well as a better understanding of their composition.

Most of the published studies of Ti(B-N) film compositions use scanning electron microscopy (SEM), wavelength-dispersive electron-probe microanalysis (EPMA) [7,8,10,12], Rutherford backscattering spectroscopy (RBS) [5], Bragg-Brentano X-ray diffraction (XRD) [2,4,7,8,9,10,12] and in some cases transmission electron microscopy (TEM) [4,6]. These techniques suffer from their relatively large analysis depths or lack of depth resolution. In this investigation we have studied PACVD-deposited thin films using Auger electron spectroscopy, which is better suited for Ti(B-N) multilayer characterization We demonstrate that a combination of techniques such as AES depth profiling and FE-SEM give a better insight into the chemistry and structure of multilayered Ti(B-N) thin films. WDS measurements were made on the same multilayered structure for comparison.

2 EXPERIMENTAL

2.1 Deposition of the multilayered coating

The base material used for the substrate was AISI H11 tool steel with the chemical composition (all in mas %): Fe, 0.39 C, 0.34 Mn, 1.07 Si, 4.93 Cr, 1.26 Mo, 0.35 V, 0.011 Ti, 0.013 P and 0.0004 S. The samples were vacuum heat treated with the same procedure used for forging dies and then plasma nitrided in a Metaplas Ionon HZIW system. The conventional and plasma heating to the working temperature took 3 hours and the nitriding lasted for 24 hours. After nitriding, the samples were polished and sputter cleaned before the multilayered PACVD films were deposited.

The PACVD deposition on the prepared steel was carried out using the standard TiN/Ti(B-N) process developed by Rübig GMBH [22] in a bipolar-pulsed glow discharge at a constant temperature of 530 °C, a pressure of 200 Pa and a bias voltage of –500 V. The deposition process was as follows: 1 hour of TiN, 8 hours of alternating low and high boron-content Ti(B-N) multilayers with the high boron content continuously increasing and, finally, 1 hour of TiB_2. The TiN films were grown using N_2 and $TiCl_4$, Ar and H_2 gasses, and for the Ti(B-N) layers, BCl_3 was also added to the deposition chamber. The purity of all the gasses used was 99.9%. The coating had a total of 19 alternating Ti(B-N) layers between TiN and TiB_2 resulting in a total layer thickness of 1.6 μm. The multilayer arrangement started with a TiN layer on the steel sample, and finished with a TiB_2 layer as the surface layer. The boron-containing coating was chosen due to its small grain size, typically 5–7 nm, resulting in an increased resistance to plastic deformation and abrasion when compared to TiN [16,20,21].

2.2 AES line scan and AES depth-profile analysis

The AES instrument used was a Thermo Scientific VG Microlab 310-F composed of two ultra-high-vacuum chambers, one for sample insertion and one for the analysis. The electron gun has a thermally assisted Schottky field-emission source that provides a stable electron beam in the range of 0.5 to 25 keV. The electron energy analyzer is of the double-focusing spherical sector type with an electrostatic input lens and can provide an energy resolution of between 0.02% and 2%. The spectrometer has five electron detectors and spectra were acquired with a constant retard ratio (CRR) of 4, which provides an energy resolution that is 0.5% of the pass energy. For the cross-section studies, samples were cross-sectioned using a JEOL Cross Section Polisher, Model SM-09010, and analyzed using an AES linescan at 10 keV beam energy. AES depth profiles of the hard coatings were also measured with a 10 keV electron beam and the sample was sputtered with a 1.2 nA current of Ar ions at 3 keV. The AES data were acquired using Eclipse V2.1 ver07 software and processed using CasaXPS software.

2.3 WDS analysis

A metallographic cross-section of the multilayered TiN/Ti(B-N)/TiB_2 sample was prepared using a classic metallographic procedure with a Gatan PECS 682 ion polisher.

Secondary-electron images and back-scattered electron images were obtained with a JEOL JSM 6500F FE-SEM, with a working distance of 7.1 mm, an accelerating voltage of 8 kV and a beam current of 0.08 nA. By reducing the accelerating voltage to 8 kV, the area of the emitted backscattered electrons was reduced to a level that enabled the separate layers to be imaged. The WDS line scans were obtained in the FE-SEM using the following standards: pure boron for boron analysis, stoichiometric TiN for nitrogen analysis and pure titanium for titanium analysis. The TiN standard was made with thin film deposition, using a Balzers Plasma Sputron; the TiN stoichiometry was confirmed by XRD [15]. The WDS analysis was performed at 5 kV and 10 kV accelerating voltages at currents of 5.0 nA and 9.2 nA, respectively, using an Oxford Instruments INCA WAVE 700.

3 RESULTS AND DISCUSSION

3.1 AES line-scan analysis

Figure 1(a) shows an SEM image of the cross-sectioned, multilayered TiN/Ti(B-N)/TiB_2 hard coating, together with the position where the AES line-scan was made across the sample. **Figure 1(b)** shows the elemental concentrations determined from the AES line scan. The N Auger peak overlaps a Ti Auger peak at 420 eV and the N concentration was calculated by comparing the overlapping peak with the 420 eV Ti Auger peak and applying the following relationships:

$$I_{385} \approx \alpha_{c_N} S_{N\,385} + \alpha_{c_{Ti}} S_{Ti\,385} \quad (1)$$

$$I_{420} \approx \alpha_{c_{Ti}} S_{Ti\,420} \quad (2)$$

giving

$$\frac{c_N}{c_{Ti}} \approx \frac{S_{Ti\,420}}{S_{N\,385}} \cdot \frac{I_{385}}{I_{420}} - \frac{S_{Ti\,385}}{S_{N\,385}} \quad (3)$$

where I_{385} and I_{420} are the peak-to-peak intensities of the overlapping Ti and N peaks at approximately 385 eV and the Ti peak at 420 eV respectively, the S are sensitivity factors for N and Ti peaks at the indicated energies, and the c are the indicated N and Ti concentrations. The combined N and Ti profile were calculated first, then decoupled using the Ti profile from the Ti peak at 420 eV. Note that B decreases while the N increases with distance from the surface, although the undulations of eight of the boron-depleted regions and eight of the boron-rich regions can be seen in the Auger linescan. There also appears to be a relatively flat region in N concentration near the interface with the steel substrate (corresponding to the TiN layer).

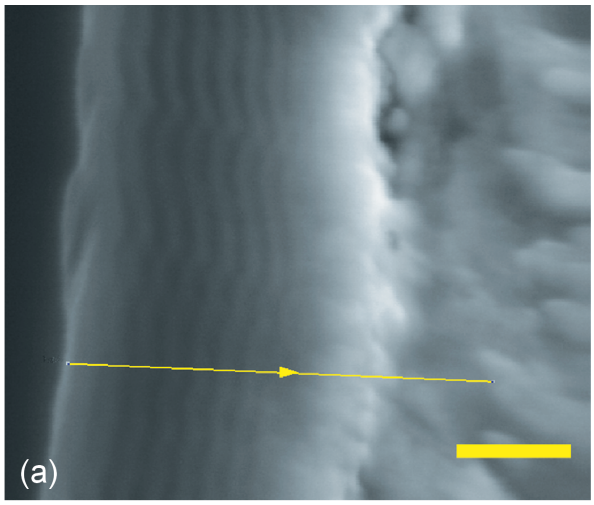

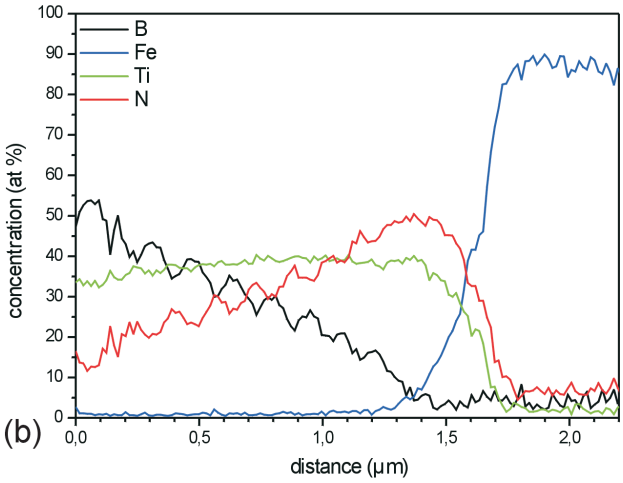

Figure 1: (**a**) SEM image of the cross sectioned TiN/Ti(B-N)/TiB_2/steel sample showing the region where the AES linescan was made. The scale marker is 600 nm long; (**b**) concentrations of Ti, N, B and Fe calculated from the AES linescan made along the line shown in part (**a**)

Slika 1: (**a**) SEM posnetek preseka vzorca TiN/Ti(B-N)/TiB_2/jeklo, prikazuje področje AES linijske analize. Merilna skala je 600 nm; (**b**) koncentracija Ti, N, B in Fe izračunana iz AES linijske analize vzdolž linije prikazane v delu (**a**)

3.2 AES depth profiling

The Auger sputter depth profile is shown in **Figure 2**. The Auger spectra were processed using equation (3), as was done for the Auger linescans. The TiB_2 layer can be seen at the first part of the depth profile. The nine boron-depleted and nine boron-rich regions can be seen in the sputter depth profile, and these are much better resolved than the corresponding regions in the Auger linescan shown in **Figure 1(b)**. Further, not all 18 alternating layers were resolved in the Auger linescan. The close agreement with the boron concentration behaviour in the Auger line scan and the Auger sputter depth profile indicates the absence of preferential sputtering in the depth profile.

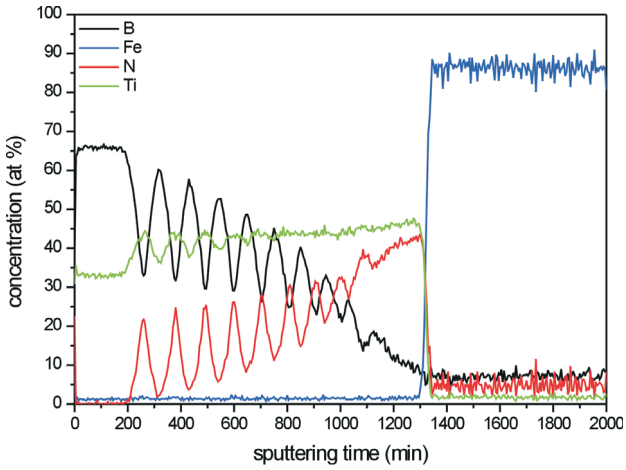

Figure 2: AES sputter depth profile of the TiB_2/Ti(N-B)/TiN multilayered hard coating showing an approximate 15 nm depth resolution

Slika 2: AES globinski profil TiB_2/Ti(N-B)/TiN večplastne trde prevleke prikazuje približno 15 nm globinsko ločljivost

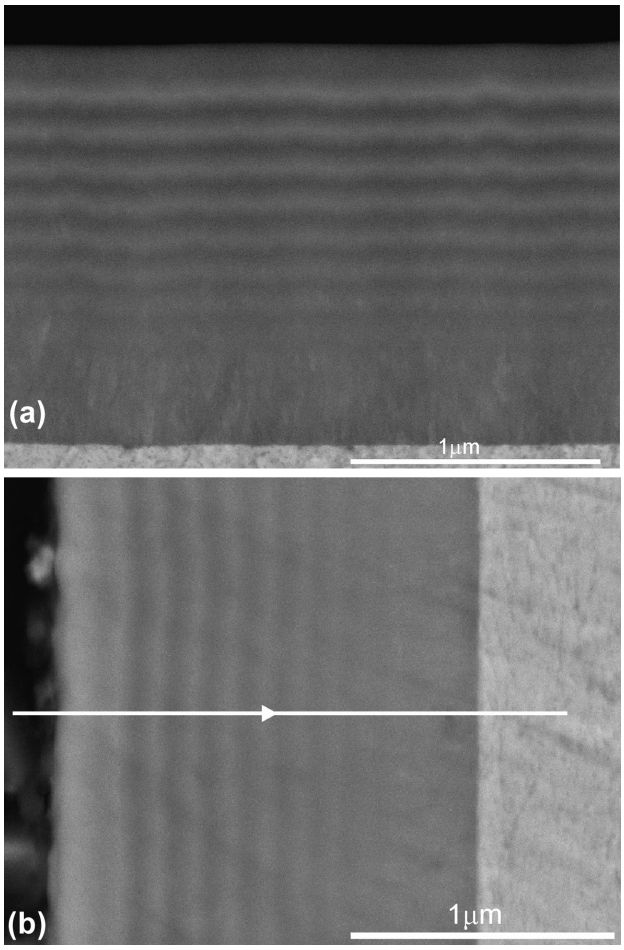

Figure 3: (**a**) Backscattered electron image (BEI) of the nanostructure of a multilayered coated sample in cross-section, (**b**) BEI of the same sample showing the region where the WDS line scans were performed

Slika 3: (**a**) BEI posnetek nanostrukturirane večplastne prevleke vzorca v preseku, (**b**) BEI posnetek istega vzorca, ki prikazuje področje WDS analize

3.3 WDS analysis

WDS measurements of the TiN/Ti(B-N)/TiB_2 multilayer were made for comparison. **Figure 3(a)** shows a backscattered electron image (BEI) of the nanostructure of a multilayered coated sample in cross-section, allowing to see the whole multilayer structure quite clearly. The first layer of the coating is TiN, and its growth seems to be columnar. Above this layer the multilayer structure of the Ti(B-N) layers are distinguished and finishes with the thicker TiB_2 layer on top. The light-grey regions represent TiN and boron-depleted Ti(B-N) layers, which have a higher average atomic number, and the dark-grey regions represent the boron-rich Ti(B-N) and TiB_2 layers, which have a lower average atomic number. The thickness of each layer was estimated to be 65 – 70 nm, except for first TiN and last TiB_2 layers which were each estimated to be approximately 150 nm thick.

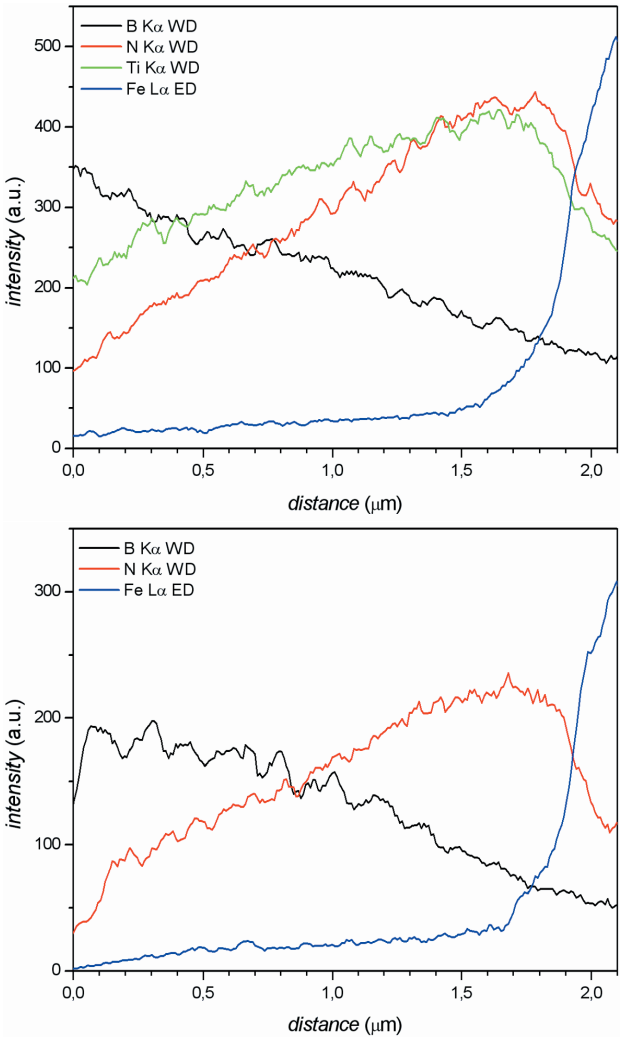

Figure 4: WDS line scans across the multilayer structure, (**a**) accelerating voltage of the primary electron beam 10 kV, (**b**) accelerating voltage of the primary beam 5 kV. The multilayered nature of the coating can be best observed from the boron linescan at 5 kV. The Ti Ka linescan is only present at 10 kV since 5 kV is to low for Ti Ka excitation.

Slika 4: WDS linijska analiza preko večplastne structure, (**a**) pospeševalna napetost primarnega elektronskega snopa 10 kV, (**b**) pospeševalna napetost primarnega elektronskega snopa 5kV. Večplastna struktura je najbolje vidna iz linijske analize bora pri 5 kV. Ti Ka linijska analiza je prisotna samo pri 10 kV, ker je 5kV premalo za vzbujanje Ti Ka.

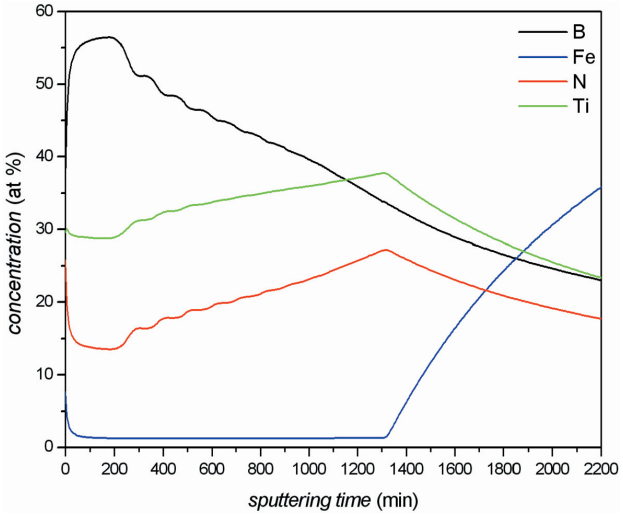

Figure 5: Cumulative depth profiles obtained with calculating the average concentrations between the surface and a given depth from the Auger depth profiles in **Figure 2**. They demonstrate that the average coating composition is heavily dependent on the analysis depth.

Slika 5: Zbirni globinski profil dobljen z izračunom poprečnih koncentracij med površino in dano globino iz Augerjevega globinskega profila na **Sliki 2**. prikazujejo je močno odvisnost poprečne sestave plasti od analizne globine.

Microchemical WDS line analyses were performed to determine the elemental distribution across the multilayer structure. The region where such an analysis was made is shown in **Figure 3(b)**. At a 10 kV accelerating voltage the B, N and Ti K_α x-ray lines are detected and measured. The Fe analysis was performed by EDS using L_a emission. For these conditions, the analyzed volume is of the order of 0.5 μm^3. By decreasing the accelerating voltage to 5 kV the analyzed volume is reduced to 0.008 μm^3. The line analysis performed at the higher accelerating voltage shows the boron, nitrogen and titanium distribution, **Figure 4(a)**. As expected, the boron concentration is highest at the top layers, and then it decreases to the multilayer-steel interface. The opposite is true for the nitrogen and titanium distributions. Using the lower accelerating voltage of 5 kV, it is possible to see an indication of a multilayer structure with observing the elemental distribution of boron, **Figure 4(b)**. However, the relatively large analysis depth compared to AES severely limited the observation of the layered structure in the coating using WDS. Due to the spatial resolution requirements of this analysis, the low intensity Fe L_α was used as it could be excited at 10 and 5 kV. This prompted the use of EDS instead of WDS for the Fe analysis. However, the inferior signal-to-noise ratio in

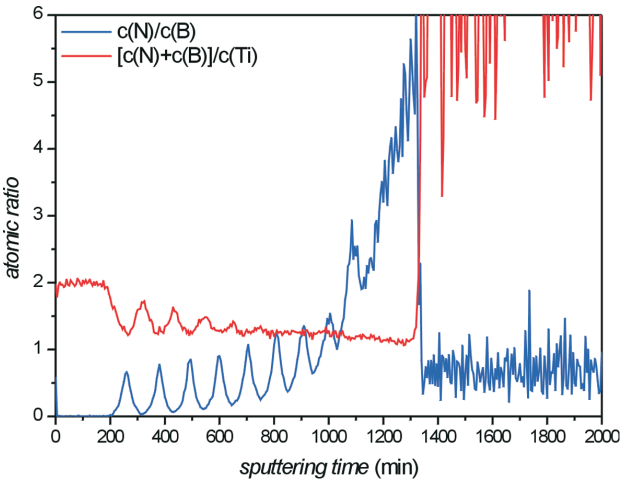

Figure 6: [c(N)+c(B)]/c(Ti) and c(N)/c(B) ratios through the thin film coating, as derived from the AES depth profile shown in **Figure 2**. Close to the surface the stoichiometry corresponds to TiB_2, although it is close to TiN near the coating-substrate interface.

Slika 6: [c(N)+c(B)]/c(Ti) in c(N)/c(B) razmerja skozi tanko plast prevleke, izpeljan iz AES globinskega profila na **sliki 2**. V bližini površine se stehiometrija ujema z TiB_2 čeprav je blizu TiN na mejni površini prevleka-substrat.

EDS means that some of the noise throughout the layers is mistaken for Fe L_α.

WDS and/or EDS analytical methods are often used to determine the chemical composition of hard coatings e.g., [15], and even in cases where the thickness of the layer is not large compared to the analysis depth an attempt is made to adjust for it by the proper choice of primary beam energy [16]. However, in the case of the multilayer coatings produced in this study, the average composition measured by a non-surface-sensitive technique would look somewhat like that shown in **Figure 5**. The average composition would be extremely dependent on the analysis depth and for small analysis depths even on the surface contamination.

It is also instructive to present depth profiling results in the form of total non-metal/titanium, and nitrogen/boron atomic ratios, as shown in **Figure 6** that shows that close to the surface the composition of the coating corresponds to TiB_2, while it approaches TiN near the coating-substrate interface. In the intermediate area, a strong variation of the B/N ratio in the Ti(B-N) layers can be clearly observed. All of this agrees with the sample manufacturing procedure, as summarized in section 2.1. The *[c(N)+c(B)]/c(Ti)* in the Ti(B-N) layers stays mostly below 1.5, which suggests that they may have a cubic structure up until hcp TiB_2, since TiN_x is cubic for x<1.5 [13].

4 CONCLUSION

We have shown that for studies of multilayer TiN/Ti(B-N)/TiB_2 hard coatings, Auger linescans and Auger sputter depth profiling are better suited to determine their composition than WDS. WDS suffers from its large analysis volume. Also, Auger sputter depth profiling is superior to Auger linescans for characterizing such films.

Acknowledgement

The authors would like to acknowledge the Ministry of Higher Education, Science and Technology of the Republic of Slovenia and ACRONI d.o.o. for financing the project L2-6093 *Electron spectroscopy of surfaces of nanostructured metallic materials*.

5 REFERENCES

[1] W. Gissler, Surf. Coat. Technol. 68/69 (**1994**), 556
[2] T. P. Mollart, M. A. Baker, J. Haupt, A. Steiner, P. Hammer, W. Gissler, Surf. Coat Technol. 74/75 (**1995**), 491
[3] T. P. Mollart, P. N. Gibson, M. A. Baker, J. Phys. D. Appl. Phys. 30 (**1997**), 1827
[4] A. Gupper, A. Fernandez, C. Fernandez-Ramos, F. Hoffer, C. Mitterer, P. Warbichler, Monatschefte fur Chemie 133/6 (**2002**), 837
[5] S. M. Aouadi, J. A. Chladek, F. Namavar, N. Finnegan, S. L. Rohde, J.Vac. Sci. Technol. B 20 (**2002**), 1967
[6] M. A. Baker, C. Rebholz, A. Leyland, A. Mathews, Vacuum 67 (**2002**), 471
[7] P. Lossbichler, C. Mitterer. Surf. Coat Technol. 96 (**1997**), 163
[8] J. Ye, S. Ulrich, K. Sell, H. Leiste, M. Stueber, H. Holleck, Surf. Coat. Technol. 467 (**2004**), 133
[9] P. Karvankova, M. G. J. Veprek-Heijman, O. Zindulka, A. Bergmaier, S. Veprek, Surf. Coat. Technol. 163 (**2003**), 149
[10] Y. H. Lu, Y. G. Shen, Z. F. Zhou, K. Y. Li, J. Vac. Sci. Technol. A 24 (**2006**), 340
[11] C. Mitterer, M. Rauter, P. Rodhammer, S. Veprek, Surf. Coat Technol. 41 (**1990**), 351
[12] P. H. Mayrhofer, C. Mitterer, Surf. Coat, Technol. 133 (**2000**), 134
[13] R. Wiedemann, V. Weihnacht, H. Oettel. Surf. Coat. Technol. 116–119 (**1999**), 302
[14] P. H. Mayrhofer, H. Willmann, C. Mitterer, Thin Solid Films, 440 (**2003**), 174
[15] P. Panjan, M. Čekada, Zaščita orodij s trdimi PVD prevlekami, Institut Jožef Stefan, Ljubljana 2005 (in Slovene)
[16] V. Leskovšek, Some aspects on PACVD, SOHN Inter. Symp. on Advanced Processing of Metals and Mat.: Principles, Technologies and Industrial, Practice, San Diego, 27–31 August 2006
[17] K.S. Klimek, H. Ahn, I. Seebach, M. Wang, K.T. Rie, Surf. Coat. Technol. 174/175 (**2003**), 1225
[18] M. Stoiber, C. Mitterer, T. Schoeberl, E. Badisch, G. Fontalvo, R. Kulmer, J. Vac. Sci. Technol. B 21 (**2003**), 1084
[19] M. Stoiber, C. Mitterer, T. Schoeberl, E. Badisch, G. Fontalvo, R. Kulmer, J. Vac. Sci. Technol. B 21 (**2003**), 1084
[20] P. H. Mayrhofer, M. H. Stoiber, C. Mitterer, Scripta Materialia 53 (**2005**), 241
[21] M. Stoiber, E. Badisch, C. Lugnoir, C. Mitterer Surf. Coat. Technol. 163 (**2003**), 451
[22] Micropuls-Plasma-Plastit Rubig GMBH&Co, http://www.rubig.com

UDK 669.14.018.298:621.791
Original scientific article/Izvirni znanstveni članek

ISSN 1580-2949
MTAEC9, 42(6)257(2008)

AN INVESTIGATION OF THE STRETCH REDUCING OF WELDED TUBES

RAZISKAVA IZTEZNE REDUKCIJE VARJENIH CEVI

S. Rešković[1], Franc Vodopivec[2]

[1]Faculty of Metallurgy, University of Zagreb, Sisak, Croatia
[2]Institute of Materials and Technology, Ljubljana, Slovenia
reskovic@simet.hr

Prejem rokopisa – received: 2008-10-20; sprejem za objavo – accepted for publication: 2008-11-12

The results of an investigation into the hot stretch reducing of high-frequency welded steel tubes are presented. The internal stresses were determined after every processing pass. The selected processing parameters ensured that the coefficient of plastic extension was maintained in the range that prevents the tearing of the tube wall and achieves the required geometrical shape as well as the planned properties of the finished tube.

Key words: welded tube, hot stretch reducing, micro-alloyed steel, internal stresses, coefficient of plastic extension

Predstavljeni so rezultati raziskave iztezne redukcije visokofrekvenčno varjenih jeklenih cevi. Po vsakem prehodu so bile določene notranje napetosti. Izbrani procesni parametri zagotavljajo, da se koeficient plastičnega podaljška ohranja v razponu, ki preprečuje trganje cevne stene in zagotavlja, da se dosežejo predpisane mere in mehanske lastnosti cevi.

Ključne besede: varjene cevi, vroče iztezna redukcija, mikrolegirano jeklo, notranje napetosti, koeficient plastičnega podaljška

1 INTRODUCTION

With proper hot working small additions of micro-alloying elements can improve the properties of hot-rolled sheets produced from structural steels [1,2]. Hot-rolled welded tubes are manufactured from hot-rolled sheets with carbide precipitates formed by deformation-induced precipitation during the final stages of hot rolling. In the technology of the stretch reducing of welded tubes, the initial tube blank is processed at an appropriate temperature and without internal tool (mandrel) to a different diameter and wall thickness [3]. The calculation of the per-pass reductions of the tube diameter and the wall thickness is relatively complex [3,4,5], and their proper sequence depends on the type of steel, the rolling temperature and the rate and the extent of reduction of the tube's diameter and the wall thickness. In this study the results of an experimental investigation on the evolution of the microstructure and internal stresses for a sequence of stretch-reducing passes for a micro-alloyed steel are presented. The findings in this investigation were used in the selection of the optimal parameters for industrial processing.

In the process of manufacturing hot-rolled welded tubes, the sheet is formed at room temperature in a tube pre-form, high-frequency welded, heated first to the normalising temperature, to homogenise the micro-structure in the weld, and then heated to the hot-rolling temperature, processed with stretch-reducing passes to the required size and air cooled [5]. The processing mill consists of several three-rolls high stands [4,5].

For proper processing, a balancing of the maximum allowed changes to the tube diameter and the wall thickness is required. Achieving the final tube size depends on the maximum allowed deformation and stressing of the steel at the temperature of every processing pass. The reduction of the diameter occurs in several passes and depends on the total reduction and the number as well as the size and design of passes. In the initial processing stands of the investigated mill, the tube diameter decreased quickly to a constant value, then it decreased more slowly towards the end pass to ensure to obtain the required tube diameter and wall thickness. The deformation was 3–5 % per pass and stand [4,5]. The maximum extent of the wall reduction depends on the steel's plastic elongation, the total and the per-pass. To prevent hot tearing of the tube wall it is necessary to know for every stand, the maximum coefficient of the steel's plastic extension (stretching), which is given as a ratio of the axial stressing and the steel's elongation [4,5],and can achieve a maximum value of $Z_t = 1$.

For $Z_t = 0.5$ the wall thickness is increased, and for a reduction of the tube diameter by 3–5%, the tube length and the wall thickness are increased. Experience shows that up to $Z_t = 0.55$, the wall thickness remains unchanged. However, for $Z_t = 1$ the tube diameter and the tube-wall thickness are reduced simultaneously and tube-wall ruptures occur frequently. For this reason, the maximum value of the coefficient of plastic extension is $Z_t = 0.7–0.8$ [4,5].

2 FRAMEWORK AND SCOPE OF THE INVESTIGATION

The fundamental processes and mechanisms of austenite hot deformation, carbide precipitation and

austenite grain growth are involved in the processing of micro-alloyed steels [6]. After proper thermomechanical processing, the hot-rolled sheet has a fine-grained and homogenous microstructure and good mechanical properties [1]. With higher temperatures, coarsening of the precipitates occurs, with the kinetics depending on the temperature, the solid solubility and the diffusivity [6,7]. With a smaller solid solubility, the coarsening rate of the precipitates is reduced, and it is also less for nitride than for carbide particles [6]. Precipitates with a diameter over a critical value and at large mutual distance accelerate the static recrystallisation of austenite, while for a small mutual distance the small precipitates may even hinder the static recrystallisation of austenite [8,9,10,11]. In niobium micro-alloyed structural steels the static recrystallisation of austenite occurs at a sufficient temperature if the per-pass rolling deformation is above approximately 12 % [12,13]. In the investigated processing the per-pass reduction was below this level, and therefore the deformation energy was released only with recovery.

The large number of point and line defects introduced into the steel by the plastic deformation produces strain hardening and softening processes with a mutual relation depending on the steel's chemical composition, the initial microstructure and the extent of deformation, the rate of deformation and the deformation temperature. Hardening is the result of an increase in the density of the deformation defects and softening corresponds to a decrease. The rates of diffusion, precipitation and precipitate coarsening can be increased in non-recrystallised austenite by up to two orders of magnitude [10,11,14] when compared to that in the recrystallised austenite, and this affects significantly the density and the mobility of the vacancies and dislocations.

The precipitation rate depends on the temperature, the degree of deformation and the content of elements affecting the recrystallisation, especially niobium. In the hot-rolled sheet used in this investigation, we found mostly particles formed by deformation- induced precipitation [1]. With high-frequency welding the steel is locally heated up to 1400 °C; however, the heating time is very short and it does not produce a significant change in the size and distribution of the precipitates. With the subsequent reheating of the tube blanks to 850 °C, the microstructure in the weld area is homogenized, while the size and the distribution of the precipitates are not affected.

The initial temperature of the stretch reducing of the welded tubes depends on the number of passes and should be sufficiently high to ensure the finishing temperature is above the austenite-to-ferrite transformation [4,5]. For low-carbon steel it is in the range 1100–950 °C. During soaking, coarsening of the austenite grains occurs and part of the niobium carbonitride is dissolved in austenite, as the solid solubility is attained only at a higher temperature. Parallel coarsening of the non-dissolved precipitates could also occur.

In the process of mastering the technology of stretch reducing high-frequency welded tubes from niobium micro-alloyed steels, in the central passes of the processing line tearing of the tube wall occurred frequently, especially in the weld area. The aim of this work was to investigate the microstructure processes that may be related to the tearing. In the frame of the investigation the microstructure, the mechanical properties and the evolution of the internal stresses generated by the deformation were investigated.

3 EXPERIMENTAL WORK

In **Tables 1 and 2** the chemical composition of the steel and the mechanical properties of the sheet determined from specimens cut out from the initial, centre and end of the coil, are shown. The microstructure of the steel sheet consisted of fine polygonal ferrite and pearlite grains (**Figure 1**).

Table 1: Composition of the steel, *w*
Tabela 1: Sestava jekla, *w*

C	Mn	Si	P	S	Al	Nb	O2	N2
0.14	0.8	0.12	0.011	0.018	0.005	0.049	0.005	0.009

The 370 mm × 3.6 mm steel band of the required length was cut out from the coil, then it was shaped to a tube blank with a diameter of 117 mm, which was high-frequency welded [15], heated to 850 °C for the homogenisation of the microstructure and the relaxation of the internal stresses, then heated to the hot-working temperature and processed within the temperature range 960–830 °C. In **Figure 2** the microstructure is shown for different parts of the welded tube: the section of the weld, the heat-affected zone, the base material and the weld. The weld is narrow and the microstructure of the

Table 2: Mechanical properties of the sheet
Tabela 2: Mehanske lastnosti traka

	R_e/MPa		R_m/MPa		A_5/%		K_{cv}/(J/mm^2)	
Direction	Axial	Transv.	Axial	Transv.	Axial	Transv.	Axial	Transv.
Coil onset	500	492	599	590	32.5	29.8	123	147
Coil centre	496	490	592	586	30.5	30.3	120	138
Coil end	495	495	590	576	30.1	31.9	118	127

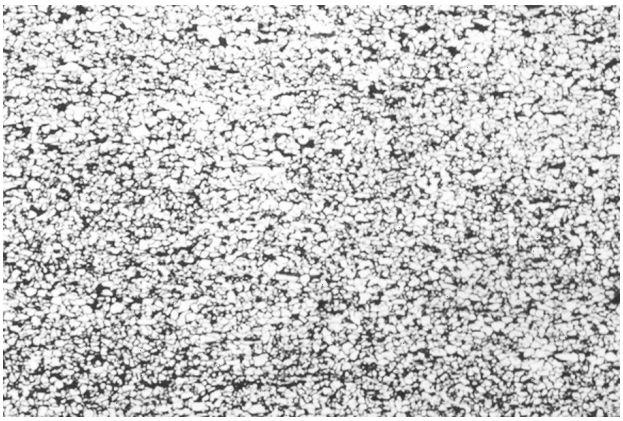

Figure 1: Microstructure of the sheet
Slika 1: Mikrostruktura traku

characteristic heat-affected zones is similar to that in the standard welds of structural steels [15].

The reduction to the final size of *d* 48.3 mm × 3.2 mm is achieved in 12 passes, applying a per-pass deformation, preventing the tearing of the tube wall, the achieving of the final diameter and ensuring that the final pass temperature is just above the austenite-to-ferrite transformation point, which strongly affects the properties of the steel in the finished tube.

The tests and examinations were carried out on samples of A, a hot rolled sheet; B, a welded tube; C, a tube after heating to the rolling temperature and water quenching, and D, a finished tube. At 12 selected points of the processing, the mill was stopped and the samples of the so-far processed tube 1 to 12 were cut out and air cooled or water quenched. Using these samples the diameter of the tube and the thickness of the tube wall were checked and the specimens for mechanical tests and optical microstructure examinations were prepared. Carbide and carbonitride particles were extracted from the steel with electrolytic dissolution and identified with X- ray diffraction analysis. For the identification of the phases found in isolates the data in [16,20] were used. The internal stresses were determined on specimens with a finely ground and etched surface. The Debye diffraction lines were checked for the wavelength and the (310) peak of α-iron, the widths of the (110), (200) and 211) lines for iron were assessed at half intensity and the internal stresses were deduced quantitatively using the method proposed in [17,18,19].

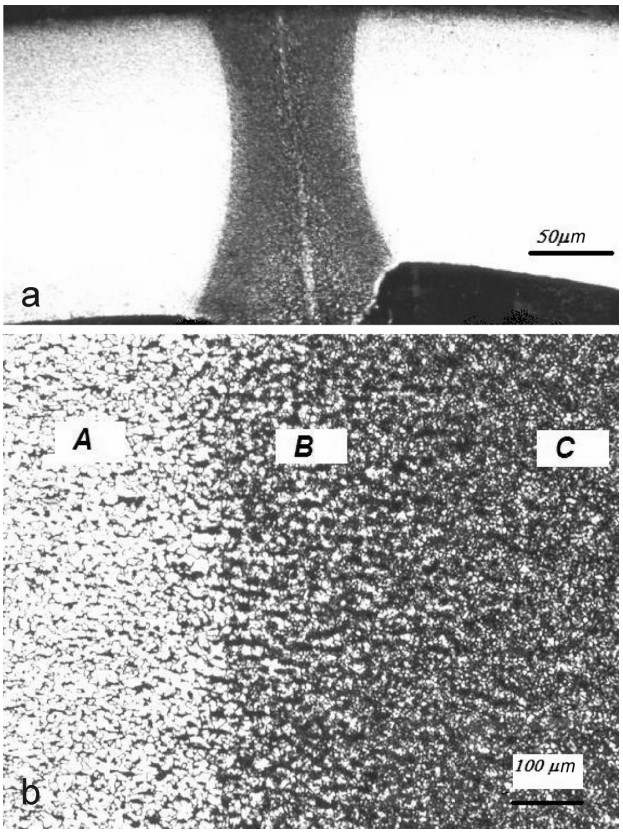

Figure 2: Tube-weld area **a)** macrography of the weld section, **b)** micrography of the welding area: A- base steel, B – heat-affected zone, C – weld
Slika 2: Področje zvara cevi **a)** makrografija prereza zvara, **b)** mikrografija področja zvara: A – osnovno jeklo; B – toplotma zona, C – var

4 RESULTS AND DISCUSSION

4.1 Processing parameters

From the data obtained on samples cut out from the tube after all stretch reducing passes the partial deformations shown in **Figures 3 and 4** were deduced. The pass temperature is also given in both figures. The per-pass decrease of the tube diameter is large and virtually constant in the initial 7 passes, after this it decreases. The decrease of the tube diameter depends on the processing procedure. As a rule, the stretch reducing in the first passes results in the maximum decrease of the tube. In **Figure 3** a decrease of 57 % of the tube diameter was obtained in the first four passes. The wall thickness is achieved by stretching, and it depends strongly on the steel extension in every pass that is lower in the previous passes [4,5]. On the investigated mill the drawing reduction of the wall thickness of the structural steel occurs in the

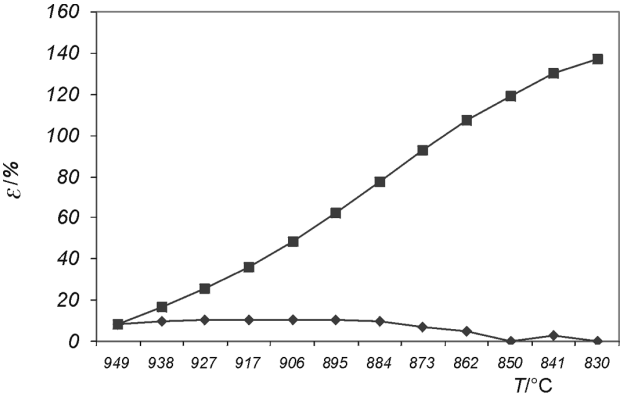

Figure 3: The per-pass (◆) and total (■) reduction of the diameter
Slika 3: Redukcija premera cevi, na vtik (◆) in skupna (■)

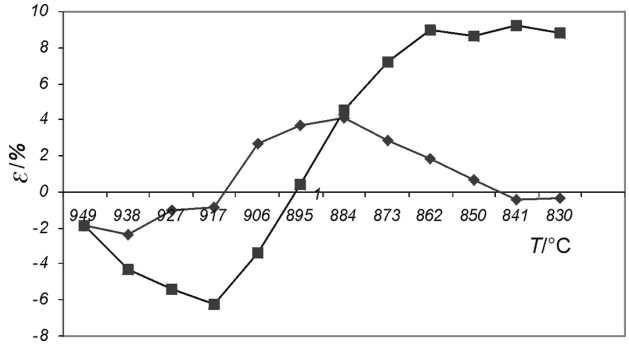

Figure 4: The per-pass (◆) and total (■) reduction of the thickness of the tube wall

Slika 4: Redukcija debeline stene cevi, na vtik (◆) in skupna (■)

temperature range from 1000 °C to 800 °C by the value Z = 0.6–0.72, and a maximum per-pass wall reduction of 2 %. For the processing of niobium micro-alloyed steel, the maximum coefficient of plastic extension is lower, i.e., Z = 0.65 % (**Figure 5**). The required tube diameter and tube-wall thickness can be achieved only with smaller per-pass reductions and, accordingly, the value of the coefficient of plastic extension is lower also.

The curve of total deformation in **Figure 3** was found to be virtually ideal for the processing of the investigated tube on the used stretch-reducing line, as the deformation parameters in **Figure 5** ensured stable processing and the required size and properties of the tube.

In the range of the analytical accuracy, the content of niobium carbo-nitride was equal for all the specimens [20]. This confirms the assumption that the content of niobium carbide is not affected by the processing parameters. It is interesting that in the weld a small quantity of niobium nitride was also detected.

4.2 Internal stresses

The difference in the shapes of the X-ray diffraction spectra for the base material and for the weld is very

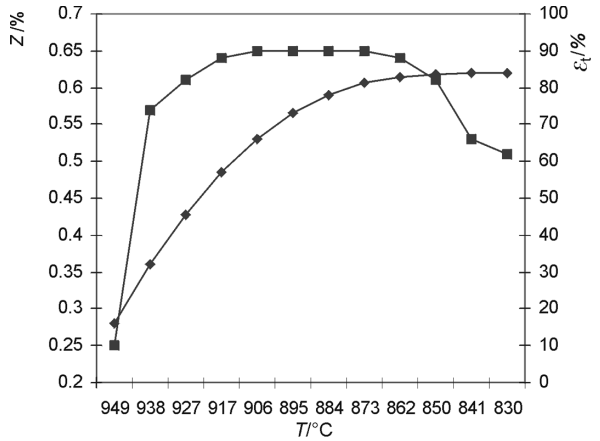

Figure 5: Change of Z(■) and the total reduction of tube ε_t (◆) in stretch reducing

Slika 5: Sprememba Z(■) in skupna redukcija cevi ε_t (◆)

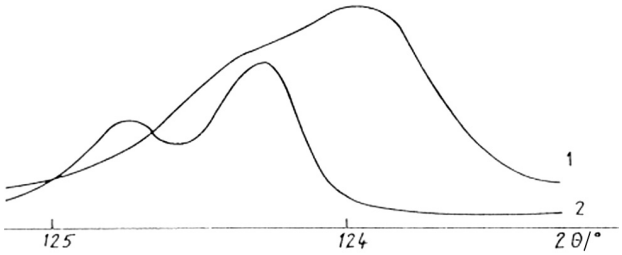

Figure 6: Welded tube. Profile of the diffraction lines (220) for the weld (1) and the base steel (2).

Slika 6: Zvarjena cev. Profil uklonskih črt (220) za zvar (1) in za osnovno jeklo (2)

clear (**Figure 6**). Since ferrite is the matrix in both cases, the absence of the Kα doublet confirms the presence of internal stresses in all the specimens water quenched from the processing temperature and used for the X-ray examination. After hot plastic deformation, the profile of the diffraction line is similar, and this indicates a partially homogenised microstructure (**Figure 7**); however, the internal stresses are still slightly greater in the weld. The diffraction line for the base material is virtually equal for the blank and the processed tube, although it is very different for the weld. The presence of the Kα doublet after stretch reduction indicates that the hot deformation had a favourable effect on the microstructure and on the internal stresses in the weld.

The intensity of internal stresses after the following processing passes is shown in **Figure 8**. The stresses remain constant in the specimens up to the third pass, then increase quickly in the following six passes, with a constant coefficient of plastic extension, and then gradually decrease in subsequent passes, parallel to a decrease in the coefficient of plastic extension. The evolution of stresses is virtually equal for the base material and the weld, and this indicates an identical reaction of both to the deformation and the equal extent of the interpass softening processes. It also confirms that the applied thermal regime of the tube blank before the start of the stretch reducing helped to avoid a greater intensity of internal stresses and a greater propensity for tearing of the tube wall in the weld area.

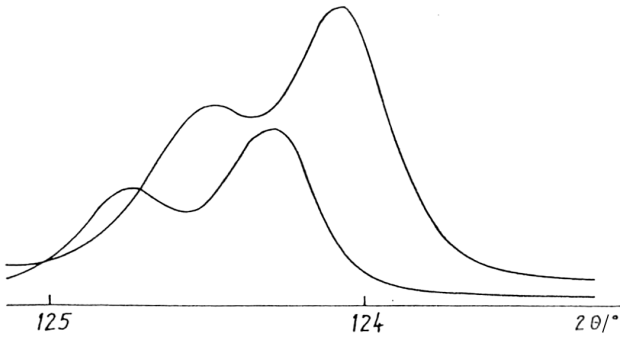

Figure 7: Finished tube. Profile of the diffraction lines (220) for the weld 1) and the base steel (2).

Slika 7: Izdelana cev. Profil difrakcijskih črt (220) za zvar (1) in za osnovno jeklo (2)

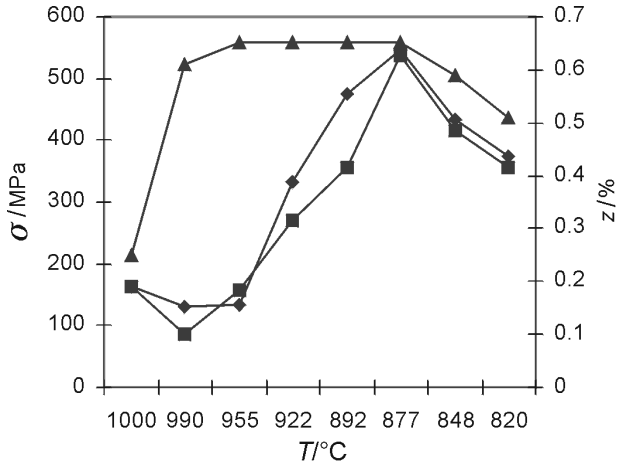

Figure 8: Evolution of internal stresses (weld ◆, base material ■) and coefficient of plastic extension Z (▲) with respect to the processing temperature.
Slika 8: Evolucija notranjih napetosti (var ◆, osnovni material ■) in koeficient plastičnega podajška Z (▲) v odvisnosti od temperature predelave

The faster cooling of the specimens for the X-ray examination explains why the internal stresses are even greater than the yield stress determined for the air-cooled specimens. The internal stresses are greater for a greater density of lattice defects generated by the plastic deformation of austenite and the decreasing extent of the recovery due to the lowering of the processing temperature. It is logical to assume that with an increased density of lattice defects the steel's hot workability is lower and that the relation between the stresses in different specimens is preserved after quenching. The first assumption is confirmed by the fact that the tube-wall tearings were more frequent for the passes with greater internal stresses and the second is the difference in the level of internal stresses for the specimens quenched after a different total deformation. In the range of the increase of the internal stresses the per-pass deformation was constant. The stresses were determined from X-ray spectra at room temperature and these are not equal to the stresses at the processing temperature. In reality, the stresses are a relative measure of the extent of the release of deformation hardening and of the residual deformation capacity of the steel, which are of essential importance for the smooth operation of the stretch-reducing line. On the basis of the assessment of the intensity of internal stresses and of the processing experience it can be concluded that the increased internal

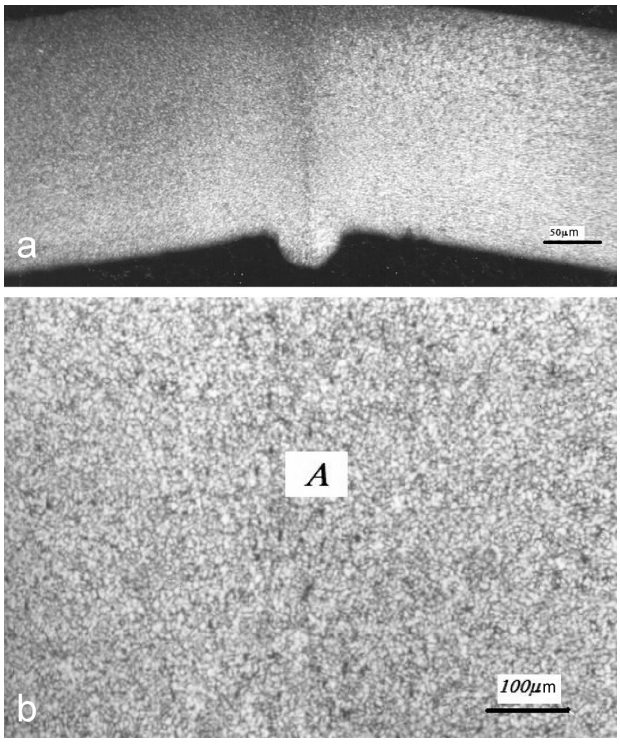

Figure 9: Section and microstructure of the finished tube wall in the weld area (A – weld zone)
Slika 9: Prerez in mikrostruktura stene cevi v področju zvara (A – področje zvara)

stresses due to the incomplete release of the deformation energy with interpass recovery and the lowering of the workability can be balanced with the selection of the proper value of the coefficient of plastic extension.

4.3 Properties of the finished tube

The mechanical properties determined for the sections of the tube with a weld and without a weld and are shown in **Table 3**. The very fine grain size (**Figure 9**) ensures that the tube has excellent mechanical properties, in accord with the standard requirements.

The mechanical and technological properties are virtually equal for the weld and the base material and confirm that the temperature-deformation regime made it possible to achieve a sufficient degree of homogenisation of the microstructure of the weld and the base material, the processing without tube-wall tearings, and the good mechanical properties of the finished tube.

Table 3: Mechanical and technological properties of the finished tube
Tabela 3: Mehanske lastnosti izdelane cevi

Spec.	R_e/MPa		R_m/MPa		A_5/%		K_{cv}/(J/mm^2)	
	Weld	B.mat.	weld	B.mat.	Weld	B.mat.	weld	B.mat.
1	502	497	590	596	32.5	31.7	104	110
2	495	492	592	609	32.5	32.7	101	122
3	496	500	592	603	31.9	32.01	106	112

5 CONCLUSIONS

The quality and reliability of the hot stretch reducing of high-frequency welded tubes depend strongly on the understanding of the processes in the steel at the operating temperature and the mastering of these processes in individual passes as well as during the entire processing line.

With the initial heating of the welded blank a sufficient homogenisation of the weld and base material's microstructure and the internal stresses were achieved. The initial hot-working temperature ensured the steel had sufficient ductility on the processing line and a sufficient finishing temperature above the austenite-to-ferrite transformation.

The per-pass changes of the tube diameter and the wall thickness ensured a smooth processing without any tube-wall tearings.

Of great importance to mastering the hot stretch reducing of tubes was understanding the per-pass evolution of the internal stresses and the choice of the per-pass deformation parameters, ensuring that we maintain the optimum value of the coefficient of plastic extension.

6 REFERENCES

[1] F. Vodopivec, S Rešković, I. Mamuzić. Evolution of substructure during the continuous rolling a microalloyed steel strip. Mat. Sci. Techn.15 (**1999**), 1293–1299

[2] S. Rešković. Studij mehanizama precipitacije i rekristalizacije u području završnog oblikovanja mikrolegiranog čelika (Investigation of the mechanisms of precipitation and recrystallisation by finishing of a microalloyed steel), Dr. Diss., University of Zagreb. 1997

[3] K. H. Staat. Streckreduzierwalzwerk, Metalurgija. 10 (**1971**), 13–22

[4] R. Križanić. Raspodjela brzina u zoni deformacije i proračun broja okretaja pri kontinuiranom toplom valjanju cijevi na izvlačno-reducirnom stanu (Deformation rate and number of revolutions by the continuous hot rolling of tubes on the stretch reducing mill). Metalurgija. 26 (**1987**), 109–116

[5] R. Križanić. Proračun površinskog presjeka stijenke cijevi pri valjanju na izvlačno-reducirnom stanu (Calculation of tube wall cross –section at rolling on the stretch reducing mill). Metalurgija. 27(**1988**), 3–11

[6] R. W. K. Honeycombe. Fundamental aspects of precipitation in microalloyed steels, HSLA Steels Technology & Applications, Proceedings of the International Conference on Technology and Applications of HSLA steels, Philadelphia, USA, (**1983**), 243–261

[7] T. Tanaka, N. Tabata, T. Hatamura. Three Stages of the Controlled-Rolling Process. Proceedings "Micro Alloying 75", Union Carbide Corporation, New York, 1977, 107–120

[8] T. M. Hoogendorn, M. J.Spanrant. Quantifying the Effect of Microalloying Elements on Structures during Processing , Ibiden, (**1977**), 57–63

[9] W. Roberts. Recent Innovations in Alloy Designing and Processing of Microalloyed Steels. HSLA Steels – Technology and Applications. Proceedings of the International Conference on Technology and Applications of HSLA STEELS, Philadelphia, Pennsylvania, USA, (**1983**), 243–251

[10] J. J. Jonas, I. Weiss. Dynamic precipitation and coarsening of niobium carbonitrides during the hot rolling of HSLA steel, Metall. Trans., 11A (**1980**), 403–410

[11] J. Jonas, I. Weiss. Effect of Precipitation on Recrystallization in Microalloyed steel. Met. Sci. 65 (**1979**), 238–245

[12] T. Tanaka, N. Tabata, T. Hatamura, C. Shiga. Three Stages of the Controlled-Rolling Process, Microalloying75, Ed. U. C. Corporation, N. York, 1977, 107–120

[13] I. Kozasu, C. Ouchi, T. Sampei, T. Okita. Hot Rolling as a High-Temperature Thermo-Mechanical Process. Ibidem, 1977, 120–129

[14] T. Gladman. Recrystallization and Grain Growth of Multi-Phase and Particle Containing Materials. Ed. N. Hansen, A. R. Jones and T. Leffers, Risd National Laboratory, Denmark, 1980, 19

[15] S. Rešković, M. Prelošćan. Zavarivost niobijem mikrolegiranog čelika visokofrekventnim postupkom (High frequency welding of a niobium microalloyed steel). Zavarivanje 35, 1992, 191–199

[16] J. T. Norton, R. E. Hiller. Structure of Cold Drawn Tubing. Trans. AIME, 99 (**1993**), 190

[17] C. N. Wagner, A. S. Tetelman. Diffraction from Layer Faults in bcc and fcc Structures, J.Appl. Phys. 33 (**1992**), 3080

[18] R. E. Smallman, K. H. Westmacott. Stacking faults in face-centred cubic metals and alloys, Phil. Mag. 2 (**1957**), 669

[19] B. Warren. X-Ray Studies of Deformed Metals. Prog. Metal Phys. 8 (**1959**), 147–202

[20] Vj. Novosel-Radović. Rentgenska difrakcija u laboratoriju Željezare Sisak 8X rays diffraction in the laboratory of Steelwork Sisak). Strojarstvo. 36 (**1994**), 9–13

UDK 669.14.018:621.791.05:539.42
Original scientific article/Izvirni znanstveni članek

ISSN 1580-2949
MTAEC9, 42(6)263(2008)

EXPERIMENTAL ANALYSIS OF CRACK INITIATION AND GROWTH IN WELDED JOINT OF STEEL FOR ELEVATED TEMPERATURE

EKSPERIMENTALNA ANALIZA NASTANKA IN RASTI RAZPOKE V ZVARU JEKLA ZA POVIŠANO TEMPERATURO

Meri Burzić[1], Živoslav Adamović[2]

[1] Institute "GOŠA", d. o. o., Milana Rakića 35, 11000 Belgrade, Serbia
[2] University of Novi Sad, "Mihajlo Pupin" Faculty of Technical Engineering, Đure Đakovića bb, 23000 Zrenjanin, Serbia
merib@neobee.net

Prejem rokopisa – received: 2008-07-10; sprejem za objavo – accepted for publication: 2008-07-22

This paper presents results of experimental investigation of crack resistance by static and variable loading of alloyed steel A-387 Gr. 11 for elevated temperature application and its welded joint. Using SEN-B, CT and Charpy pre-cracked specimens, the significance of heterogeneity of microstructure and mechanical properties of welded joints on fracture toughness and fatigue crack initiation and propagation, at room and working temperatures, is evaluated.

Keywords: Alloyed steel, welded joint, fracture toughness, crack propagation rate, fatigue crack, fatigue threshold

V članku je predstavljena eksperimentalna raziskava odpornosti razpoke pri statični in izmenični obremenitvi pri jeklu A-387Gr 11 za uporabo pri povišani temperaturi in zvarih tega jekla. Z uporabo SEN-B-, CT- in Charpy-preizkušancev z razpoko smo ocenili pomen heterogenosti mikrostrukture in mehanskih lastnosti zvara za žilavost loma in za začetek ter za napredovanje utrujenostne razpoke pri sobni in pri delovni temperaturi.

Ključne besede: legirano jeklo, zvar, žilavost loma, hitrost napredovanja razpoke, prag utrujenosti

1 INTRODUCTION

The in-service behaviour of alloyed steel A-387 Gr. 11 Class 1, for pressure vessels, used for high temperature applications, depends on the properties of its welded joint, with parent metal (BM), heat-affected-zone (HAZ) and weld metal (WM) as constituents. Critical locations, regarding integrity of welded joint can be formed in HAZ and WM [1]. Qualification of specified welding technology of plates, 96 mm thick, of steel A-387 is performed according to standard EN 288-3 [2].

While determining the plane strain fracture toughness, K_{Ic}, of welded joint constituents with heterogeneous microstructure, one must bear in mind, in order to hold the validity of theoretical assumptions and meanings of fracture toughness as measured property, that fracture mechanics is based on material homogeneity, including the region of crack tip.

A characteristical property of the welded joint is the heterogeneity of microstructure and mechanical properties, together with, irregular internal stress distribution with residual stresses and stress concentration. These important problems do not exclude experimental determination of plane strain fracture toughness, K_{Ic}, of welded joint and its constituents, although they present difficulties in the interpretation of measured values and obtained results [3–5].

For better understanding of crack occurrence and its growth effect in welded joints of steel for elevated temperatures, applied in equipment for high pressure, it is necessary to quantify the parameters controlling the strain behaviour in crack tip vicinity and crack resistance. Therefore, in this paper the effect of heterogeneity of microstructure and mechanical properties on fracture toughness, K_{Ic}, fatigue crack growth rate, da/dN, and fatigue threshold stress intensity factor range, ΔK_{th}, of A-387 steel and its welded joint constituents is experimentally investigated at room temperature (20 °C) and at working temperature (540 °C) [6].

2 MATERIAL FOR TESTING

The welded joint sample (350 × 500 × 96) mm with double "U" weld metal in the middle of the steel A-387 was used for this investigation [6]. Two welding procedures were applied [6]:

- shielded metal manual arc welding (SMAW) with coated electrode LINCOLN Sl 19G (AWS: E8018-B2 for root weld passes;
- Submerged arc welding (SAW), applying as consumable wire LINCOLN LNS 150 and flux LINCOLN P230, for filler passes.

The welded sample and scheme of cutting out of specimens from welded joint (OM, HAZ and WM) are shown in **Figure 1**. The chemical composition and mechanical properties of A-387 1 steel are given in **Tables 1 and 2**. The chemical composition of electrode LINCOLN Sl 19G and wire LINCOLN LNS 150

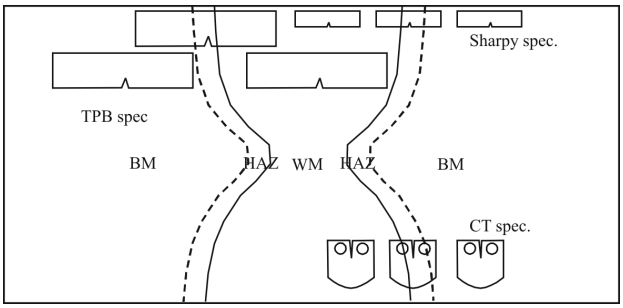

Figure 1: Scheme of testing sample of double "U" weld metal and specimens sampling [6]
Slika 1: Shema preizkušanca z dvojnim U-zvarom in odvzem vzorcev [6]

according to certificates is given in **Table 3**, and the mechanical properties according to certificates are given in **Table 4**.

Table 1: Chemical composition of tested steel A-387
Tabela 1: Kemična sestava jekla A-387, ki je bilo uporabljeno za preizkuse

Chemical composition, *w*/%						
C	Si	Mn	P	S	Cr	Mo
0.15	0.29	0.54	0.022	0.011	0.93	0.47

Table 2: Required mechanical properties of tested steel A-387
Tabela 2: Predpisane mehanske lastnosti za jeklo A-387

Yield stress, min.	Tensile strength	Elongation	Impact energy
$R_{p0,2}$/MPa	R_m/MPa	*A*/%	*KV*/J
315	490-620	25	> 85

Table 3: Chemical composition of filler metal [6]
Tabela 3: Kemična sestava deponiranega materiala [6]

Filler material	Chemical composition, *w*/%						
	C	Si	Mn	P	S	Cr	Mo
LINCOLN Sl 19G	0.08	0.045	0.35	0.025	0.025	1.10	0.50
LINCOLN LNS 150	0.11	0.18	0.37	0.020	0.020	1.04	0.47

Table 4: Mechanical properties of filler metal [6]
Tabela 4: Mehanske lastnosti deponiranega materiala [6]

Filler material	Yield stress $R_{p0,2}$/MPa	Tensile strength R_m/MPa	Elongation *A*/%	Impact energy *KV*/J
LINCOLN Sl 19G	505	640	23	> 95
LINCOLN LNS 150	490	610	26	> 100

3 TENSILE PROPERTIES

Tensile testing of specimens taken from parent metal, from weld metal, and from butt welded joint, were performed on an machine in displacement control, at room and at working temperature. The specimen from WM for testing at room temperature, was machined from

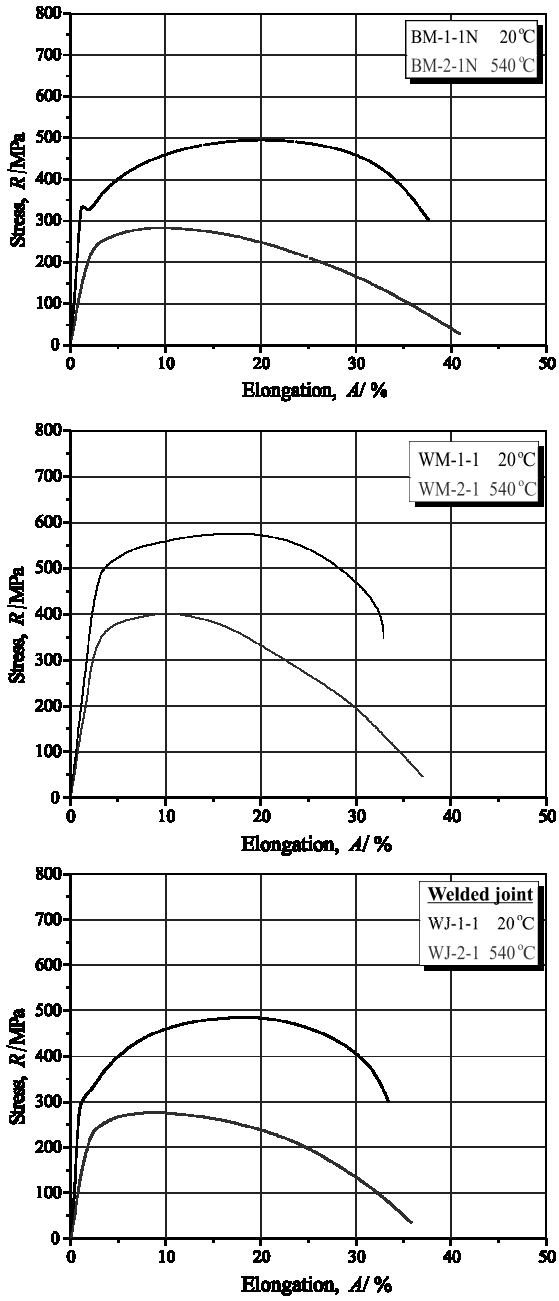

Figure 2: Diagrams stress – elongation: a) BM, b) WM, c) welded joint
Slika 2: Odvisnosti napetost–podaljšek: a) BM, b) WM, c) zvarni spoj

the available material, according to standard EN 895 [7]. For easier comparison of results the specimen from BM is of the same dimensions according the standard EN 10002-1 were used. Specimen from welded joint was made according EN 895. For testing at the temperature of 540 °C the same specimen design according to standard ASTM E1475-00 [8] was used for all welded joint consituents with dimensions adopted to available equipment.

Typical stress – strain curves for specimens from BM, WM and from welded joint, tested at room and

working temperature, are given in **Figure 2**. The testing results at room and at working temperatures are given in **Table 5** for BM, in **Table 6** for WM and in **Table 7** for the specimens of welded joint.

The effect of testing temperature on tensile properties is clear. At higher temperature the values of yield stress and tensile strength are smaller, and elongation values are increased, as seen in **Figure 2** and in **Tables 5–7** [7]. However, this conclusion is very simplified and apparent, as it will be discussed.

Table 5: Results of tensile testing of BM specimens
Tabela 5: Rezultati nateznih preizkusov BM-preizkušancev

Specimen	Testing temperature °C	Yield stress $R_{p0,2}$/MPa	Tensile strength R_m/MPa	Elongation A/%
OM-1-1N	20	330	495	37.6
OM-1-2N		318	479	36.1
OM-1-3N		324	488	38.7
OM-2-1N	540	219	284	40.1
OM-2-2N		212	279	39.6
OM-2-3N		226	303	39.9

Table 6: Results of tensile testing of WM specimens
Tabela 6: Rezultati nateznih preizkusov WM-preizkušancev

Specimen	Testing temperature °C	Yield stress $R_{p0,2}$/MPa	Tensile strength R_m/MPa	Elongation A/%
OM-1-1N	20	491	576	32.7
OM-1-2N		504	592	31.6
OM-1-3N		496	585	33.9
OM-2-1N	540	338	401	36.9
OM-2-2N		331	396	36.2
OM-2-3N		345	409	37.8

Table 7: Results of tensile testing of welded joint specimens
Tabela 7: Rezultati nateznih preizkusov WM-preizkušancev

Specimen	Testing tempe-rature °C	Yield stress $R_{p0,2}$/MPa	Tensile strength R_m/MPa	Elongation* A/%	Location of fracture
ZS – 1 – 1	20	322	488	33.5	BM
ZS – 1 – 2		319	497	32.2	BM
ZS – 1 – 3		315	491	31.9	BM
ZS – 2 – 1	540	221	278	35.8	BM
ZS – 2 – 2		224	285	34.6	BM
ZS – 2 – 3		217	277	37.9	BM

*measured at L_0 = 100 mm, as comparative value (is not material property)

The basic requirement in welded structures design is to assure the required strength. In most welded structures this is achieved with superior strength of WM compared to BM (overmatching effect). In tested case this is achieved at room and at working temperatures (**Figure 2 a, b, Tables 5, 6**). An additional proof of ovetmatching is the fracture of specimens from welded joint in BM and that the difference of values of yield stress and tensile strength in **Tables 5 and 7** is minor, at the level of measurement error. It is to notice the good agreement between yield stress and tensile strength values from test (**Table 5**) and specified values (**Table 2**). The obtained results of tensile properties of WM, **Table 6** and **Figure 4b**, confirmed that welding technology was properly specified (welding procedure specification – WPS – is a separate document), including preheating and post-weld heat treatment.

Special attention in tensile properties should be paid to elongation. When material is homogenious, as here BM and WM should be considered, elongation is usefull for comparison. For welded joint, the elongation value is meaningless, since in measuring length of 100 mm enter BM i WM, of different tensile properties, but also a part of HAZ is included, in which tensile properties are unknown. Nevertheless, the character of obtained tensile curves shows that material is ductile and it has an approximate ratio of unifirom and non-uniform elongation 1 : 2 (**Figure 2**). From the aspect of in-service behaviour of the welded structure, it is to underline that for real values elongation is elastic, and only locally and in limited amount also plastic, so the elongation values from **Figure 2 and Tables 5–7** can serve only for comparison and can not be the base for material behaviour assessment, especially HAZ, occurrence and crack propagation.

In the performed test, of special importance is that the obtained strength values at the working temperature are within specified levels. This will significantly contribute to crack resistance evaluation of the statically and variably loaded heterogenious structure, such as welded joint and heat-affected-zone are.

4 EXAMINATION OF MICROSTRUCTURE

A macrograph of butt welded joint of A-387 steel is given in **Figure 3**. Clearly recognized are: parent metal (BM) and weld metal (WM), and also heat-affected-zone (HAZ) in between [6].

Figure 3: Macrograph of welded joint
Slika 3: Makroposnetek zvarnega spoja

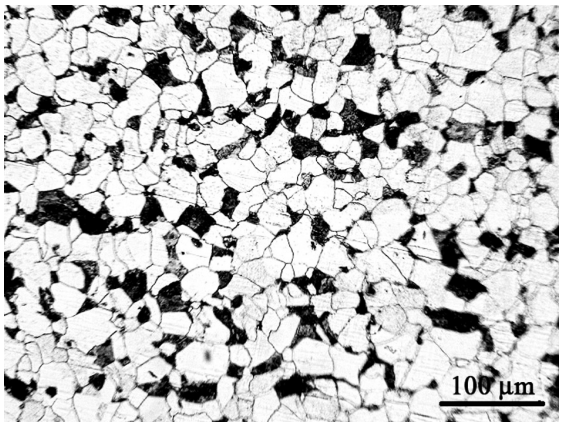

Figure 4: Microstrukture of parent metal (BM)
Slika 4: Mikrostruktura osnovnega materiala

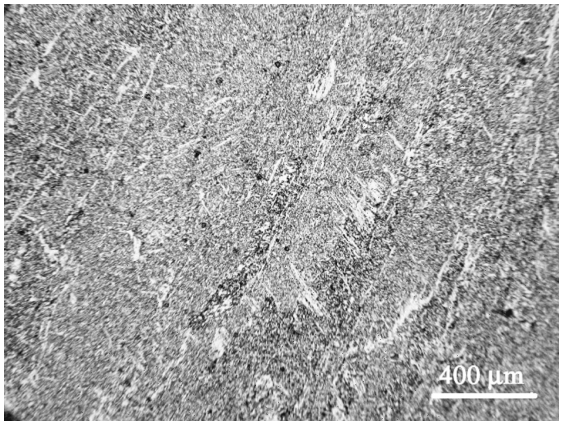

Figure 5: Microstrukture of weld metal (WM)
Slika 5: Mikrostruktura vara

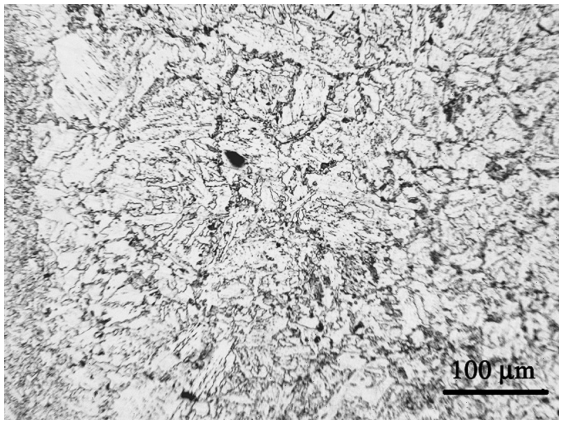

Figure 6: Microstrukture of the heat-affected-zone (HAZ)
Slika 6: Mikrostruktura toplotne zone

The uniform microstructure of parent metal, in addition to light polygonal crystals of ferrite, contains of pearlite as polygonal dark micro-constituent. The BM microstructure is presented in **Figure 4** with solidification grain size 5 according to ASTM [6]. The weld metal microstructure is bainite and grain boundary ferrite, **Figure 5** [6]. HAZ microstructure comprises from coarse grained bainite which is located next to the WM and fine grained bainite, next to the BM, **Figure 6** [6]. One has to have in mind that this local microstructure can significantly differ from microstructures at other locations in HAZ.

5 FRACTURE TOUGHNESS TESTING

The effect of microstructure and mechanical properties heterogeneity of welded joint constituents on the plane-strain fracture toughness, K_{Ic}, can be assessed locating a fatigue pre-crack tip on the specimen in different regions and following the regions of fracture growth.

5.1 Procedure and testing results

Fracture toughness testing were performed using three-points bend, 17.5 mm thick specimens (SEN-B), **Figure 7a**, and 8 mm thick, compact tension specimens (CT), **Figure 7b** to according the standard ASTM E1820 [9]. Three-point bend (SEN-B) specimens were tested at room temperature. Only CT specimens were tested at working temperature.

Fracture toughness, K_{Ic}, a measure of fracture toughness, J_{Ic}, is determined based on J-integral critical value, by testing according to ASTM E813-89 standard [10]:

$$K_{Ic} = \sqrt{\frac{J_{Ic} \cdot E}{1-\nu^2}} \qquad (1)$$

where: E – elasticity modulus, and ν – Poisson's ratio.

For the determination of the J-integral a single specimen testing method by successive partial unloading was applied. By data pairs applied force, F, – crack opening displacement, δ, the points of basic relationship curve were obtained (**Figure 8**, left). The procedure for the determination of critical value, as measure of the fracture toughness, J_{Ic}, requires the design of resistance curve (J-R curve), shown in **Figure 8**, right, in which

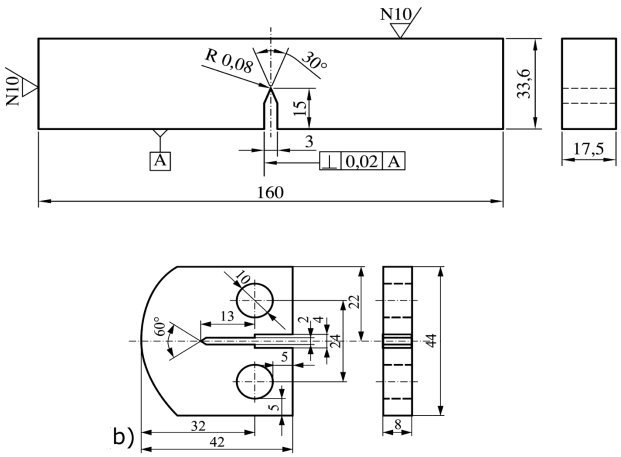

Figure 7: Specimen for fracture mechanic testing: **a)** SEN-B specimen, **b)** CT specimen
Slika 7: Preizkušanci za preizkuse mehanike loma: **a)** SEN-B, **b)** CT

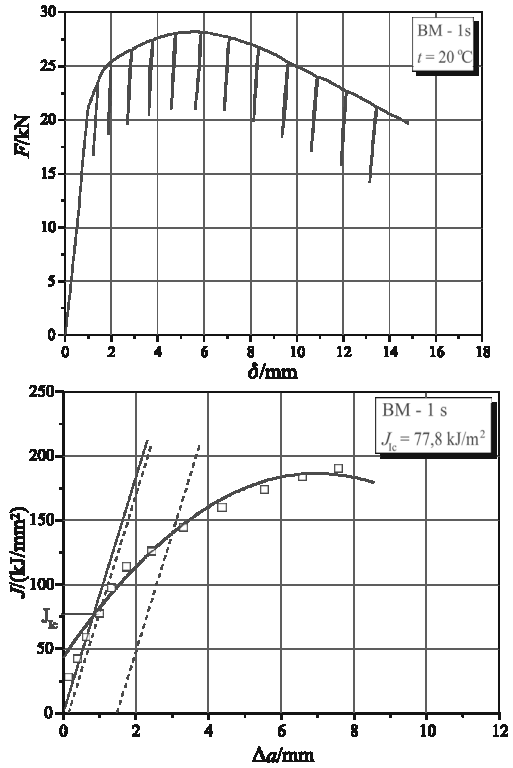

Figure 8: Diagrams $F - \delta$ (a) and $J - \Delta a$ (b) for the specimen with a notch in BM for room temperature

Slika 8: Odvisnosti $F - \delta$ (a) in $J - \Delta a$ (b) za preizkušanec z razpoko v BM pri sobni temperaturi

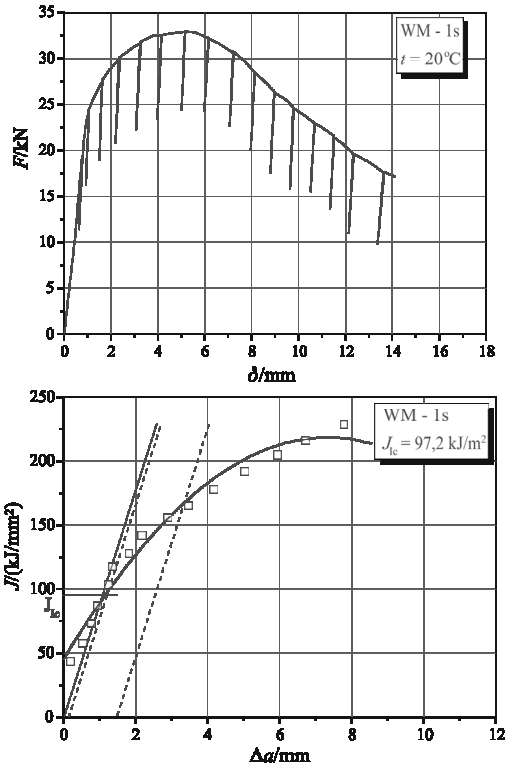

Figure 10: Diagrams $F - \delta$ (a) and $J - \Delta a$ (b) for the specimen with a notch in WM for room temperature

Slika 10: Odvisnosti F – δ (a) in $J - \Delta a$ (b) za preizkušanec z razpoko v WM pri sobni temperaturi

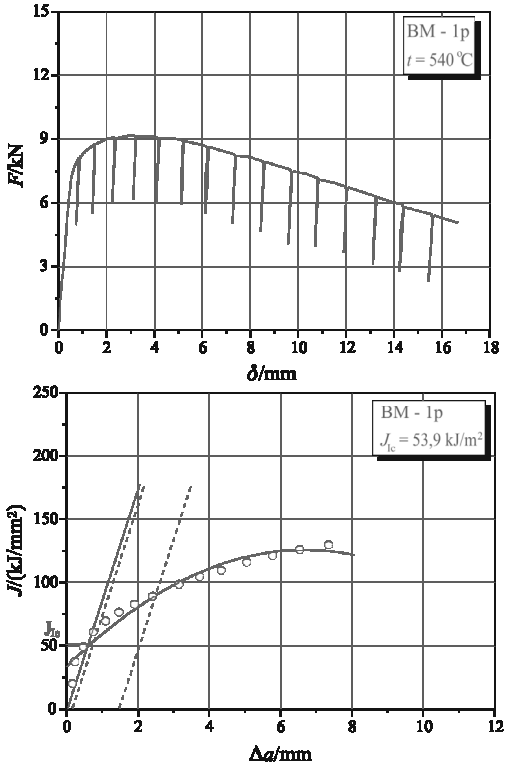

Figure 9: Diagrams $F - \delta$ (a) and $J - \Delta a$ (b) for the specimen with a notch in BM for operating temperature

Slika 9: Odvisnosti $F - \delta$ (a) in $J - \Delta a$ (b) za preizkušanec z razpoko v BM pri delovni temperaturi

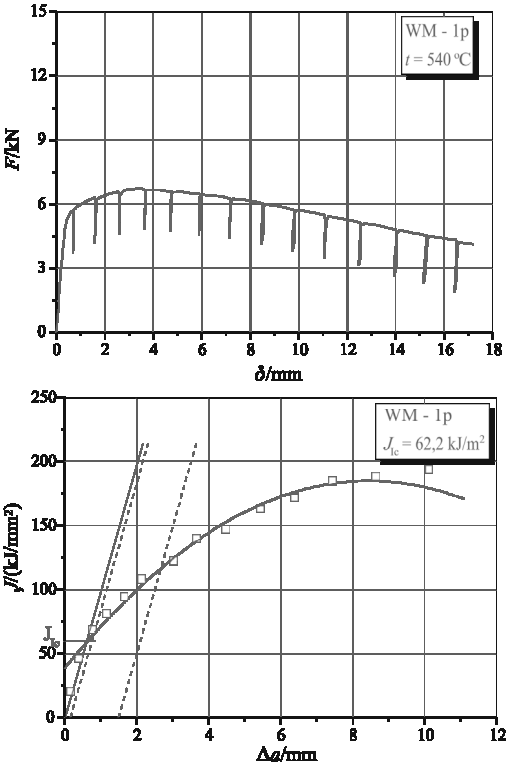

Figure 11: Diagrams $F - \delta$ (a) and $J - \Delta a$ (b) for the specimen with a notch in WM for operating temperature

Slika 11: Odvisnosti $F - \delta$ (a) in $J - \Delta a$ (b) za preizkušanec z razpoko v WM pri delovni temperaturi

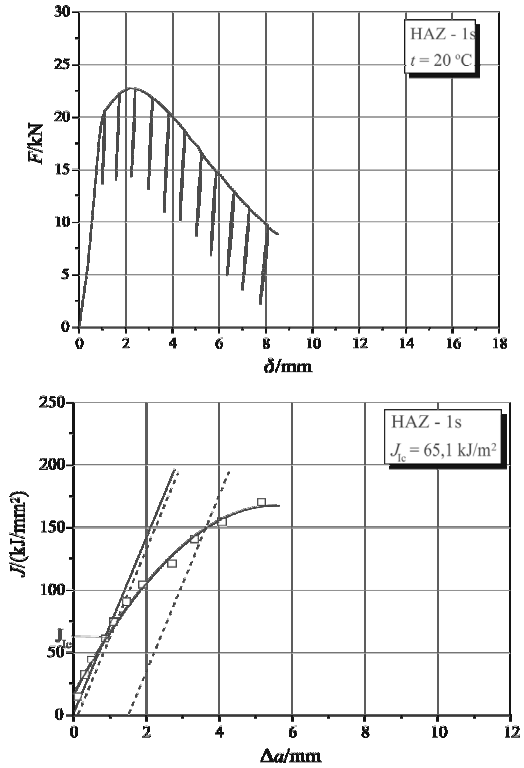

Figure 12: Diagrams $F - \delta$ (a) and $J - \Delta a$ (b) for the specimen with a notch in HAZ for room temperature

Slika 12: Odvisnosti $F - \delta$ (a) in $J - \Delta a$ (b) za preizkušanec z razpoko v HAZ pri sobni temperaturi

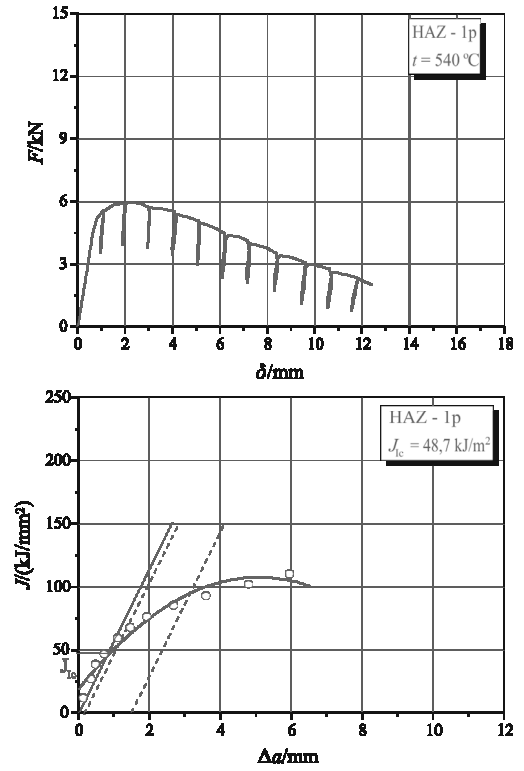

Figure 13: Diagrams $F - \delta$ (a) and $J - \Delta a$ (b) for the specimen with a notch in HAZ for operating temperature

Slika 13: Odvisnosti $F - \delta$ (a) in $J - \Delta a$ (b) za preizkušanec z razpoko v HAZ pri delovni temperaturi

crack increase is determined based on compliance change. Basic, but more expensive, is the procedure in ASTM E813 standard with the multi specimens (of the same size) method with different length of fatigue pre-crack, and different compliance.

In a single specimen test, the specimen is unloaded in intervals to about 30 % of the actually attained level of force chosen by experience with the type of material. Based on the change of line slope of the compliance, C, with crack extension, the crack increase, Δa, between two successive unloadings, corresponding to the attained value of force, is determined as:

$$\Delta a_i = \Delta a_{i-1} + \left(\frac{b_{i-1}}{\eta_{i-1}}\right) \cdot \left(\frac{c_i - c_{i-1}}{c_{i-1}}\right) \qquad (2)$$

The next steps are the determination of critical value, J_{Ic}, and use of this value in Eq. (1) for the calculation of the fracture toughness, K_{Ic}, according the single specimen compliance method.

5.2 Discussion of fracture toughness testing results

The obtained diagrams are presented in **Figure 8** for specimens of BM tested at room temperature and in **Figure 9** for specimens tested at 540 °C. The corresponding curves for WM are given in **Figures 10 and 11**, and for HAZ in **Figures 12 and 13** [6,11]. The calculated values of fracture toughness, K_{Ic}, are given in **Table 8** for the specimens notched in BM, WM and HAZ.

The microstructural and mechanical heterogeneities of a welded joint affect its resistance to crack propagation. Therefore, in specification for fracture mechanics testing conditions should prescribe not only the test procedure and location of a fatigue crack, but also the method of interpretation and meaning of the obtained results [6].

The character of curves varies depending on the notch i.e. fatigue crack, tip location and testing temperature. It is possible to observe an almost identical character of individual curves in each group, the difference between the diagrams for individual specimens lies exclusively in the maximal force value, F_{max}, which is directly dependent on the fatigue crack length, a, and on testing temperature [6].

The maximal value of K_{Ic} at room temperature was obtained for specimens notched in WM (mean K_{Ic} value $\approx$145 MPa m$^{1/2}$). Somewhat lower K_{Ic} values exhibited the specimens notched in BM (mean value K_{Ic} $\approx$130 MPa m$^{1/2}$). The scatter of results is small, 10–15 MPa m$^{1/2}$ in terms of minimum and maximum values. Lower K_{Ic} values belong to specimens notched in HAZ. The differences do not indicate an important reduction of properties [6]. The close K_{Ic} values for BM and HAZ are related to the microstructure. Namely, both constituents have ferrite-pearlite microstructures of similar crack resistance at static loading. It should be next in mind that in performed testing the location of fatigue crack tip is a

random one, and that in HAZ can exist the regions of different microstructure and lower fracture toughness.

Table 8: Results of testing the critical *J*-integral, J_{Ic}, and the critical stress intensity factor, K_{Ic}

Tabela 8: Rezultati preizkusa kritičnega *J*-integrala, J_{1c} in kritičnega faktorja intenzitete napetosti K_{IC}

Desig-nition	Testing tempera-ure °C	Critical J-integral J_{Ic}/(kJ/m^2)	Critical stress intensity factor, K_{Ic}/(MPa m$^{1/2}$)	Critical crack length a_c/mm
BM-1s	20	77.8	132.4	52.8
BM-2s		75.2	130.3	51.1
BM-3s		73.2	128.4	49.7
BM-1p	540	53.9	90.2	46.1
BM-2p		49.7	87.4	43.4
BM-3p		55.1	92.1	48.1
WM-1s	20	97.2	148.0	66.0
WM -2s		93.7	145.3	63.6
WM -3s		92.2	143.1	61.7
WM -1p	540	62.2	97.8	54.3
WM -2p		60.3	96.3	52.6
WM -3p		55.6	92.5	48.5
HAZ-1s	20	65.1	121.1	44.2
HAZ -2s		70.2	125.2	47.4
HAZ -3s		71.3	125.6	47.9
HAZ -1p	540	48.7	86.6	42.5
HAZ -2p		46.8	85.2	41.6
HAZ -3p		47.3	85.9	42.2

By applying the fundamental formula of fracture mechanics:

$$K_{Ic} = \sigma\sqrt{\pi \cdot a_c} \tag{3}$$

and introducing the value of allowable stress $\sigma_{doz} = \sigma$, for the shape factor equals to unity, approximate values of critical crack length, a_c, can be calculated, (**Table 8**). Largest crack length, a_c, can occur under static load in WM, but without brittle fracture occurrence.

For static loading, the given differences in K_{Ic} value should not have significant effect on structural safety. It is obvious that allowable stress, lower than yield stress, will produce higher values for critical crack length and if in the tested material the crack of length less than critical, there is no danger of brittle fracture. Such a crack has to be detected and its length assessed by convenient non-destructive testing method. After the integrity analysis it is possible, under defined conditions, allow for structure service even in crack growth period. Important data for a decision about the extended service of cracked component are crack growth rate and its dependance on applied load. The chages of K_{Ic} value are then important, since critical crack length, a_c, is directly depended on K_{Ic} value.

The effect of temperature on fracture toughness K_{Ic}, is given in **Table 8**. The reduction of 35–45 % in fracture toughness at working temperature compared to room temperature depends on fatigue crack tip location (BM, WM, HAZ), with maximum value of K_{Ic} in the specimen notched in WM. Obtained $J - \Delta a$ curves are of almost identical character, only the value of maximum force F_{max}, is different, and it is directly related to the fatigue crack length a.

5.3 Fatigue analysis by fracture mechanics

If a structural component is continuously exposed to variable loads, fatigue crack may initiate and propagate from severe stress raisers if the stress intensity factor range at fatigue threshold, ΔK_{th}, is exceeded.

A basic contribution of fracture mechanics in fatigue analysis is the division of fracture process to crack initiation period and the growth period to critical size for fast fracture. The total number of cycles to fracture, N_u, is divided into number of cycles for fatigue crack initiation, N_i, and for its growth to the value critical for fracture, N_p: ($N_u = N_i + N_p$)

The development in the research of material behaviour for variable loading is achieved applying experimental and theoretical approaches. The analysis of stress and strain state at growing fatigue crack tip by applying linear elastic fracture mechanics (LEFM) enabled to develop the Paris equation for metals and alloys, which relates fatigue crack growth rate da/dN to stress intensity factor range ΔK through coefficient C and exponent m [12]:

$$\frac{\mathrm{d}a}{\mathrm{d}N} = C(\Delta K)^m \tag{4}$$

The standard ASTM E647 [13] defines the testing of pre-cracked specimen for fatigue crack growth rate measurement, da/dN, and for the calculation of the stress intensity factor range, ΔK. Two basic requirements in ASTM E647 are: the crack growth rate should be above 10^{-8} m/cycle to avoid fatigue threshold region and load should be of constant amplitude.

Standard Charpy size specimen, fatigue pre-cracked in different welded joint constituents, and instrumented by foil RUMUL RMF A-5, of measuring length 5 mm (**Figure 14**), for continuous monitoring of crack length, were tested at room temperature under variable loading for the determination of fatigue crack growth rate, da/dN, and stress-intensity factor range at fatigue threshold, ΔK_{th}. The testing was performed in load control, by

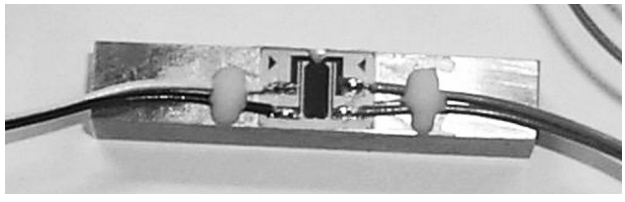

Figure 14: Charpy specimen instrumented by foil RUMUL RMF A-5 for continuous monitoring of crack length

Slika 14: Charpy preizkušanec s merilno folijo RUMUL RMF A-5 za zvezno merjenje dolžine razpoke

Table 9: Parameters of Paris equation
Tabela 9: Parametri Parisove enačbe

Specimen designation	Test temperature	Stress-intensity factor range at fatigue threshold	Coefficient	Exponent	Crack growth rate d*a*/d*N* at ΔK = 10 MPa $m^{1/2}$
	°C	ΔK_{th}/(MPa $m^{1/2}$)	*C*	*m*	nm/cycle
BM–1s	20	6.8	$2.98 \cdot 10^{-13}$	3.62	$1.24 \cdot 10^{-09}$
WM–1s		6.8	$3.88 \cdot 10^{-13}$	3.82	$2.56 \cdot 10^{-09}$
HAZ–1s		6.7	$3.05 \cdot 10^{-13}$	4.01	$3.12 \cdot 10^{-09}$
BM–1p	540	5.9	$3.11 \cdot 10^{-13}$	4.08	$3.74 \cdot 10^{-09}$
WM–1p		6.2	$3.27 \cdot 10^{-13}$	4.14	$4.51 \cdot 10^{-09}$
HAZ–1p		6.1	$3.38 \cdot 10^{-12}$	3.17	$5.00 \cdot 10^{-09}$

three-points bending on the FRACTOMAT high-frequency resonant pulsator.

CT specimens were tested on working temperature, since at 540 °C the measuring foils can not be used, and load line displacement is measured instead.

The relations d*a*/d*N* – ΔK are presented in **Figure 15** for the specimens pre-cracked in the parent metal (PM), in **Figure 16** for specimens pre-cracked in the weld metal (WM) and in **Figure 17** for specimens pre-cracked in the heat-affected-zone (HAZ). The values of coefficient *C* and exponent *m,* with the values of stress-intensity factor range at fatigue threshold, ΔK_{th}, are given in **Table 9**.

The dominant almost linear middle part of curve in **Figures 15–17** is covered by Paris law and is practically most important, since it allows to define the difference between fatigue crack low growth rates (initiation) close to fatigue threshold, and high rates (K_{Ic}), when fracture occurs. The application of Paris equation is very convenient for fatigue of structures produced of materials of elevated and high strength. As it can be seen from **Table 9**, the position of the fatigue crack-tip and the testing temperature significantly affect the ΔK_{th} values and the fatigue-crack growth [6]. For comparison of the properties of welded joint constituents the crack growth rates are calculated for different values of stress-intensity factor range ΔK. As a referent value ΔK

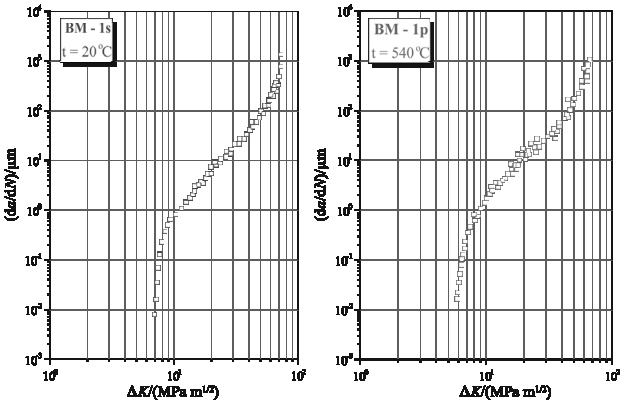

Figure 15: Fatigue crack growth rate per cycle, *da/dN*, vs. stress intensity factor range, ΔK, specimens pre-cracked in parent metal, tested at room temperature (left) and at 540 °C (right)

Slika 15: Rast utrujenostne razpoke na cikel d*a*/d*N* v odvisnosti od faktorja intenzitete napetosti ΔK, preizkušanec z razpoko v osnovnem materialu; preizkus pri sobni temperaturi (levo) in pri 540 °C (desno)

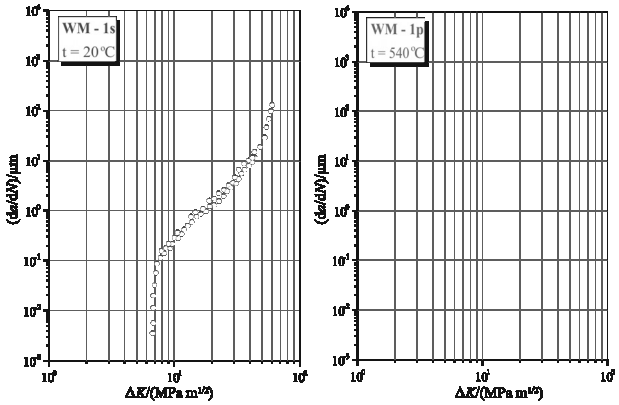

Figure 16: Fatigue crack growth rate per cycle, *da/dN*, vs. stress intensity factor range, ΔK, specimens pre-cracked in weld metal, tested at room temperature (left) and at 540 °C (right)

Slika 16: Rast utrujenostne razpoke na cikel d*a*/d*N* v odvisnosti od faktorja intenzitete napetosti ΔK, preizkušanec z razpoko v varku, preizkus pri sobni temperaturi (levo) in pri 540 °C (desno)

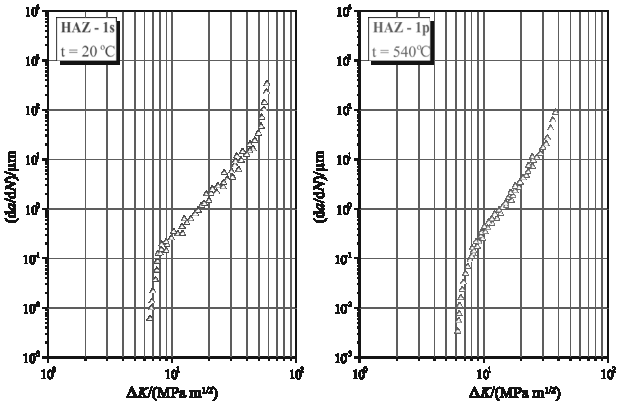

Figure 17: Fatigue crack growth rate per cycle, *da/dN*, vs. stress intensity factor range, ΔK, specimens pre-cracked in heat-affected-zone, tested at room temperature (left) and at 540 °C (right)

Slika 17: Rast utrujenostne razpoke na cikel d*a*/d*N* v odvisnosti od faktorja intenzitete napetosti ΔK, preizkušanec z razpoko v toplotni zoni, preizkus pri sobni temperaturi (levo) in pri 540 °C (desno)

= 10 MPa√m is accepted, which is within a middle part of the diagram, where Paris law is valid, **Figures 15–17**.

The fatigue crack-growth rate at room temperature, d*a*/d*N*, is $1.24 \cdot 10^{-09}$ μm/cycle for the specimen of BM, $2.56 \cdot 10^{-09}$ μm/cycle for specimen of WM and $3.12 \cdot 10^{-09}$ μm/cycle for specimen of HAZ At the temperature of 540 °C, corresponding values are higher: ($3.74 \cdot 10^{-09}$; $4.51 \cdot 10^{-09}$; $5.00 \cdot 10^{-09}$ for BM, WM and HAZ, in respect [6]. The behaviour of welded joint and its constituents should affect the change of curve slope in validity part of Paris law. Materials of lower fatigue-crack growth rate have lower slope in the diagram d*a*/d*N*\ *vs.* ΔK [6]. Slow growth is confirmed for specimens cracked in BM and WM, since for the same growth rate, greater factor intensity range is required. The maximum fatigue crack growth rate is expected when stress intensity factor range approaches to plane strain fracture toughness, when brittle fracture is possible [14].

In spite of significant differences in fatigue-crack growth rate, the obtained values are still low and acceptable. That means that tested steel and its welded joint exhibited acceptable level of fatigue-crack growth resistance and can be successfully applied for variable loading in case of detected crack-like defects, primarily for low-cycle fatigue.

6 CONCLUSIONS

The following conclusions were derived:

- The resistance to crack growth and obtained values of K_{Ic} and a_c of the welded joint are affected by its microstructural and mechanical heterogeneity and by the testing temperature. Feritte-lamelar pearlite microstructure of the WM has a better resistance to crack growth in static loading condition than the feritte-pearlite microstructure of BM of uniform grain size, and the feritte-pearlite microstructure of HAZ of different grain size. Obtained close K_{Ic} values of BM and HAZ are explained by the position of fatigue crack tip in HAZ region of the microstructure similar to that in BM.
- The testing temperature influences the fracture toughness K_{Ic} and the crack critical length a_{cr} values. The reduction of fracture toughness is of 35–45%, depending on fatigue crack tip location (BM, WM i HAZ). Specimen notched in WM has the highest value K_{Ic}, whereas for BM and HAZ obtained K_{Ic} values are lower. Results obtained at working temperature are proportionally lower compared to results at room temperature, and are a consequence of lower material properties at elevated temperature.
- Notch location and crack initiation, as well as testing temperature affect values of fatigue threshold ΔK_{th} and fatigue crack growth parameters.
- The minimum fatigue-crack growth rate exhibited the specimens pre-cracked in BM, and the maximum fatigue crack-growth rate in specimens pre-cracked in HAZ. This is directly connected to the effects that microstructural heterogeneity in HAZ regions has on fatigue-crack growth rate, d*a*/d*N*.
- Specimens of welded joint constituents at working temperature (540 °C) exhibited two to four-fold higher crack-growth rates when compared to room temperature under variable loads in tests of the fatigue threshold and fatigue crack growth parameters that this is explained by reduced material properties at elevated temperature.

7 REFERENCES

[1] S. Sedmak, A. Sedmak, Integrity of Penstcok of Hydroelectric Powerplant, Structural Integrity and Life, 5 (**2005**) 2, 59–70

[2] JUS EN 288-3:1992, Specification and approval of welding procedures for metallic materials – Part 3: Welding procedure tests for arc welding of steels, Službeni list SRJ, (**1995**), 25

[3] J. Vojvodic Tuma, A. Sedmak, Analysis of the unstable fracture behaviour of a high strength low alloy steel welment, Engineering Fracture Mechanics, 71 (**2004**), 1435–1451

[4] E. O. Argoub, A. Sedmak, M. A. Esasamei, Structural Integrity Assessment of Welded Plate with a Crack, Structural Integrity and Life, 4 (**2004**) 1, 39–46

[5] K. Gerić, PhD Thesis, University of Belgrade, Faculty of Tehnology and Metallurgy, Belgrade, 1997

[6] M. Burzić, PhD Thesis, University of Novi Sad, Technical faculty, 2008

[7] EN 895, Welded butt joints in metallic materials – Transverse tensile test, 1995

[8] ASTM E 1475-00, Standard Test Method for Measurement of Creep Crack Growth Rates in Metal, Annual Book of ASTM Standards 03.01.2000, 936–950

[9] ASTM E 1820-99a, Standard Test Method for Measurement of Fracture Toughness, Annual Book of ASTM Standards, 03.01, 1999

[10] ASTM E813-89, Standard Test Method for J_{Ic}, A Measure of Fracture Toughness, Annual Book of ASTM Standards, 03.01. 1993, 651

[11] M. Burzić, Z. Burzić, J. Kurai, The prediction of residual life of reactors in RNP, CertLab Pančevo, 2006

[12] P. C. Paris, F. Erdogan, A Critical Analysis of Crack Propagation Laws, Trans. ASME, Journal Basic Eng., 85, 4, 528

[13] ASTM E647, Standard Test Method for Constant-Load-Amplitude Fatigue Crack Growth Rates Above 10-8 m/cycle, Annual Book of ASTM Standards, 03.01. 1995, 714

[14] M. Burzić, Z. Burzić, J. Kurai, Dž. Gačo, Fatigue Behaviour of Alloyed Steel for High Temperature, First Serbian (26th YU) Congress on Theoretical and Applied Mechanics, Kopaonik, Serbia, 2007, 1085–1090

UDK 669.14.018.8:620.193
Original scientific article/Izvirni znanstveni članek

ISSN 1580-2949
MTAEC9, 42(6)273(2008)

THE ROLE OF CHLORIDE SALTS ON HIGH TEMPERATURE CORROSION OF 321 STAINLESS STEEL

VLOGA KLORIDNIH SOLI PRI VISOKOTEMPERATURNI KOROZIJI NERJAVNEGA JEKLA 321

Neelofar Amin, Mohammed Misbahul Amin, Shamsul Baharin Jamaludin, Kamarudin Hussin

School of Materials Engineering, PPK Bahan Taman Muhibah UniMAP, University Malaysia Perlis, 02600 Jejawi, Perlis, MALAYSIA
neelofaramin@yahoo.com

Prejem rokopisa – received: 2008-04-20; sprejem za objavo – accepted for publication: 2008-07-07

The effect of $CaCl_2$ and $BaCl_2$ salt coatings on the high temperature corrosion of 321 stainless steel at 950 °C in a slow current of air for the period of 72 hours were studied. The 321 alloy was severely attacked by calcium- and barium-chlorides due to formation of volatile chlorides. The data have been complemented by oxidation kinetics measurements and morphological structures were analyzed using scanning electron microscope (SEM). The elemental distribution on the alloy surface deposits were characterized by using energy dispersive X-ray (EDAX) analysis. The alkaline earth metal chloride salts have deleterious effect on the protectivity of the scale and rapid degradation of the alloy is noted.

Key words: 321 stainless steel, Hot Corrosion, $CaCl_2$, $BaCl_2$, Scale

Raziskan je bil vpliv prekritij s solmi $CaCl_2$ in $BaCl_2$ na visokotemperaturno oksidacijo nerjavnega jekla 321 v počasnem toku zraka pri 950 °C v trajanju do 72 h. Zaradi nastanka volatilnih kloridov sta oba klorida zlitino močno napadla. Določena je bila kinetika oksidacije, morfologija pa je bila določena z opazovanjem v vrstičnem mikroskopu. Porazdelitev elementov v depozitu na površini je bila določena z energijsko disperzivno spektrometrijo (EDAX). Kloridi alkalnih kovin močno zmanjšajo varovalnost škaje in povzročijo hitro degradacijo zlitine.

Ključne besede: nerjavno jeklo 321, vroča korozija, $CaCl_2$, $BaCl_2$, škaja

1 INTRODUCTION

The intensification of process engineering in almost every branch of modern technology, and development of new technologies make increasingly higher requirements for metallic construction materials, especially for their heat and scaling resistance. The increase in operating efficiency of certain installations or plants is generally achieved by the application of higher temperatures and pressures and higher flow velocities of gases and vapours which creates gas corrosion hazard for the construction materials[1–7].

The corrosion process under hot gases or vapours being a mixture of many aggressive components, proceeds usually many times faster and is characteristic by a non-uniform attack of metal surface[8-12]. It became obvious that chloride, always present in such industrial gases, is one of the most dangerous aggressive components of the above mentioned atmospheres[13,14].

In this study, the 321 stainless specimens were subjected to treatments of $CaCl_2$ and $BaCl_2$, oxidised at 950 °C for times ranging 12 h to 72 h was chosen in order to highlight the corrosion phenomena.

Finally the results of morphologies were carried out by using SEM (model Jeol 6460-LA) as well as energy-dispersed X-ray spectroscopy profiles of elements of deposits on the surface of corroded 321 alloy were presented.

2 EXPERIMENTAL

The present study has been carried out using commercially available 321 stainless steel. Its chemical composition was as follows: C–0.08 %, Mn–2 %, Si–1 %, Cr–17.5 %, Ni–10.5 %, P–0.045 %, S–0.03 % and Fe-balance. The 321 stainless steel sheets were cut into small pieces of size (20 × 12 × 3) mm. The surface of each specimens was polished mechanically with (180, 320, 600) grades of silicon carbide paper. The specimens were coated with $CaCl_2$ and $BaCl_2$ in a preheated condition to obtain a layer of salt deposition [13]. The coated specimens were dried and weighed, followed transferred into a crucible. The salt coated alloy were oxidised at 950 °C for the periods of 72 h in slow current of air and mass changes were recorded at every 12 h of interval. For each condition, two series of specimens were corroded in accordance with reference [14].

The microstructural and microchemical characterization were performed using Jeol 6460-LA scanning electron microscope equiped with a energy dispersive X-ray spectrometer and analyzer.

3 RESULTS

Figure 1 shows the curve of mass change versus exposure time of 321 stainless steel coated with $CaCl_2$ and $BaCl_2$, oxidized at 950 °C in slow blowing air. The

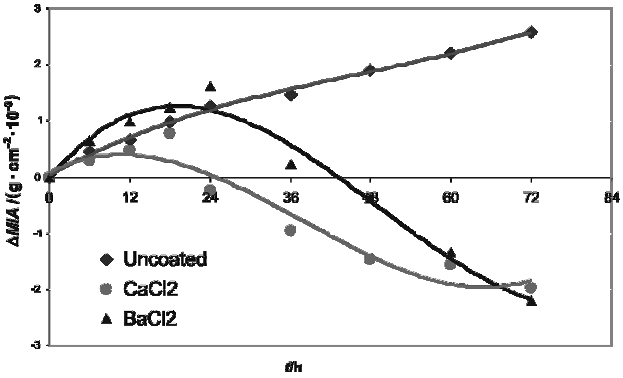

Figure 1: Oxidation behavior of 321 stainless steel without coated, coated with $CaCl_2$ & $BaCl_2$ as shown by a plot of mass change vs time, oxidized at 950 °C for 72 h

Slika 1: Oksidacija nerjavnega jekla 321 brez prekritja in z njim s $CaCl_2$ in $BaCl_2$. Sprememba mase v odvisnosti od časa pri oksidaciji do 72 hr pri 950 °C

graph of the mass change increases by increasing the exposure times shows for the uncoated alloy, a parabolic curve. The specimens coated with calcium and barium chloride exhibited the weight gain upto 24 h and mass loss with further increase of annealing time. The conclusion is that chlorides are more reactive in presence of metal because of the formation of volatile metallic chloride. The greater activity of calcium chloride is explained by the weaker bonding of calcium chloride than that of barium chloride.

Morphological Studies of 321 stainless steels

In **Figure 2** (**a, b**) the 321 alloy coated with $CaCl_2$ is shown, the scales formed are rough exhibiting a tendency to deform, wrinke and microcrack. The formation of metallic chlotide may have proceeded through the formation of intermediate volatile species, f.i. CrO_2Cl_2. some of which evaporate and some of decompose and accumulate at the alloy/salt interface in the form of Cr_2O_3.

The SEM micrograph of specimen coated by $BaCl_2$ exposed at 950 °C for 72 h (**Figure 3 a, b**) showing the presence of internal and pitting corrosion. The specimens exposed at 950 °C were badly deteriorated by layers of oxides and metallic chloride. The deposit film shows the presence of voids and pores especially in the outer layers of the scale.

Energy Dispersive X-Ray Analysis (EDAX)

Figures 4 and 5, the EDAX spectra, elements and compounds had been verified the content of the elements of the specimen coated by calcium chloride and barium chloride exposed at 950 °C for 72 h. The results of spectra and elements showed that the surface was mainly

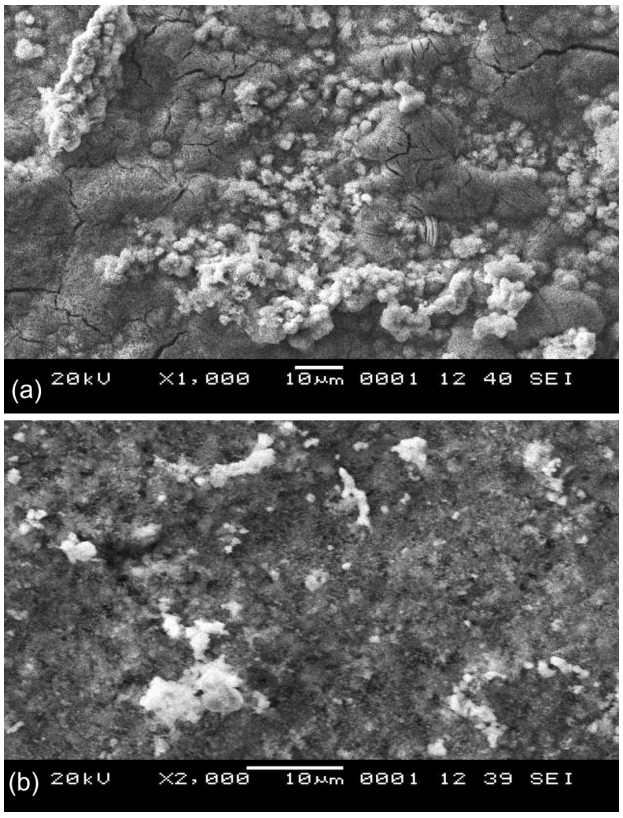

Figure 2: Outer surface of the scale formed on 321 stainless steel coated with $CaCl_2$, oxidised at 950 °C for 72 h

Slika 2: Zunanja površina škaje, ki je nastala pri 72-urni oksidaciji nerjavnega jekla 321, prekritega s $CaCl_2$

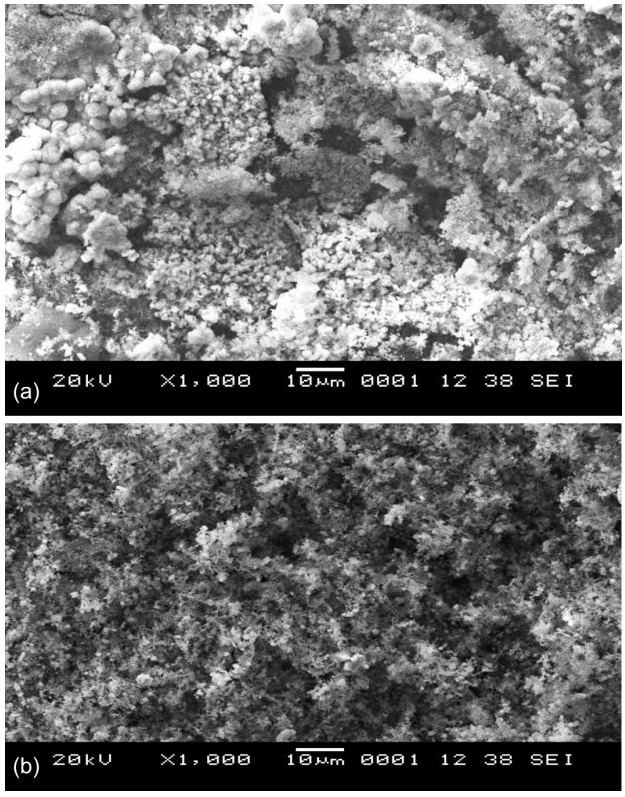

Figure 3: Outer surface of scales formed on 321 stainless steel coated with $BaCl_2$, oxidised at 950 °C for 72 h

Slika 3: Zunanja površina škaje, ki je nastala pri 72-urni oksidaciji nerjavnega jekla 321, prekritega z $BaCl_2$

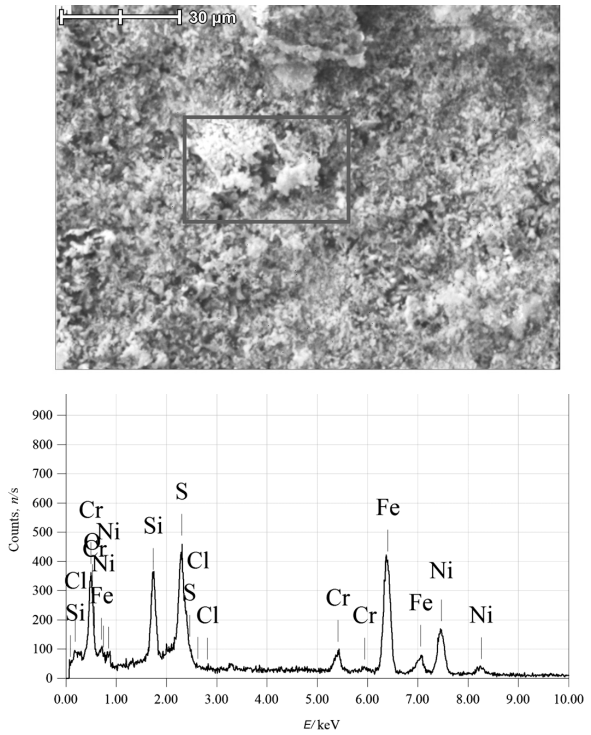

Figure 4: EDAX spectra of the elements on the specimen coated with $CaCl_2$, oxidized at 950 °C for 72 h in blowing air

Slika 4: Posnetek analizirane površine in EDAX-spekter elementov v vzorcu, prekritem s $CaCl_2$, ki je bil oksidiran v zračnem toku 72 h pri 950 °C

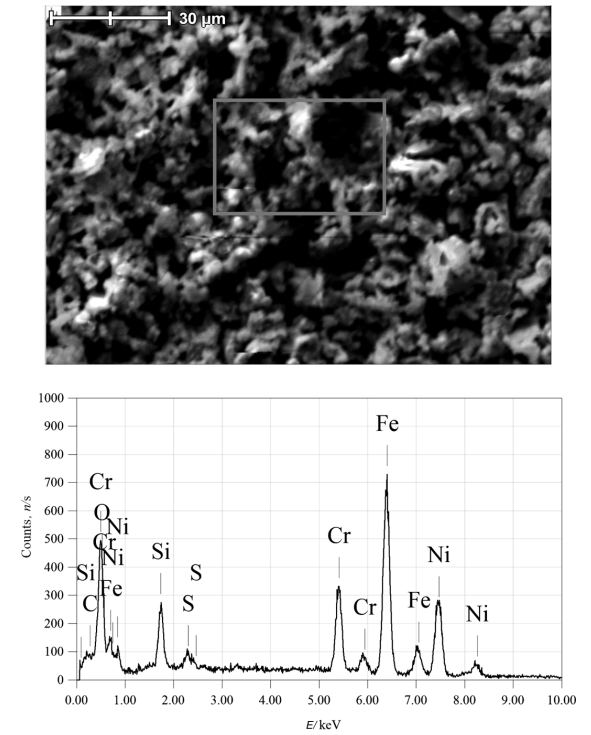

Figure 5: EDAX spectra of the elements and compounds of the specimen coated with $BaCl_2$, oxidized at 950 °C for 72 h in blowing air

Slika 5: Posnetek analizirane površine in EDAX-spekter elementov v vzorcu, prekritem z $BaCl_2$, ki je bil oksidiran v zračnem toku 72 h pri 950 °C

composed of nickel (Ni), chromium (Cr), iron (Fe) and oxygen (O). The results were logically acceptable because 321 stainless steel containing 17.5 % of chromium, 10.5 % of nickel and iron as balance.

Tables 1, 2 show the elemental analysis results of specimen coated with calcium- and barium- chloride that exposed at 950 °C for 72 h. According to the results in **Tables 1, 2**, iron oxide, FeO, was the main oxide product, it appearance as the site product while corrosion occur. Iron oxide formed when iron (Fe), reacting with oxygen in air, the equation shown as below:

$$2Fe + O_2 \rightarrow 2FeO$$

Besides that, Cr_2O_3 also occur in great quantities as the protective films for the stainless steel. In addition, the surface also accompanied with other oxides such as NiO, Cr_2O_3, SiO_2 and Chloride with small amount.

Table 1: Composition of the scale on the specimen coated with calcium chloride, oxidized at 950 °C for 72 h in blowing air from EDAX. Deduced from the EDAX analysis.

Tabela 1: Sestava škaje na vzorcu, prekritem s kalcijevom kloridom, ki je bil oksidiran v zračnem toku 72 h pri 950 °C. Preračunano iz EDAX-analize.

Element	*E*/keV	Mass, *w*/%	Compound	Mass, *w*/%
O		30.63		
Si	1.739	5.46	SiO_2	11.68
S	2.307	4.79	SO_3	0.96
Cl	2.621	0.36	Cl	0.36
Cr	5.411	3.63	Cr_2O_3	5.31
Fe	6.398	39.03	FeO	50.20
Ni	0.851	16.10	NiO	31.49
Total		100.00		100.00

Table 2: Composition of the scale on the specimen coated with barium chloride, oxidized at 950 °C for 72 h in blowing air from EDAX. Deduced from the EDAX analysis.

Tabela 2: Sestava škaje na vzorcu, prekritem z barijevom kloridom, ki je bil oksidiran v zračnem toku 72 h pri 950 °C. Preračunano iz EDAX-analize.

Element	*E*/keV	Mass, *w*/%	Compound	Mass, *w*/%
O		24.78		
Si	1.739	2.24	SiO_2	4.80
S	2.307	1.20	SO_3	0.29
Cl	2.621	1.12	Cl	1.29
Cr	5.411	10.18	Cr_2O_3	13.60
Fe	6.398	37.29	FeO	47.98
Ni	7.471	23.19	NiO	32.04
Total		100.00		100.00

4 DISCUSSION

The corrosive environment of calcium chloride and barium chloride effect onto the hot corrosion behavior of 321 stainless steel at 950 °C, exhibiting the breakdown of protection film on stainless steel caused the formation of a volatile, CrO_2Cl_2. The reaction can be described as follows [12,13]:

$$CaCl_2 + Cr_2O_3 + 3/2O_2 \rightarrow CrO_2Cl_2 + CaCrO_4$$

The formation of volatile products such as CrO_2Cl_2 and $CaCrO_4$, exerts sufficient vapour pressure to break the passivation of oxides on 321 stainless steel. Once the passive film breaksdown, the molten $CaCl_2$ further attacks the stainless steel and lead to corrosion. The equation:

$$2Fe + 2CaCl_2 + O_2 \rightarrow 2CaO + 2FeCl_2$$

$$2Cr + 3CaCl_2 + 3/2O_2 \rightarrow 2CrCl_3 + 3CaO$$

$$Cr + CaCl_2 + 3/2O_2 \rightarrow CrO_2Cl_2 + CaO$$

The chlorides formed such as CrO_2Cl_2 and $CrCl_3$ were released at the salt interface and get oxidized to release chlorine gas:

$$4CrCl_3 + 6O_2 \rightarrow 4CrO_3 + 6Cl_2$$

$$4CrO_2Cl_2 + 2O_2 \rightarrow 4CrO_3 + 4Cl_2$$

The chloride might be entrapped between inner oxide layers of the alloy and get condensed on cooling and appear as distinct and discrete phase in the scales [13]. $BaCl_2$ has undergone the same reaction as $CaCl_2$.

Since calcium is more electronegative than barium, the bonding of calcium chloride is weaker than that of the barium chloride. All common metals are very soluble in chloride form and so the reaction rate is increased. The presence of chloride ions in the electrolytic solution affects nearly every aspect of the corrosion behavior. The oxide layer that protects the steel breaks down in the presence of chloride, causing pits to form. This type of corrosion can lead to structural failures [3].

Temperature is a factor in activation controlled corrosion. Raising the temperature will also increase the corrosion rate as the activation energy decreases with temperature. Increasing solution temperature increased the susceptibility to both pitting and active dissolution [1].

The corrosion rate of each test decreases with the increasing of exposure times. It is because of the decrease of the concentration of chloride ions with time, most of the chloride ions that leads to corrosion has reacted with the chromium oxyde film protecting the surface of the steel and activate the unprotected surface [12]. This determined the concentrations of chloride solution will affect the corrosion rate. The chemical reactions of chloride ions are:

$$Fe^{2+} + 2Cl^- \rightarrow FeCl_2$$

At high temperatures in chloride salts increased the susceptibility to both pitting and active dissolution, resulted in increased corrosion current densities and peak current densities [4].

5 CONCLUSION

The results of the study shown the increased chloride content, the easily the passive region shrinks and simultaneously with the formation of corrosion of metallic chloride and fluxing products exhibiting the profuse deteriotion of the surface of the 321 stainless steel.

The patterns of the graphs follow the kinetic theory of reaction where the reactions rates were directly proportional to the increasing of temperature. It means as the temperature increases in the time for the initiating corrosion attack is decreased. The $CaCl_2$ coated alloy shown higher weight loss than the coated with $BaCl_2$.

Pitting corrosion, internal corrosion and stress corrosion cracking were the commonest corrosion found in 321 stainless steel in presence of chloride.

From the results of EDAX, iron oxide, FeO, Cr_2O_3 and NiO occur in great quantities on the corroded stainless steel surface in addition to other oxides such as SO_3, SiO_2 and chloride with small composition.

ACKNOWLEDGEMENT

The authors would like to thankfully acknowledged for the financial assistance in the form of Fundamental Research Grant Scheme: Vote-9003-00144 from Ministry of Higher Education, Malaysia.

6 REFERENCES

[1] Mrowec S, Werber T., Gas corrosion of metals, National Bureau of Standards, Washington D.C. (1978)

[2] Rahmel A., Schwenck W., Korrosion und Korrosionschudz von Stahlen, Verlag Chemie Weinheim, 1977, Chapter 6

[3] Stringer J., Hot corrosion of high temperature alloys, Proc. Intnl. Symp., High Temperature Alloys, Electrochemical Society Inc., Princton, N. J., (**1976**), 513

[4] Hart A. B., Cutler A. J. B., Deposition and corrosion in gas turbine, Appl. Sci. Publishers, London 1973, 371

[5] Attia A. A., Salih S. A., Baraka A. M., J Electrochem. Acta, (**2002**), 48:113

[6] Chester T. Sims T. Hagel W. C., The Superalloy, John Wiley & Sons, New York, 1972

[7] Badawy W. A. Alkharafi F. M. Al-Hassan E. Y., Corros. Prevention & Control, (**1999**) 46, 51

[8] Kolman, D. G., Ford, D. K., Butt, D. P. Nelson, T. O., Corrosion of 304 stainless steel exposed to nitric acid-chloride environments. Materials Corosion and Environment Effects, Laboratory Los Alamos, National Laboratory, (**2005**), 209

[9] Nishimura R., Maeda Y., Strees corrosion cracking of sensitized type 316 austenitic stainless steel in hydrochloric acid solution – effect of sensitizing time. *Corrosion Science.* 45 (**2003**) 8, 1847–1862

[10] Abdallah M., Rhodanine Azosulpha. Drugs as corrosion inhibitors for corrosion of 304 stainless steel in hydrochloric acid solution. *Journal of Corrosion Science.* 44 (**2001**) 4, 717–728

[11] Huntz A. M., Lefevre B., Cassino F., Mat. Sci. Eng. A290 (**2000**), 190–197

[12] M. Misbahul Amin, Hot corrosion behavior of inconel-600 alloy in presence of NaCl and Na_2CO_3 at 850 °C. *Prakt. Metallogr* (**1993**), 30:5

[13] M. Misbahul Amin, The CsCl- and $CsNO_3$-induced high temperature oxidation of Nimonic-90 alloy at 1123K. *Applied Surface Science.* 115 (**1996**) 355–360

UDK 641.87:543.272.61
Izvirni znanstveni članek/Original scientific article

ISSN 1580-2949
MTAEC9, 42(6)277(2008)

RAZTAPLJANJE CO_2 V EMBALIRANI VODI ALI BREZALKOHOLNI PIJAČI IN S TEM POVEZANE MOŽNE POŠKODBE

PROBLEMS ASSOCIATED WITH THE DISSOLUTION OF CO_2 IN THE CASE OF BOTTLED WATER AND NON-ALCOHOLIC BEVERAGES

Darko Drev[1,2], Mitja Peček[1,2], Jože Panjan[2]

[1]Inštitut za vode Republike Slovenije, Univerza v Ljubljani, Hajdrihova 28c, 1000 Ljubljana, Slovenija
[2]Fakulteta za gradbeništvo in geodezijo, Jamova 2, 1000 Ljubljana, Slovenija

Prejem rokopisa – received: 2008-06-05; sprejem za objavo – accepted for publication: 2008-08-13

Pri vodi in brezalkoholni pijači, ki ima raztopljen ogljikov dioksid, lahko nastane pri odpiranju plastenke ali steklenice poškodba. Ta poškodba je lahko posledica izmeta zamaška in pijače v obraz, pa tudi eksplozije steklenice. To se lahko zgodi, če je v vodi prevelik tlak raztopljenega CO_2 in je tudi zamašek pokvarjen. Eksplozija steklenice lahko nastane pri nekvalitetnem materialu. Pravilno izdelan zamašek bi moral med odpiranjem v steklenici postopno zmanjševati tlak. Če se to ne zgodi in je v plastenki velik tlak CO_2, lahko pride do izmeta zamaška v obraz ter tudi burnega iztoka tekočine iz plastenke. Takšni primeri niso samo teoretični, temveč se dogajajo tudi v praksi. Eksplozija steklenice nastane predvsem takrat, kadar so v steklu prekomerne napetosti kot posledica nehomogenosti materiala in neustrezne izdelave.

Ključne besede: brezalkoholne pijače, ogljikov dioksid, CO_2, plastenke, tlak, poškodbe

In the case of bottled water or bottled non-alcoholic beverages that contain dissolved carbon dioxide, opening the (glass or plastic) bottle can prove dangerous to the person opening it. Unscrewing the bottle cap can cause the cap or the contained liquid to be ejected away from the bottle with sufficiently high speed to cause physical harm to a person, or the entire bottle can explode. A properly functioning cap reduces bottle pressure slowly and continuously during the bottle opening process. The ejection of the cap and contained liquid is caused by exceedingly high pressure in the bottle, while both the ejection effect or the explosion of the bottle is caused by a malfunction of the bottle cap due to insufficient homogeneity of the materials used or inadequate processes applied in the production of the cap.

Key words: non-alcoholic beverages, carbon dioxide, CO_2, plastic bottle, problems

1 UVOD

Pri izbiri materiala za embaliranje vode in brezalkoholnih pijač niso pomembne samo tiste njegove lastnosti, ki zagotavljajo higiensko neoporečnost, temveč tudi druge lastnosti, kot so na primer: možnost enostavne manipulacije, nizka cena, možnost reciklaže itd. [Spellman, 1999], [Havelaer, 2003]. Glede higienske neoporečnosti lahko prištevamo steklo med kemijsko in fizikalno najprimernejše materiale za embaliranje pijač. Glavna pomanjkljivost steklene embalaže je lomljivost in s tem povezane težave pri transportu in ravnanju z njo [Nölle,1997]. V zadnjih dvajsetih letih se zato embalira vedno več vode in brezalkoholnih pijač v plastenke [Drev, 2005]. Med polimernimi materiali se za najmanjše plastenke največ uporablja od 250 ml do 2,5 l polietilentereftalat (PET), pri večjih posodah pa tudi polietilen (PE), polivinilklorid (PVC), polistiren (PS), polipropilen (PP) itd. Razlog za to je enostavno delo in nizka cena embalaže. Pri embalirani vodi in brezalkoholnih pijačah pa ne smemo pozabiti na zamaške. Ti so pogosto izdelani iz drugačnega materiala kot steklenice oziroma plastenke. Pri steklenicah so navadno kovinski zamaški s polimernimi ali plutovinastimi tesnili, pri plastenkah pa gre navadno za podoben material kot pri plastenki ali pa za katerega izmed standardnih termoplastov (PE, PP, PVC). V tem članku se omejujemo le na problematiko možnih poškodb pri odpiranju steklenic ali plastenk. Velika težava pa nastane, če steklenico ali plastenko raznese v navzočnosti ljudi. Pri tem so lahko posledice eksplozije steklenice mnogo hujše kot pri plastenki. Drobci stekla lahko poškodujejo ljudi na večji razdalji in mnogo huje, kot je to možno pri plastenki. Eksplozije steklenic ali plastenk, v katerih je embalirana gazirana pijača, so posledica prevelikega tlaka CO_2 v posodi ter tudi napak in s tem povezanih strižnih napetosti v materialu. Pri steklu, ki je krhko, so lahko včasih te strižne napetosti tako velike, da se lahko razleti steklenica tudi brez povečanega tlaka CO_2 v notranjosti. Pri plastični embalaži pa to ni mogoče. Strižne napetosti so posledica različnih raztezkov in skrčkov v materialu, ki nastanejo zaradi nehomogenosti materiala, temperaturne razlike, migracijskih procesov itd.

2 TEORETIČNI DEL

2.1 Raztapljanje ogljikovega dioksida v vodi

Maksimalna količina CO_2, ki se lahko raztopi v kokakoli ali vodi, je določena s Henryjevim zakonom (**slika 1**). Ta zakon pravi, da je pri dani temperaturi količina

plina, ki se raztopi v tekočini, premo sorazmerna njegovemu parcialnemu tlaku (**slika 1**).

$$n_i = K_i\, p_i \quad (1)$$

Tu pomenijo:
n_i [mol/m^3] – količina plina, ki se raztopi v tekočini
K_i [mol Pa^{-1}m^{-3}] – konstanta Henryjevega zakona
p_i [Pa] – parcialni tlak plina

V **tabelah 1 in 2** so prikazane Henryjeve konstante in konstante C za glavne sestavine zraka.

Tabela 1: Henryjeve konstante za vodo in pline pri 298 K (de.wikipedia.org/wiki)
Table 1: Henry's constants for the solubility of some gases in water at 298 K

Enačba:	$k_{H,cp} = \frac{C_{voda}}{p_{plin}}$	$k_{H,cp} = \frac{p_{plin}}{C_{voda}}$	$k_{H,px} = \frac{p_{plin}}{x_{voda}}$	$k_{H,cc} = \frac{C_{voda}}{p_{plin}}$
Enota:	$\frac{\text{mol}_{plin}}{1 \cdot \text{bar}}$	$\frac{1 \cdot \text{bar}}{\text{mol}_{plin}}$	$\frac{\text{bar} \cdot \text{mol}_{plin}}{\text{mol}_{plin}}$	[brez dimenzije]
O_2	$1{,}3 \cdot 10^{-3}$	769,23	$4{,}259 \cdot 10^{4}$	$3{,}180 \cdot 10^{-2}$
H_2	$7{,}8 \cdot 10^{-4}$	1282,05	$7{,}099 \cdot 10^{4}$	$1{,}907 \cdot 10^{-2}$
CO_2	$3{,}4 \cdot 10^{-2}$	29,41	$0{,}163 \cdot 10^{4}$	0,8317
N_2	$6{,}1 \cdot 10^{-4}$	1639,34	$9{,}077 \cdot 10^{4}$	$1{,}492 \cdot 10^{-2}$
He	$3{,}7 \cdot 10^{-4}$	2702,7	$14{,}97 \cdot 10^{4}$	$9{,}051 \cdot 10^{-3}$
Ne	$4{,}5 \cdot 10^{-4}$	2222,22	$12{,}30 \cdot 10^{4}$	$1{,}101 \cdot 10^{-2}$
Ar	$1{,}4 \cdot 10^{-3}$	714,28	$3{,}955 \cdot 10^{4}$	$3{,}425 \cdot 10^{-2}$
CO	$9{,}5 \cdot 10^{-4}$	1052,63	$5{,}828 \cdot 10^{4}$	$2{,}324 \cdot 10^{-2}$

Henryjeva konstanta je odvisna od temperature:

$$C = \frac{\Delta_{solv} H}{R} = \frac{-\mathrm{d}\ln(K_i)}{\mathrm{d}(1/T)} \quad (2)$$

Tu pomenijo:
$\Delta_{solv}H$ [J/mol] – entalpija
R [J/molK] – plinska konstanta
C [K] – konstanta
T [K] – temperatura

Tabela 2: Konstante C za različne pline
Table 2: Constants C for different gases

plin	O_2	H_2	CO_2	N_2	He	Ne	Ar
C /K	1700	500	2400	1300	230	490	1300

Ugotavljamo, da se pri dvakrat povečanem tlaku pri isti temperaturi dvakrat poveča količina raztopljenega plina. Seveda pa velja tudi nasprotno: če se tlak zmanjša, se zmanjša količina plina, ki je lahko raztopljena v tekočini in ta plin se iz tekočine izloči.

Plinska enačba za parcialni tlak posameznega plina:

$$p_i = (m_i/M_i)\, RV/T \quad (3)$$

Če plinsko enačbo za parcialni tlak združimo z Daltonovim zakonom, dobimo:

$$p = p_1 + p_2 + \ldots + p_n = (m_1/M_1 + m_2/M_2 + \ldots + m_n/M_n) \cdot RV/T \quad (4)$$

$$x_i = m_i/m \quad (5)$$

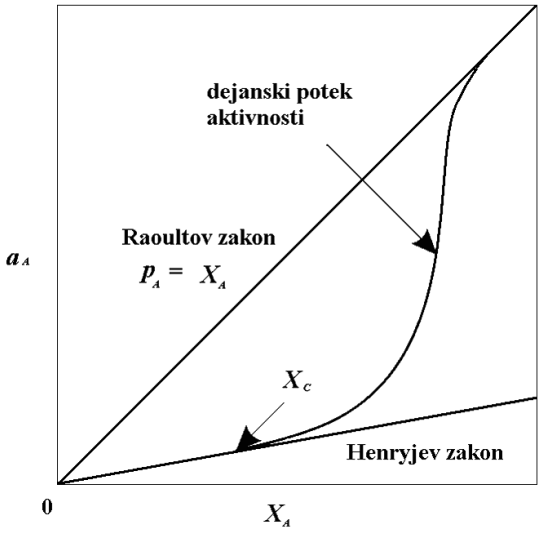

Slika 1: Prikaz topnosti plina CO_2 v vodi po Henryjevem zakonu in primerjava topnosti za idealne raztopine po Raoulovem zakonu [2]
Figure 1: Solubility of the gas CO_2 in water according to the Henry's law and comparison of the solubility to ideal solutions according to the Raoult's law [2]

Iz Daltonovega zakona tako dobimo enačbo za parcialni tlak posameznega plina:

$$p_i = (x_i/M_i)\, M_{zmesi}\, p \quad (6)$$

Tu pomenijo:
p [Pa] = tlak zmesi plinov v celoti
p_i [Pa] = parcialni tlak posameznega plina
x_i [mol/mol] = masni delež posameznega plina v zmesi
M_i [g/mol]= molska masa plina (masa enega kilo mola plina)
M_{zmesi} [g/mol] = molska masa zmesi

V termodinamiki ne govorimo o koncentracijah, temveč o aktivnostih določene komponente. Tudi v našem primeru je aktivnost CO_2 nekoliko drugačna od koncentracije in je podana z naslednjo enačbo:

$$a_A = \frac{p_A}{p_A^0} \quad (7)$$

Tu pomenijo:
a_A = aktivnost plina
p_A = parcialni tlak realneg plina
$p_A{}^0$ = parcialni tlak realnega plina

V idealni raztopini velja, da je parcialni tlak linearno sorazmeren deležu komponente v raztopini. Čim večji je njen delež, tem višji je parcialni tlak.

Ogljikov dioksid se raztaplja v vodi po Henryjevem zakonu v odvisnosti od temperature in tlaka (**tabeli 3, 4**). S **slike 2** je razvidno, da se pri enakem tlaku polnjenja raztopi različna količina CO_2 pri različnih temperaturah. Če je bila na primer pozimi v polnilnici temperatura samo 10 °C, poleti pa 30 °C, je lahko nastala pri pritisku polnjenja 3 bar približno 100-odstotna razlika v količini raztopljenega CO_2. Zato je pomembno, da so polnilnice tudi zaradi teh razlogov klimatizirane.

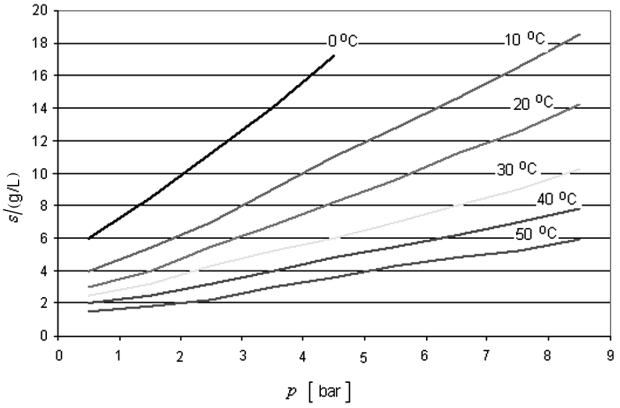

Slika 2: Odvisnost topnosti CO_2 v vodi od tlaka in temperature v okolici

Figure 2: Dependence of the CO_2 solubility in water on pressure and temperature

V primeru, da je bila gazirana brezalkoholna pijača polnjena pozimi pri relativno nizki temperaturi (na primer 10 °C), brezalkoholno pijačo pa odpira oseba poleti v naravi, kjer nima hladilnika ali hladilne torbe, bo lahko temperaturna razlika vsaj 20 °C. Ta razlika pa povzroča sproščanje CO_2 in s tem znatno povečan tlak.

Tabela 3: Topnost CO_2 v odvisnosti od parcialnega pritiska CO_2 pri 1 bar [16]

Table 3: Solubility of CO_2 at a partial pressure for CO_2 of 1 bar abs [16]

T/°C	0	10	20	30	40	50	80	100
Topnost CO_2 v vodi [*s*/cm^3 /g]	1,8	1,3	0,88	0,65	0,52	0,43	0,29	0,26

Disociacijska konstanta ogljikove kisline je odvisna od temperature (Lide, 1991).

Tabela 4: Odvisnost disociacijske konstante ogljikove kisline (K_{1A}) od temperature

Table 4: Dissociation constant (K_{1A}) of carbonic acid at various temperatures

Temperatura *T*/°C	0	5	10	15	20	25	30	35	40	45	50
$K_{1A}.10^7$	2,64	3,04	3,4	3,1	4,6	4,5	4,1	4,0	5,4	5,3	5,9

$$CO_2\ (l) + H_2O\ (l) \Leftrightarrow H_2CO_3\ (l)$$

$$K = \frac{c[H_2CO_3]_l}{c[CO_2]_l\, c[H_2O]_l} = \frac{c[H_2CO_3]_l}{c[CO_2]_l 55{,}5}$$

Tu pomenijo:

(*l*) = tekočina (liquid)

K = ravnotežna konstanta

$$K_r = 55{,}5 \cdot K = \frac{c[H_2CO_3]_l}{c[CO_2]_l} \approx 0{,}0017 \qquad (8)$$

2.2 Migracijski procesi voda-plastenka-okolica

Plastenke so praktično neprepustne za migracijske procese snovi iz okolice v vodo in iz vode v okolico. Pri steklenicah so ti migracijski procesi še mnogo manjši. Za pločevinke pa pogosto to ne velja v celoti. Procesi raztapljanja kovinskih ionov v vodi so znatni, posebno še, če kakovost pločevine ni najboljša. Če so v vodi prisotni razni dodatki (brezalkoholne pijače), se lahko ti procesi še pospešijo.

Migracijski procesi so odvisni od:
- lastnosti materiala,
- lastnosti permeatov,
- tlaka in koncentracije permeata,
- naknadne oksidacije v vodi,
- sestave atmosfere,
- drugih dejavnikov.

Pri plastenkah se pojavljajo zelo minimalni procesi prodiranja plinastih produktov iz atmosfere v tekočino (vodo, kokakolo) in iz tekočine v atmosfero (**slika 3**). Nobena plastika ni povsem neprepustna za pline, kot sta na primer kisik (O_2) in ogljikov dioksid (CO_2). Poleg migracijskih procesov plinastih produktov pa se lahko raztapljajo določene druge snovi iz embalaže v tekočino in obratno [Gächter,1989]. Vsi ti procesi morajo biti zelo minimalni, kar se doseže z ustrezno izbiro plastike in dovolj tesnim zamaškom. Materiali za izdelavo plastenk za živila morajo biti iz ustreznih materialov ter tudi atestirani. PET – polietilentereftalat je v osnovi zelo primeren za embaliranje živil, vendar pa ne vsak, temveč le tisti, ki je bil izdelan na ustrezen način in tudi atestiran. Na primer, PET- regenerat se ne sme več uporabljati za embaliranje živil, ker ni dovolj kemijsko stabilen.

Prepustnost CO_2 skozi stene plastenke je odvisna od difuzijskega koeficienta in koncentracij CO_2 v tekočini in v zraku:

$$F_x = -D\frac{\mathrm{d}c}{\mathrm{d}x} = -D\frac{c_1 - c_2}{l} \qquad (9)$$

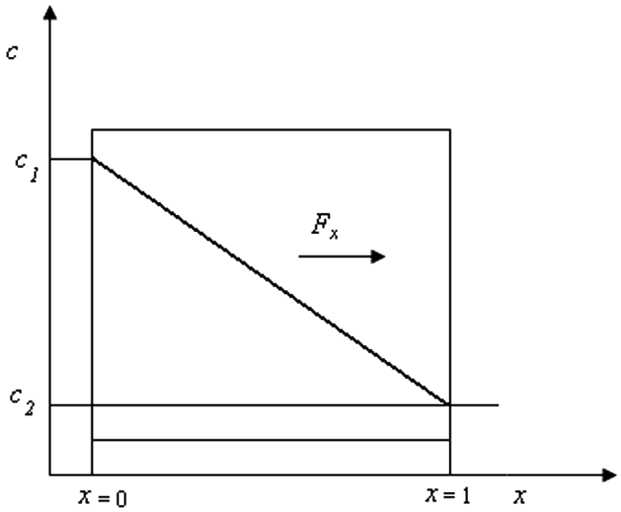

Slika 3: Prikaz difuzijskega toka CO_2 skozi steno plastenke

Figure 3: Sheme of the diffusion flow of CO_2 through the plastic bottle wall

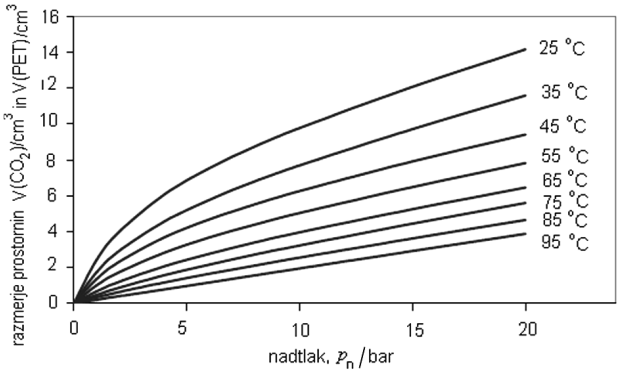

Slika 4: Topnost CO_2 v PET (59 % amorfnega dela) v odvisnosti od nadtlaka p_n in zunanje temperature [9]
Figure 4: Solubility of CO_2 in PET (59% of amorphous faze) in dependence of the pressure and temperature [9]

Tu pomenijo:
F_x [m s^{-1}] – tok
p_1 [Pa] – parcialni pritisk
D [m^2 s^{-1}] – difuzijski koeficient
c [mg/m^3] – koncentracija
l [m] – debelina folije

Prepustnost PET-embalaže je odvisna od »topnosti« CO_2 v polimeru (**slika 4**). "Topnost" je odvisna od temperature, kristaliničnosti, molske mase PET ter dodatkov v plastiki. Prepustnost poveča delež amorfne oblike, nizka molekulska masa ter velika količina dodatkov. Zato je pri embaliranju vode in brezalkoholnih pijač zelo pomembno, da je material relativno čist in ima ustrezno molekulsko maso. Na **sliki 5** je prikazan primer vpliva temperature na topnost CO_2 pri določeni sestavi PET. Na **sliki 6** pa je prikazana prepustnost O_2 za polimerne materiale PET za plastenke.

Tabela 5: Prepustnost PET plastike za pline [15]
Tabele 5: Permeability of a PET layer plastics for gases [15]

Material	μCO_2 [cm^{3}mm/(m^{2}d bar)]	μO_2 [cm^{3}mm/(m^{2}d bar)]
PET	16	4
OPET	8	2
PEN	2	0,5
PVDE oslojen	0,05	0,03
EVOH	0,05	0,01
SiO_2	0,01	0,002

V **tabeli 3** je prikazana prepustnost plastenke za CO_2 in O_2 in nekaterih drugih materialov, ki se uporabljajo za embaliranje pijač. Iz vseh navedenih podatkov je razvidno, da so PET-plastenke praktično neprepustne za CO_2 in druge pline. Zato ostanejo v plastenki še dolgo časa prevelike koncentracije CO_2, ki so bile vnesene pri polnjenju. To povzroča potencialno nevarnost poškodb.

2.3 Vpliv pH vrednosti na količino plinastega ogljikovodika in s tem tudi na pritisk v plastenki

V kisli vodi in gaziranih brezalkoholnih pijačah sta v ravnotežju raztopljeni in plinasti CO_2 :

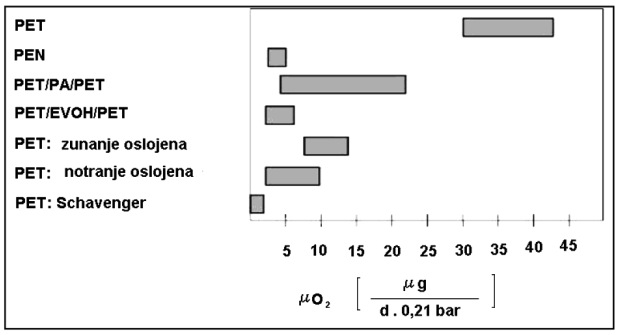

Slika 5: Prikaz prepustnosti O_2 za PET plastenke [12]
Figure 5: Permeability of PET plastic bottels for oxygen [12]

$$H_2O + CO_2 \Leftrightarrow H_2CO_3 \Leftrightarrow H^+ + HCO_3^- \Leftrightarrow 2H^+ + CO_3^-$$

$$H_2CO_3 \rightleftharpoons HCO_3^- + H^+$$

$$K_{a1} = \frac{c\left[H^+\right] \cdot c\left[HCO_3^-\right]}{c\left[H_2CO_3\right]} = 4{,}3 \cdot 10^{-7} \qquad (10)$$

$$HCO_3^- \rightleftharpoons CO_3^{2-} + H^+$$

$$K_{a2} = \frac{c\left[H^+\right] \cdot c\left[CO_3^{2-}\right]}{c\left[HCO_3^-\right]} = 6 \cdot 10^{-11} \qquad (11)$$

$$K_{a1} = \frac{x \cdot c\left[HCO_3^-\right]}{c\left[H_2CO_3\right]}$$

$$\left(\approx \frac{x \cdot c\left[HCO_3^-\right]}{c\left[CO_2 + H_2CO_3\right]} \approx \frac{x \cdot c\left[HCO_3^-\right]}{c\left[CO_2\right]_l}\right) \qquad (12)$$

$$K_{a2} = \frac{x \cdot c\left[CO_3^{2-}\right]}{c\left[HCO_3^-\right]} \qquad (13)$$

Tu pomenijo:
x [mol/L]= c[H$^+$]
K_{a1}[mol/L]= konstanta razpada H_2CO_3
K_{a2}[mol/L]= konstanta razpada HCO_3^-

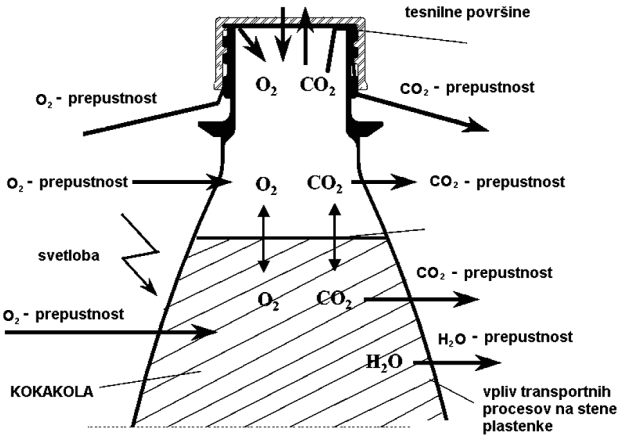

Slika 6: Prikaz migracijskih procesov v plastenki z brezalkoholno pijačo [9]
Figure 6: Migration processes in soft drink plastic bottle [9]

Kot je razvidno iz ravnotežne reakcije, je vsebnost plinastega CO_2 odvisna delno tudi od kemije in ne samo od Henryjevega zakona o topnosti CO_2 v vodi. Določene raztopljene snovi vplivajo na pH-vrednost, ta pa na ravnotežje plinastega in raztopljenega CO_2.

Ker se lahko s časom spreminja sestava raztopljenih snovi v vodi, se spreminja tudi pH-vrednost. S tem se spreminja tudi razmerje med topnih in plinastim CO_2.

Koncentraciji vodikovih $c[H^+]$ ali hidroksilnih ionov $c[OH^-]$ sta povezani preko konstante disociacije vode, zato je pH-vrednost merilo za koncentracijo vodikovih $c[H^+]$ in hidroksilnih ionov $c[OH^-]$.

$$H_2O \Leftrightarrow [H^+] + [OH^-]$$

Za konstanto disociacije velja naslednja formula:

$$\frac{c[H^+] \cdot c[OH^-]}{c[H_2O]} = K_{H_2O} = 1{,}8 \cdot 10^{-16} \qquad (14)$$

$$c[H_2O] = \frac{1\text{L}}{M_{H_2O}} = \frac{1000\ \text{g/L}}{18\ \text{g/L}} = 55{,}5\ \text{mol/L}$$

$$c[H_2O] \cdot 1{,}8 \cdot 10^{-16} = 55{,}5 \cdot 1{,}8 \cdot 10^{-16} = 1 \cdot 10^{-16} = K_w \qquad (15)$$

$$\lg c[H^+] + \lg c[OH^-] = -14 \qquad (16)$$

$$pH = -\lg c[H^+] \qquad (17)$$

Tu pomenijo:

K_{H2O}[mol/L]= konstanta razpada vode

K_w [(mol/L)^2] = ionski produkt vode

Na podlagi zgoraj navedenih reakcij in enačb lahko izračunamo ravnotežje med CO_2 in pH vrednostjo kot je prikazano na **sliki 7**.

Iz navedenega je razvidno, da se z zmanjšanjem pH-vrednosti poveča količina plinastega CO_2. To pa se lahko zgodi zaradi kemičnih reakcij raztopljenih substanc v brezalkoholni pijači. Te reakcije so navadno zanemarljive, saj mora ostati nespremenjena kakovost ustekleničenih brezalkoholnih pijač.

CO_2 pa nastaja tudi pri biokemijskih procesih razgradnje raztopljenih organskih snovi v vodi oziroma brezalkoholni pijači. Za to so potrebne bakterije in ustrezni pogoji. Pri embalirani vodi in brezalkoholnih pijačah mora biti zagotovljena sterilnost embalaže in pijače, zato so takšne reakcije malo verjetne. Vendar pa jih ne moremo v celoti izključiti, posebno še pri sadnih sokovih, kjer je velika količina hraniva za razvoj bakterij.

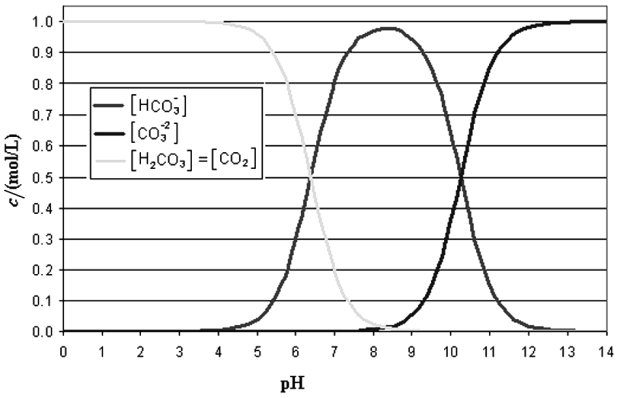

Slika 7: Ravnotežje CO_2 – pH-vrednost [7]
Figure 7: pH-CO_2 equilibra [7]

3 PRAKTIČNI DEL

3.1 Primer sproščanja CO_2 zaradi dviga temperatur in dodajanja topila v gazirano brezalkoholno pijačo

a) Povečanje tlaka zaradi dviga temperature

- Pri preiskavi gazirane mineralne vode je bila izmerjena količina 3,8 mg CO_2/l.
- Iz grafikona na **sliki 2** je razvidno, da se z dvigom temperature od 15 °C na 40 °C poveča tlak CO_2 iz 1 bar na približno 4 bar.
- 3 bar nadtlaka lahko povzroči burno sprostitev brezalkoholne pijače tako kot je prikazano na **sliki 8**.
- Pri steklenicah z velikimi napetostmi v materialu pa lahko nastane celo eksplozija steklenice. Steklenice za brezalkoholne pijače so navadno preizkušene na tlak 7 bar.

b) Sproščanje CO_2 zaradi raztapljanja drugih snovi, ki dvigujejo pH vrednost

3.2 Izračun pH vrednosti za gazirano mineralno vodo pred dodatkom $NaHCO_3$ in po njem:

- raztopili smo 1 g $NaHCO_3$ v 1 L gazirane mineralne vode;
- v gazirani mineralni vodi je bila izmerjena vsebnost CO_2; 3,8 mg/L = 0,086 mol/L in 7,7 mg HCO_3^-/L = 0,126 mol HCO_3^-/L;
- pufer H_2CO_3 in $NaHCO_3$ ima pH = 6,4;
- izračun pH-vrednosti pred dodatkom $NaHCO_3$:

$$pH = 6{,}4 + \lg \frac{c[HCO_3^-]}{c[CO_2]} = 6{,}4 + \lg \frac{0{,}126\ \text{mol/L}}{0{,}086\ \text{mol/L}} =$$
$$6{,}4 + 0{,}16 = 6{,}56$$

- izmerjena pH vrednost gazirane mineralne vode je bila približno 6,5;
  1 mol H_2CO_3 = 62 g
  1 mol CO_2 = 44 g
  1 mol HCO_3^- = 61 g
  1 mol $NaHCO_3$ = 84 g
- v 1 L gazirane mineralne vode smo dodali 10 g $NaHCO_3$ (0,12 mol);
- sprostila se je znatna količina CO_2, pri čemer se pH-vrednost ni opazno spremenila;
  izračun pH vrednosti po dodatku $NaHCO_3$:

$$pH = 6{,}4 + \lg \frac{c[HCO_3^-]}{c[CO_2]} = 6{,}4 +$$
$$+ \lg \frac{(0{,}126 + 0{,}12)\ \text{mol/L}}{0{,}086\ \text{mol/L}} = 6{,}4 + 0{,}45 = 6{,}85$$

– Izmerjena pH-vrednost po dodatku $NaHCO_3$ je bila približno 6,5, kar ni bistvena sprememba glede na prvotno stanje.

3.3 Sproščanje CO_2 zaradi dodatka $NaHCO_3$ v kokakolo:

– pred dodatkom $NaHCO_3$ je bila izmerjena vrednost pH = 3;
– po dodatku 1 g $NaHCO_3$ v 1 L Coka cole je nastala burna reakcija sproščanja CO_2, približno tako kot je prikazano na sliki 8;
– po dodatku $NaHCO_3$ je imela Coka cola pH = 6;
– pri Coka coli je poleg ogljikove tudi znatna količina fosforne kisline. Zato je treba upoštevati poleg ravnotežnih reakcij H_3CO_3 tudi ravnotežne reakcije H_3PO_4

$$H_3PO_4 \rightleftharpoons H_2PO_4^- + H^+$$

$$K_1 = \frac{c[H^+] \cdot c[H_2PO_4^-]}{c[H_3PO_4]} = 1 \cdot 10^{-2}$$

$$H_2PO_4^- \rightleftharpoons HPO_4^{-2} + H^+$$

$$K_2 = \frac{c[H^+] \cdot c[H_2PO_4^{2-}]}{c[H_2PO_4^-]} = 1 \cdot 10^{-7}$$

$$HPO_4^{-2} \rightleftharpoons PO_4^{-3} + H^+$$

$$K_3 = \frac{c[H^+] \cdot c[PO_4^{3-}]}{c[HPO_4^{2-}]} = 1 \cdot 10^{-12}$$

$$pH = -\lg c[H^+] = 3$$

$$c[H^+] = -\lg c[H^+] = 10^{-3} \text{ mol/l}$$

Izračun sproščene količine CO_2 po dodatku $NaHCO_3$:

$$c[H_2CO_3] = \frac{c[HCO_3^-] \cdot c[H^+]}{4{,}3 \cdot 10^{-7}} = \frac{[0{,}09 + 0{,}01] \cdot [0{,}001]}{4{,}3 \cdot 10^{-7}}$$

$$= \frac{10^{-4}}{4{,}3 \cdot 10^{-7}} = 232 \text{ mol/L}$$

232 mol/L CO_2 = 4 g/L CO_2

3.4 Poškodbe pri odpiranju plastenk

Oseba iz manjšega kraja na Dolenjskem, ki je odpirala dvolitrsko plastenko kokakole, je dobila zaradi tega poškodbe. Zamašek ji je vrglo v levo ličnico, hlape in tekočino pa v levo oko. V trenutku jo je močno zapeklo in na to oko ni videla nič več. Zaradi tega je morala poiskati zdravniško pomoč v bolnišnici. Na okulističnem oddelku je ostala 13 dni. Delne posledice poškodbe pa so ostale. Odškodnino za nastalo poškodbo poskuša iztožiti na sodišču.

V navedenem primeru je bil v plastenki povišan tlak CO_2 ter tudi pokvarjen zamašek. Tega ni bilo možno enostavno odpreti, temveč so bili za to potrebni dodatni napori. Zaradi tega se je v kokakolo vnašala dodatna kinetična energija, ki je sproščala vsebnost neraztopljenega CO_2. Poleg tega pa odpiranje pokvarjenega zamaška ni povzročalo postopnega sproščanja tlaka v plastenki.

Slika 8: Prikaz burne ekspanzije Coka cole po odstranitvi zamaška
Figure 8: Ejection of liquid after removal of the Coca-cola bottle cap

Poznan je primer iz Nemčije, ko je plastenka s kokakolo eksplodirala v rokah devetletnega otroka. Zardi poškodb, ki jih je pri tem dobil otok, je bila izplačana odškodnina 10.000 DM.

Podobno kot za navedena primera kokakole je poznano še več primerov poškodb z drugimi gaziranimi brezalkoholnimi pijačami in ustekleničeno kislo vodo.

V fazi polnjenja se je lahko raztopila dvakrat večja količina CO_2 kot pri nekoliko višji temperaturi pri enakem tlaku. Če se steklenica oziroma plastenka gazirane pijače pred odpiranjem še precej obrača, se znatni del raztopljenega CO_2 sprosti. Razlog za to je vnos kinetične energije v vodo, kar vpliva na dodatno sproščanje CO_2. Količina neraztopljenega CO_2 se tako nekajkrat poveča, kar po Henryjrevem zakonu pomeni tudi zvišanje tlaka v plastenki. V takem primeru lahko pride pri odpiranju plastenke do približno takšnega pojava, kot je prikazan na **sliki 8**.

4 SKLEPI

Količina raztopljenega CO_2 v vodi ali brezalkoholni pijači ni pomembna samo zaradi zdravstvenih in kulinaričnih zahtev, temveč lahko vpliva tudi na poškodbe uporabnikov. Te so sicer zelo redke, vendar pa jih ne smemo zanemariti. V članku smo analizirali

vzroke poškodb in se v konkretnih primerih omejili le na poškodbe, ki lahko nastanejo zaradi prevelike količine CO_2 pri odpiranju plastenk. Obravnavali pa smo problem bistveno širše, tj. z vidika nastajanja prekomerne količine plinastega CO_2 v ustekleničeni pijači. Količina raztopljenega in plinastega ogljikovega dioksida je v glavnem definirana z osnovnimi plinskimi zakoni (Henryjev zakon), kar se pogosto pozablja. Tudi vrsta in količina raztopljenih snovi imata določen vpliv na topnost oziroma sproščanje CO_2. Veliko bolj problematično pa je nastajanje CO_2 pri biokemijskih procesih (alkoholno vretje, itd.), kar povzroča še večjo nevarnost poškodb pri odpiranju steklenic. Prekomerna količina CO_2 pa ni nevarna le pri odpiranju steklenic, temveč tudi med hranjenjem. Če je tlak tako velik, da ga embalaža več ne zdrži, nastane eksplozija. Eksplozije plastenk niso tako problematične kot eksplozije steklenic, saj je steklo krhko in trdo. Drobci stekla lahko zletijo v zrak ter povzročijo precejšnje poškodbe navzočih ljudi.

Varnejše odpiranje steklenic in plastenk morajo omogočiti tudi zamaški. Neustrezni zamaški so ena izmed velikih hib, ki jih lahko ugotovimo potrošniki v vsakdanjem življenju. Pri plastenki mora biti izdelan zamašek tako, da zagotavlja popolno zaprtje vsebine, dokler ga ne začnemo odvijati. Ko začnemo odpirati plastenko, mora priti do enostavnega razdvajanja fiksnega dela (če obstaja) od zamaška z navojem. Navojni del bi moral biti narejen tako, da se pri odvijanju postopno sprošča tlak. Odpiranje steklenic s kovinskim pokrovom ni problematično, če uporabljamo ustrezno odpiralo. Pri dvigovanju pokrovčka se tlak postopno izenačuje. Bistveno večji problem pa so ustekleničene pijače z zamaški.

5 LITERATURA

[1] Brydson, J. A., Plastics Materials, Butterworth Heinemann, 1999

[2] Dean, J. A., Lange's Handbook of Chemistry, McGraw, Inc., 1992

[3] Drev, D., Problematika embalirane vode. V: Roš, Milenko (ur.). Zbornik referatov. Ljubljana: Slovensko društvo za zaščito voda, 2005, 128–138

[4] Frimmel, F. H., Wasser und Gewasser, Ein Handbuch (Gebundene Ausgabe), Spektrum Akademischer Verlag, 1999

[5] Gächter, R., Müller, H., Taschenbuch der Kunststoff – Additive, Hanser Verlag, Wien, 1989

[6] Havelaer, A. H., Melse, J. M., Quantifying public health risk in the WHO Guidalines for Drinking – Water Quality, RIVM report 73401022/2003, 2003

[7] Lide, D. R., CRC Handbook of Chemistry and Physics, 71 ed. Boca Raton, Ann Arbor, Boston: CRC Press, 1991

[8] Jolly, W. L. Modern Inorganic Chemistry (2nd Edn.). New York: McGraw-Hill, 1991

[9] Müller, K., O_2 – Durchlässigkeit von Kunststoffflaschen und Verschlüssen – Messung und Modellierung der Stofftransportvorgänge, PhD Thesis, Technische Universität München, 2003

[10] Mette, M., Ein Beitrag zur Gasdurchlässigkeit Permeabler Getränkenflaschen unter dem Aspekt der Haltbarkeit des Füllgutes-Teil 1, Brauindustrie, 3 (**2003**), 150–153

[11] Nölle, G., Technick der Glasherstellung, Wiley VCH Verlag, (1997)

[12] Orzinski, M., Untersuchung der Permeation von anorganische Gasen und organische Verbindungen durch barriereverbesere Kunststoffflaschen und ihre messtechnische Erfassung, PhD Thesis, Technische Universität Berlin, D83, 2007

[13] Preeti, C., Multi-component transport of gases and vapors in poly(ethylene terephtalate), PhD Thesis, Georgia Institute of Technology, 2006

[14] Pravilnik o preskušanju izdelkov in snovi, ki prihajajo v stik z živili, (Uradni list RS, 131/039)

[15] Palzer, G., Establishment of a standard test precedure for PET bottle materials with respect to chemical inertness behavior including the preparation of a certified PET reference material, PhD Thesis, Technische Universität München, 2001

[16] Physical and engineering data, January 1978 ed. The Hague: Shell Internationale Petroleum Maatschappij BV, 1978

[17] Spellman, F. R. The drinking water handbok, CRC PRESS, 1999

[18] Uredba Evropskega parlamenta in Sveta, 27. oktober 2004 o materialih in izdelkih, namenjenih za stik z živili, in o razveljavitvi direktiv 80/590/EGS in 89/109/EGS

[19] Uredba o izvajanju Uredbe Evropskega parlamenta in Sveta ES o materialih in izdelkih, namenjenih za stik z živili in o razveljavitvi direktiv 80/590/EGS in 89/109/EGS, (Uradni list RS, 53/05, 66/06)

[20] Witt G. Taschenbuch der Fertigungstechnik, Hanser, 2005

UDK 543.428.3:669.25
Izvirni znanstveni članek/Original scientific article

ISSN 1580-2949
MTAEC9, 42(6)285(2008)

PRIPRAVA Co-FERITNIH NANODELCEV Z OZKO PORAZDELITVIJO VELIKOSTI Z METODO TERMIČNEGA RAZPADA OLEATOV

PREPARATION OF Co-FERRITE NANOPARTICLES WITH A NARROW SIZE DISTRIBUTION BY THE THERMAL DECOMPOSITION OF OLEATES

Sašo Gyergyek[1], Darko Makovec[1], Mihael Drofenik[1,2]

[1]Odsek za sintezo materialov, Institut »Jožef Stefan«, Jamova 39, 1000 Ljubljana, Slovenija
[2]Fakulteta za kemijo in kemijsko tehnologijo, Univerza v Mariboru, Smetanova 17, 2000 Maribor, Slovenija
saso.gyergyek@ijs.si

Prejem rokopisa – received: 2007-10-30; sprejem za objavo – accepted for publication: 2008-07-23

V prispevku opisujemo sintezo nanodelcev kobaltovega ferita z ozko porazdelitvijo velikosti z metodo termičnega razpada organskega kompleksa. Sinteza nanodelcev je potekala v dveh stopnjah. V prvi smo sintetizirali železov in kobaltov oleat z reakcijo kobaltovega (II) in železovega (III) klorida z natrijevim oleatom v mešanici topil. V drugi stopnji smo raztopino oleatov, ki smo ji dodali različne količine oleinske kisline, segreli do vrelišča topila (heksadeken 282 °C ali oktadeken 316 °C). Na povišani temperaturi oleati razpadejo in tvorijo oksidne nanodelce. Na nanodelce je vezan monomolekulski sloj oleinske kisline, ki omogoča dispergiranje nanodelcev v nepolarnih topilih. Povprečna velikost nanodelcev kobaltovega ferita je odvisna od temperature, časa siteze in količine dodane oleinske kisline. Sintetizirani nanodelci v območju velikosti med 9 nm in 20 nm izkazujejo ferimagnetno vedenje ter magnetne lastnosti, ki se spreminjajo s povprečno velikostjo nanodelcev. Predpostavili smo mehanizem nastanka nanodelcev kobaltovega ferita, ki vključuje koalescenco manjših nanodelcev in njihovo rekristalizacijo.

Ključne besede: kobaltov ferit, nanodelci, magnetni nanodelci

A synthesis method for the preparation of narrow-size-distribution Co-ferrite nanoparticles by thermal decomposition of oleates is presented. A two-step method was used to produce the nanoparticles. In the first step cobalt and iron oleates were synthesized by reacting iron (III) and cobalt (II) chlorides with sodium oleate in a mixture of solvents. In the second step the oleates solution, to which different amounts of oleic acid were added, was heated to the solvents' boiling point (hexadecene 282 °C or oktadecene 316 °C). At elevated temperatures oleates decompose and oxide nanoparticles are formed. The nanoparticles are than coated with a mono-molecular layer of oleic acid, are hydrophobic and can be dispersed in non-polar organic solvents. The average size of the cobalt ferrite nanoparticles depends on the temperature, time of the synthesis and the concentration of oleic acid. In the size range between 9 nm and 20 nm the synthesized nanoparticles exhibited ferromagnetic behavior and size-dependent magnetic properties. A mechanism for the formation of cobalt ferrite nanoparticles with re-crystallization of nanoparticles composed of smaller nanoparticles is proposed.

Key words: cobalt ferrite, nanoparticles, magnetic nanoparticles

1 UVOD

Magnetni nanodelci, kot so npr. feritni, so pomemben material zaradi značilnih magnetnih, magnetorezistivnih in magnetooptičnih lastnosti,[1] ki jih v grobozrnatem materialu ne opazimo.[2-4] Njihova uporaba se razteza od tehnološke, kot so magnetne tekočine[5] in magnetno hranjenje informacij,[6] do biomedicinske, kot sta na primer ciljna dostava zdravil[7] ali povečanje kontrasta pri slikanju z NMR-tehniko.[8]

Kobaltov ferit je tehnološko zanimiv predstavnik skupine feritnih materialov zaradi velike energije magnetne anizotropije in velikih magnetooptičnih koeficientov.[9] Tako je bilo razvitih veliko različnih sinteznih metod za pripravo nanodelcev kobaltovega ferita, kot so sol-gel,[10] hidrotermalna sinteza,[11] koprecipitacija,[12] koprecipitacija v mikroemulzijah[13] in koprecipitacija s segrevanjem z mikrovalovi,[14] v zadnjem času pa tudi termični razpadi organskih kompleksov, kot je npr. razpad oleatov.[15] Zadnja omenjena metoda omogoča sintezo nanodelcev z ozko porazdelitvijo velikosti in enostavno prilagajanje velikosti nanodelcev s spreminjanjem sinteznih pogojev. Pri tej metodi raztopimo predhodno sintetizirane oleate v nepolarni tekočini z visokim vreliščem. Pri povišani temperaturi vrelišča oleati razpadajo in nastanejo nanodelci ferita, ki so prekriti z monomolekulskim slojem oleinske kisline. Za oleinsko kislino je znano, da dobro stabilizira suspenzije nanodelcev v nepolarnih topilih.[16] Tako lahko sintetizirane nanodelce dispergiramo v nepolarnih topilih, kot so npr. dekan, heksan ali toluen, in pripravimo magnetne tekočine ali pa z reakcijami zamenjave ligandov nanodelce ustrezno funkcionaliziramo.[17]

Nastanek monodisperznih delcev je odvisen od ločitve nukleacije delcev od njihove rasti.[18] Zagotovitev takšnih pogojev je pri večini sinteznih metod praktično nemogoča. Pri segrevanju oleatov v topilu z visokim vreliščem pa lahko takšne pogoje do neke mere izpolnimo. Poglaviten vzrok je stopenjski razpad oleatov pri različnih temperaturah. V primeru sinteze maghemita s termičnim razpadom železovega oleata $Fe(ol)_3$ je bilo ugotovljeno, da ena molekula oleinske kisline disociira

pri temperaturi 220 °C – 240 °C, kar povzroči nukleacijo, drugi dve pa pri temperaturi okoli 300 °C. Disociacija drugih dveh oleinskih kislin povzroči intenzivno rast jeder, ki so nastala pri nižji temperaturi.[15] Tako sta nukleacija in rast ločeni za približno 60 °C.

Pri tem delu smo sintetizirali Co-feritne nanodelce s termičnim razpadom oleatov. Poudarek je bil na raziskavah vpliva sinteznih pogojev na povprečno velikost nanodelcev in na njihove magnetne lastnosti. S spremljanjem časovnega poteka pa smo poskušali priti do podrobnejših informacij o mehanizmu nastanka nanodelcev kobaltovega ferita, saj prisotnost oleatov z različnima kationoma in s tem z različnim temperaturnim vedenjem, najverjetneje modificira predpostavljen mehanizem nastanka, opažen pri nanodelcih maghemita (gama Fe_2O_3).

2 EKSPERIMENTALNI DEL

Nanodelce kobaltovega ferita smo pripravili po modificirani dvostopenjski metodi termičnega razpada železovega (III) in kobaltovega (II) oleata.[15] V prvi stopnji smo sintetizirali kobaltov (II) in železov (III) oleat. V bučki z obrusom smo raztopili 20 mmol železovega (III) klorida, 10 mmol kobaltovega (II) klorida in 80 mmol natrijevega oleata v topilu s sestavo: 30 mL vode, 40 mL etanola in 70 mL heksana. Reakcijsko mešanico smo refluktirali 4 h pri vrelišču zmesi topil. Med refluktiranjem nastaneta železov (III) in kobaltov (II) oleat, ki sta netopna v vodni fazi in se sproti ekstrahirata v heksansko fazo. Po 4 h refluksa ločimo oleate od vodne faze v liju ločniku. Heksansko fazo, ki vsebuje raztopljene oleate, smo sprali z destilirano vodo. Oleate smo izolirali z odparevanjem heksana pri 60 °C. 24 g oleatov smo raztopili v 133 g heksadekena ali oktadekena. V drugi stopnji smo k raztopinam oleatov dodali različne količine oleinske kisline (OA), raztopine segreli s hitrostjo segrevanja ≈3 K/min do vrelišča topila (heksadeken 282 °C in oktadeken 316 °C) in refluktirali krajši čas 0,5 h ali daljši čas 3 h. **Tabela 1** prikazuje sintezne pogoje. Nad 250 °C je mogoče opaziti burno reakcijo, ki je posledica termičnega razpada oleatov. Nanodelce smo izolirali s flokulacijo, ki jo povzroči dodatek acetona v velikem prebitku, in s centrifugiranjem pri 5000 min^{-1}, 10 min. Dodatek acetona močno spremeni dielektrično konstanto medija, kar povzroči tudi zmanjšanje topnosti stranskih produktov in nezreagiranih reaktantov. Te smo odstranili z večkratnim intenzivnim spiranjem oborine s heksanolom. Heksanol se je izkazal kot primeren medij za čiščenje produktov, saj zaradi delno polarnega značaja ne omogoča nastanka stabilnih suspenzij hidrofobnih nanodelcev, hkrati pa je dobro topilo za oleate. Po spiranju smo čiste delce dispergirali v heksanu, s centrifugiranjem na 5000 min^{-1}, 10 min pa odstranili aglomerate. Nanodelce smo karakterizirali z rentgensko praškovno difrakcijo (XRD) (Bruker AXS D4 ENDEAVOR), presevno elektronsko mikroskopijo (TEM) (Jeol 2010F) in z meritvami magnetnih lastnosti z magnetometrom z vibrirajočim vzorcem (VSM) (Lake Shore 7307 VSM). Vzorce za TEM smo pripravili s sušenjem razredčene stabilne suspenzije nanodelcev v heksanu na mrežici za TEM, vzorce za druge raziskave pa smo pripravili z izolacijo nanodelcev iz heksanske suspenzije z acetonom. Povprečno velikost nanodelcev smo ugotovili iz širitve uklonov XRD-spektrov (d_{XRD}) z računalniškim programom Topaz™, povprečno velikost in standardni odklon pa iz merjenja velikosti vsaj 100 nanodelcev na TEM-posnetku (d_{TEM}).

3 REZULTATI IN DISKUSIJA

Pri povišani temperaturi oleati razpadajo in tvorijo oksidne nanodelce. Takšni nanodelci so prevlečeni z monomolekularskim slojem oleinske kisline tudi v primeru, ko v reakcijsko zmes oleinska kislina (OA) ni bila dodana. Med sintezo oleatov nastaja OA s hidrolizo natrijevega oleata. Zaradi nepolarnega značaja se ekstrahira v heksansko fazo. Nizka temperatura odparevanja heksana in visoka tempratura vrelišča OA je razlog, da je delež OA očitno dovolj velik, da stabilizira suspenzijo nanodelcev tudi v primeru, ko OA nismo dodali k raztopinam oleatov. Sloj OA, ki je vezan na površino, preprečuje njihovo aglomeracijo in omogoča dispergiranje nanodelcev v nepolarnih topilih.

Produkt sinteze so kristalinični spinelni nanodelci, kar je razvidno iz XRD- spektrov na **sliki 1**. Izjema je vzorec, pripravljen s segrevanjem krajši čas (0,5 h) pri končni temperaturi (vzorec CF2). Difraktogram tega vzorca prikazuje razen uklonov, značilnih za spinelno strukturo, tudi široke uklone, ki se skladajo s strukturo CoO. Delci v vseh vzorcih so sferične oblike z ozko

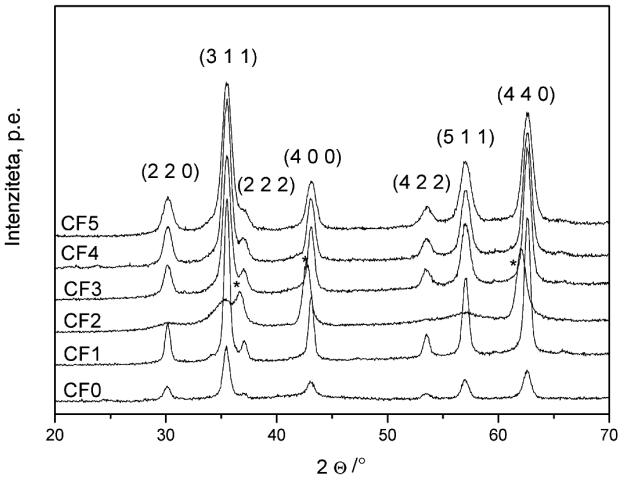

Slika 1: XRD-spektri nanodelcev Co-ferita. Spektri so indeksirani v skladu s spinelno strukturo. Pri vzorcu CF2 so z * označeni refleksi CoO.

Figure 1: XRD-spectra of Co-ferrite nanoparticles. Spectra are indexed according to spinel structure. CoO reflections are marked by * in the spectrum of the sample CF2.

Tabela 1: Vpliv temperature (T), časa sinteze (t) in količine dodane OA izražene z masnim razmerjem med maso oleatov in maso OA (m_{OA}/m_{OL}) na povprečno velikost nanodelcev (d_{XRD}) in (d_{TEM}), in na magnetne lastnosti nanodelcev (M_s-nasičena magentizacija, M_r-remanentna magnetizacija in H_{ci}-koercitivnost)

Table1: Effect of temperature (T), synthesis time (t) and amount of added OA expressed by mass ratio between mass of OA and mass of oleates (m_{OA}/m_{OL}) on average nanoparaticles size (d_{XRD}) and (d_{TEM}), and magnetic properties of nanoparticles (M_s-saturation magnetization, M_r-remanent magnetization and H_{ci}-coercitivity)

Oznaka vzorca	T/°C	t/h	m_{OA}/m_{OL}	d_{XRD}/nm	d_{TEM}/nm	$M_s/10^{-4}$ T/g	$M_r/10^{-4}$ T/g	H_{ci}/(79,6 A m^{-1})
CF0	316	0,5	0	15	–	–	–	–
CF1	316	3	0	21	20 ± 2	57	28	1873
CF2	316	0,5	0,3	10*	16 ± 2	10	0,4	79
CF3	316	3	0,3	14	11 ± 2	49	14	720
CF4	316	3	0,6	13	14 ± 1	35	11	402
CF5	282	3	0	10	9 ± 2	49	4	41

*samo velikost spinelnih nanodelce

porazdelitvijo velikosti (**Slika 2**). Meritev velikosti nanodelcev na TEM-posnetkih ($d_{TEM,}$ **tabela 1**) je pokazala relativno ozko porazdelitev velikosti s standardnim odklonom od povprečne velikosti 10 % – 20 %. Velikost, ugotovljena na TEM-slikah, se dobro sklada z velikostjo, določeno iz XRD- spektrov (d_{XRD}, **tabela 1**), kar dokazuje dobro kristaliničnost nanodelecv. Izjema je vzorec, pripravljen s segrevanjem krajši čas (vzorec CF2), kjer je velikost, določena iz XRD-spektrov (10 nm za spinelne nanodelce), precej manjša od velikosti, ugotovljene na TEM slikah. Večanje velikosti nanodelcev z višanjem temperature sinteze (vzorca CF1 in CF5) je verjetno povezano predvsem s hitrejšim razpadanjem oleatnih kompleksov, kar pospešuje rast kristalitov.[15] Na velikost nanodelcev vpliva tudi dodatek OA, ki se veže na površino nanodelcev, in s tem verjetno otežuje prenos snovi do rastočega nanodelca kar povzroči zmanjšanje velikosti nanodelcev z naraščanjem dodane količine OA (vzorci CF1, CF3 in CF4).

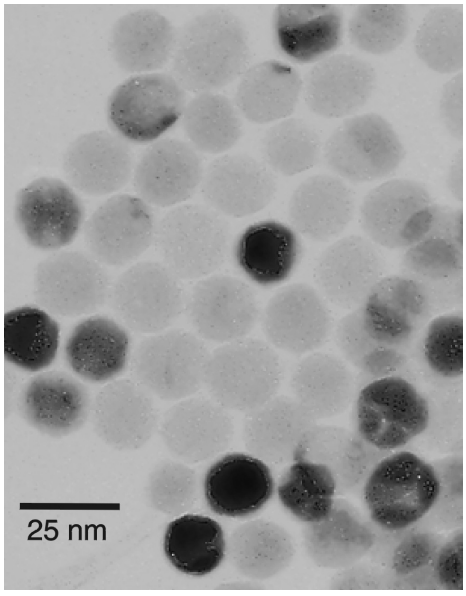

Slika 2: TEM-posnetek nanodelcev CF1

Figure 2: TEM-image of nanoparticels CF1

Povprečna velikost nanodelcev ima ključen vpliv na magnetne lastnosti materiala (**tabela 1** in **slika 3**). Z manjšanjem povprečne velikosti nanodelcev se zmanjšujejo tudi magnetizacija, remanenca in koercitivnost. Zaradi velikega razmerja med površino in volumnom nanodelcev je znaten delež atomov na površini nanodelca. Ker je sloj površinskih atomov neurejen, ne prispeva k magnetnemu momentu nanodelca oz. zmanjša magnetizacijo nanodelcev v primerjavi z grobozrnatim materialom. Delež površinskih atomov raste z manjšanjem povprečne velikosti nanodelcev, kar se izraža z manjšanjem nasičene magnetizacije z manjšanjem povprečne velikosti nanodelecev. Prav tako se z zmanjševanjem povprečne velikosti nanodelcev veča delež OA, ki je vezana na površini in redči magnetno fazo. Energija magnetne anizotropije se manjša z volumnom nanodelca, kar se izraža z manjšanjem remanence in koercitivnosti. Zopet je izjema vzorec po krajšem času sinteze (vzorec CF2), pri katerem magnetizacija ne doseže nasičenja niti pri relativno visokem polju 796 kA m^{-1}. Slabe magnetne lastnosti se ne skladajo z velikostjo delcev, opaženih s TEM. Analiza XRD-spektra

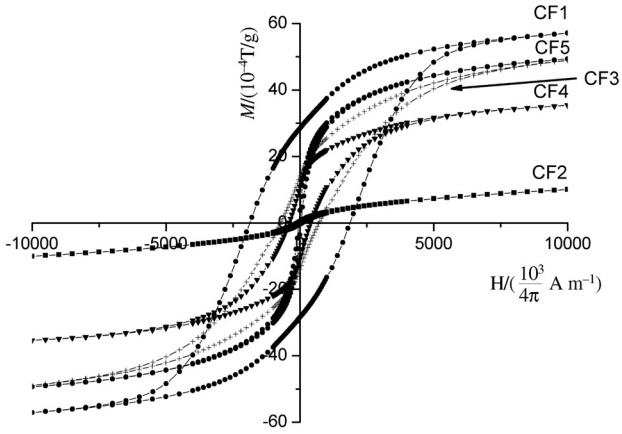

Slika 3: Krivulje odvisnosti magnetizacije od magnetnega polja, izmerjene pri sobni temperaturi

Figure 3: Room temperature magnetisation curves as a function of magnetic field

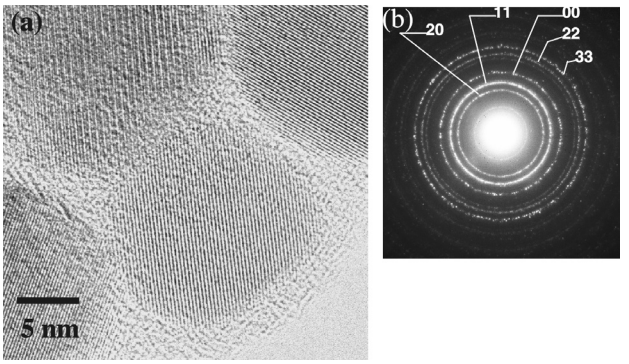

Slika 4: HRTEM-posnetek nanodelcev CF1 **(a)** in pripadajoča elektronska difrakcija **(b)**
Figure 4: HRTEM-image of nanoparticles CF1 **(a)** and selected area electron diffraction **(b)**

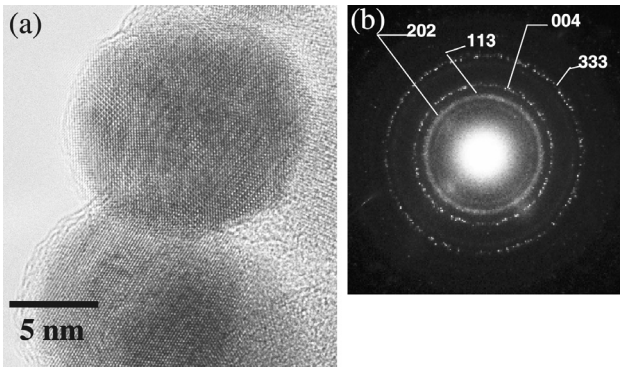

Slika 5: HRTEM-posnetek nanodelcev CF2 **(a)** in pripadajoča elektronska difrakcija **(b)**
Figure 5: HRTEM-image of nanoparticles CF2 **(a)** and selected area electron diffraction of **(b)**

vzorca sicer kaže na prisotnost dveh faz, vendar tega na TEM-posnetku ni opaziti. EDS-analiza na posameznega nanodelca pokaže skoraj identično sestavo kot pri vzorcu, ki je bil sintetiziran daljši čas (vzorec CF1). Nizke vrednosti za magnetne lastnosti tega vzorca (vzorec CF2), ki je bil sintetiziran krajši čas, so verjetno posledica slabše kristaliničnosti, kar lahko opazimo z visokoločljivostno TEM (HRTEM). HRTEM nanodelcev po daljšem času sinteze (vzorec CF1) kaže periodično mrežno sliko, ki se sklada z njihovo dobro kristaliničnostjo (**slika 4a**). Pripadajoča elektronska difrakcija prikazuje ostre obroče refleksov, katerih oddaljenost od centralnega pramena ustreza spinelni strukturi (**slika 4b**). Na HRTEM-sliki nanodelcev je po krajšem času sinteze (vzorec CF2) jasno viden neenakomeren kontrast – manjša področja z urejeno periodičnostjo se menjajo z neurejenimi področji (**slika 5a**). S slabšo urejenostjo kristalne strukture nanodelcev CF2 se sklada pripadajoča elektronska difrakcija (**slika 5b**), ki kaže razširjene obroče refleksov. Širina refleksov se ne sklada z velikostjo nanodelcev. Na osnovi podrobne analize HRTEM lahko ugotovimo, da je vsak nanodelec sestavljen iz domen urejenega materiala, ki se nekoliko razlikujejo v svoji orientaciji. Bistveno slabše magnetne lastnosti nanodelcev CF2, sintetiziranih krajši čas, je torej očitno posledica njihove slabe kristaliničnosti.

Posebna notranja nanostrukturiranost, ki jo kažejo nanodelci po krajšem času sinteze, je verjetno posledica kompleksnega, relativno zapletenega mehanizma njihovega nastanka. Pri povišani temperaturi nastanejo nanodelci CoO in nanodelci železovega oksida spinelne strukture (magnetit ali maghemit), ki se nato koalescirajo in tvorijo večje sferične nanodelece. Po daljšem času pri temperaturi sinteze kompozitni delci rekristalizirajo v nanodelce kobaltovega ferita, ki imajo urejeno notranjo strukturo. Podoben mehanizem nastanka nanodelcev, ki vključuje rekristalizacijo aglomeratov manjših nanodelcev, je bil opažen tudi pri sintezi nanodelcev Fe_3O_4 s podobnim postopkom.[19] Na kinetiko nastanka nanodelcev kobaltovega ferita ima močan vpliv tudi prisotnost OA. Vzorec CF0, ki smo ga pripravili brez dodane OA, je vseboval le spinelne nanodelce (**slika 1**), čeprav je bil pripravljen pod enakimi pogoji kot kompozitni nanodelci CF2. Oleinska kislina torej očitno zavre hitrost procesov med sintezo.

4 SKLEP

Pri tem delu smo raziskovali sintezo nanodelcev kobaltovega ferita z metodo termičnega razpada oleatov. Metoda omogoča pripravo nanodelcev z ozko porazdelitvijo velikosti, povprečna velikost nastalih nanodelcev pa je odvisna od temperature, časa sinteze in koncentracije OA. Sintetizirani nanodelci v območju velikosti med 9 nm in 20 nm izkazujejo ferimagnetno vedenje ter magnetne lastnosti, ki se spreminjajo s povprečno velikostjo nanodelcev. Predpostavili smo mehanizem nastanka nanodelcev kobaltovega ferita, ki vključuje koalescenco manjših nanodelcev in njihovo rekristalizacijo.

5 LITERATURA

[1] E. Tirosh, G. Shemer, G. Markovich, Chem. Mater. 18 (**2006**), 465–470
[2] R. C. Ashoori, Nature, 379 (**1996**), 413–419
[3] I. M. L. Billas, A. Chatelain, W. A. de Heer, Science, 265 (**1994**), 1682–1684
[4] T. Hyeon, S. L. Seung, J. Park, C. Yunhee, N. B. Hyon, J. Am. Chem. Soc., 123 (**2001**), 12798–12801
[5] R. E. Rosenweg, Ferrohydrodynamics, Dover Publications, New York, 1985
[6] D. H. Han, H. L. Luo, Z. Yang, J. Magn. Magn. Mater., 161 (**1996**), 376–378
[7] U. Häfeli, W. Schüt, J. Teller, M. Zborowski, Scientific and Clinical Applications of Magnetic Carriers, Plenum, New York, 1997
[8] Q. A. Pankhurst, J. Connolly, S. K. Jones, J. Dobson, Applications of magnetic nanoparticles in biomdecine, J. Phys. D:Appl. Phys., 36 (**2003**), R167–R181
[9] W. F. J. Fontijn, P. J. van der Zaag, L. F. Feiner, R. Metselaar, M. A. C. Devillers, J. Appl. Phys., 85 (**1999**), 5100–5105

[10] T. Meron, Y. Rosenberg, Y. Lareah, G. Markovich, J. Magn. Magn. Mater, 292 (**2005**), 11–16
[11] M. Rozman, M. Drofenik, J. Am. Ceram. Soc., 78 (**1995**), 2449–2455
[12] Y. I. Kim, D. Kim, S. C. Lee, Physica B, 337 (**2003**), 42–51
[13] D. Makovec, A. Košak, M. Drofenik, Nanotechnology, 15 (**2004**), S160–S166
[14] F. Bansebaa, F. Zavaliche, P. L. Ecuyer, R. W. Cochrane, T. Veres, J. Colloid Interface Sci., 277 (**2004**), 104–110
[15] J. Park, K. An, Y. Hwang, J. G. Park, H. J. Noh, J. Y. Kim, J. H. Park, N. M. Hwang, T. Hyeon, Nature Materials, 3 (**2004**), 891–895
[16] A. Košak, D. Makovec, A. Žnidaršič, M. Drofenik, Mater. Tehnol., 39 (**2005**), 37–41
[17] M. Lattuada, T. A. Hatton, Langmuir, 23 (**2007**), 2158–2168
[18] T. Sugimoto, Monodispersed Particles, Elsevier, Amsterdam, 2001
[19] D. Caruntu, G. Caruntu, Y. Chen, C. J. O'Connor, G. Goloverda, V. L. Kolesnichenko, Cehm. Mater., 16 (**2004**), 5527–5534
[20] X. Batlle, A. Labarta, J. Phys. D: Appl. Phys., 35 (**2002**) R15–R42

UDK 669.14.018.298:669.18
Professional article/Strokovni članek

ISSN 1580-2949
MTAEC9, 42(6)291(2008)

CENTRELINE FORMATION OF THE Nb(C,N) EUTECTIC IN 0.15 % C; 0.0071 % N; 0.022 % Nb; 0.033 % Al AND 0.003 % S STRUCTURAL STEEL

SREDINSKO IZCEJANJE IN NASTANEK EVTEKTIKA Nb(C,N) V KONSTRUKCIJSKEM JEKLU Z 0,15 % C; 0,0071 % N; 0,022 % Nb; 0,033 % Al IN 0,003 % S

Jure Bernetič[1,2], Boštjan Bradaškja[1,2], Gorazd Kosec[1], Borut Kosec[2], Erika Bricelj[1]

[1]ACRONI, d. o. o., Cesta Borisa Kidriča 44, SI-4270 Jesenice, Slovenia
[2]Faculty of Natural Science and Engineering, Department of Materials and Metallurgy, University of Ljubljana, Aškerčeva 12, SI-1000 Ljubljana, Slovenia
jure.bernetic@acroni.si

Prejem rokopisa – received: 2008-09-23; sprejem za objavo – accepted for publication: 2008-10-22

During a routine control, a very small through thickness reduction of area was found for one tensile specimen of a 90-mm plate. Careful investigations of the fracture and the section of specimens cut from the as-solidified continuously cast 250-mm slab showed that the cause was the presence of coarse particles of niobium carbo-nitride as a constituent of the quasi-eutectic Fe-Nb(C,N) that forms because of the centerline segregation of niobium.

Key words: structural steel, heavy plates, reduction of area, eutectic niobium carbo-nitride

Pri rutinski kontroli lastnosti jekla je imel raztržni preizkušanec 90-milimetrske mm plošče zelo majhno kontrakcijo v smeri debeline. Preiskava prelomne površine in prereza preizkušancev, izrezanih iz kontinurino litega 250-milimetrskega slaba, je pokazala, da je vzrok zanjo prisotnost velikih zrn niobijevega karbonitrida v spačenem evtektiku Fe-Nb(C,N), ki je nastal zaradi sredinske segregacije niobija.

Ključne besede: konstrukcijsko jeklo, debele plošče, kontrakcija v smeri debeline, evtektik niobijevega karbonitrida

1 INTRODUCTION

The reduction of area in the through thickness direction is an essential mechanical property of thick steel heavy plates intended for fillet welds. In the standard EN 10164[1] three quality classes, Z15, Z25 and Z35, with minimal average values for the through thickness reduction of area of three tests, 15 %, 25 % and 35 %, and minimal individual values, 10 %, 15 % and 25 %, respectively, are specified. During routine testing in a mechanical laboratory for one specimen only 9.5 % of the through thickness reduction of area was found, although the declared plate class was Z35. The sample is shown in **Figure 1**. According to Vodopivec et al. [2] the content of sulphur is the primary reason for the low ductility in the through thickness direction because of the lamelar tearing with fracture propagation also along the interface between the sulphide inclusion and the ferrite matrix. The mass fraction of sulphur in the tested steel, which was only 0.003 %, excludes the possibility of a low reduction of area due to sulphide inclusions.

Figure 1: Macroscopic image of S 355 J2+N structural steel, showing the reduction of area specimen taken from a 90-mm heavy plate in the thickness direction

Slika 1: Makroskopski posnetek kontrakcijskega preizkušanca konstrukcijskega jekla S 355 J2+N. Preizkušanec je vzet po debelini iz 90-milimetrske debele plošče

A small amount of niobium was added to the investigated structural steel to achieve the required mechanical properties. The addition of Nb could also affect the through thickness ductility of heavy plates because of the formation of coarse niobium carbo-nitride particles as constituents of the degenerated eutectic Fe-Nb(C,N), which may form with a high content of niobium or because of defective solidification of the steel[3].

To identify the cause of the low reduction of area, detailed investigations of specimens cut at different distances from the surface of the as-solidified slab were carried out.

2 EXPERIMENTAL

The structural steel (S 355 J2+N) was melted in an EAF (electric arc furnace), VD (vacuum degassing) treated, continuously cast and cut into slabs of dimensions (250 × 1085 × 4770) mm. The slabs were cooled to

Table 1: Chemical composition of the S 355 J2+N steel grade in mass fractions *w*/%
Tabela 1: Kemijska sestava jekla S 355 J2+N v masnih deležih *w*/%

Element	C	Si	Mn	P	S	Cr	Cu	Ni	Al	Nb	Ti	N
w/%	0.15	0.49	1.10	0.018	0.003	0.14	0.29	0.12	0.033	0.022	0.005	0.0071

room temperature and after surface grinding reheated in a pusher-type furnace to a temperature of 1250 °C and hot rolled to 90-mm-thick plates. The chemical composition of the heat is listed in **Table 1**. First, samples perpendicular to the slab casting direction were examined after grinding and deep-etching for 40 min in 25 % H_2SO_4 at 70 °C, which revealed the as-cast macrostructure. From this specimen, samples 1, 2 and 3 in the thickness direction were cut out for metallographic examination, as shown in **Figure 2**. From the 90-mm heavy plate, specimens were cut out in the thickness direction and submitted for tensile testing and examinations with optical and scanning electron microscopes (SEM) as well as energy-dispersive X-ray spectroscopy (EDXS).

3 RESULTS AND DISCUSSION

Figure 3 shows a secondary-electron image of a fracture surface of one specimen with coarse niobium carbo-nitride inclusions and small MnS inclusions. The spots of the EDXS analyses of both inclusions are marked with arrows in **Figure 3** and the results are given in **Table 2**. In the mapping micrographs in **Figure 4** the bright areas represent the element in the particles and show the morphology of the particles and the main elements in large inclusions. Most of the particles observed on the fracture surface showed a large content of niobium. On the basis of fractographs it was concluded that niobium-containing particles (Nb,Ti)(C,N) were the main cause for the poor through thickness reduction of area of the steel plate.

From the location of the fracture of the tensile specimen shown in **Figure 1,** we assumed that the source of the coarse precipitates was a very strong centreline segregation during the solidification of the steel slab.

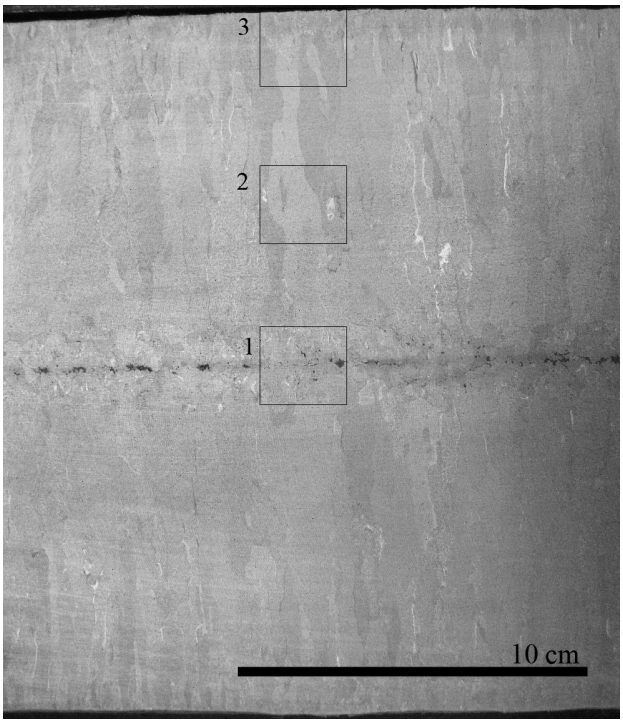

Figure 2: As-cast sample taken from slab perpendicular to the casting direction
Slika 2: Vzorec iz slaba pravokotno na smer ulivanja jekla

Table 2: Results of the spot EDXS analyses. The place of the analysis is marked with an arrow in **Figure 3**.
Tabela 2: Rezultati točkovne EDXS analize. Mesto analize na **sliki 3** je označeno s puščico.

	Element	Fe	Mn	S	Ti	Nb
conc. *w*/%	(Nb,Ti)(C,N)	28.661	0.728	–	3.853	66.758
	MnS	3.747	70.306	25.861	–	–

Tabela 3: Results of the spot EDXS analyses. The place of the analysis is marked with an arrow in **Figure 5**.
Table 3: Rezultati točkovne EDXS analize. Mesto analize na **sliki 5** je označeno s puščico.

	Element	C	Fe	Mn	S	Ti	Nb	Al	Pb
conc. *w*/%	(Nb,Ti) (C,N)	3.18	33.09	–	–	3.76	59.97	–	–
	MnS	–	3.56	61.89	33.09	–	–	–	–
	Pb	2.01	9.16	–	–	–	–	1.62	84.46

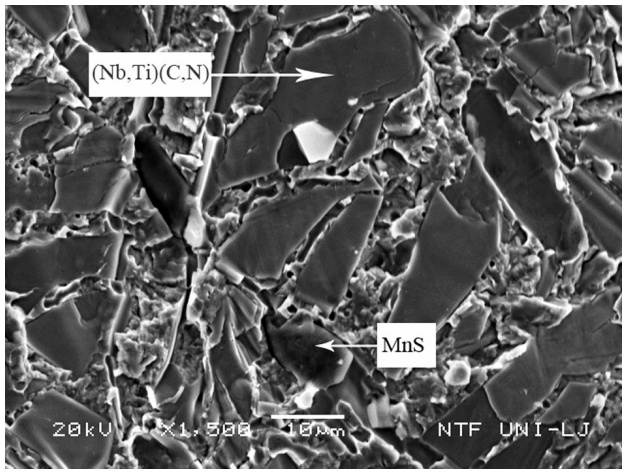

Figure 3: SEM fractograph (secondary electron image) of the reduction of area specimen. The analysed particles are marked with arrows, and the EDXS analyses are presented in **Table 2**
Slika 3: SEM-slika (sekundarni elektroni) prelomne površine kontrakcijskega preizkušanca. Točke opravljene EDXS analize prikazujeta puščici, rezultati so podani v **tabeli 2**

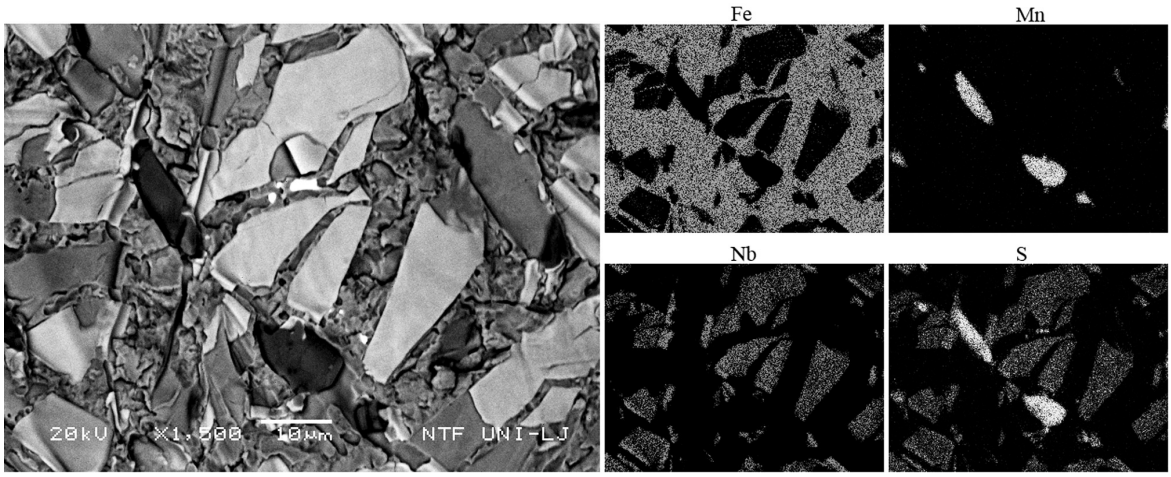

Figure 4: EPMA mapping of Nb(C,N) and MnS particles
Slika 4: Ploskovna mikroanaliza delcev Nb(C,N) in MnS

This conclusion is confirmed by the fact that from three samples, as shown in **Figure 2,** the niobium-rich precipitates were only found in the specimen cut from the slab centre in sample number 1. The precipitates are very similar to the Fe-Nb(C,N) eutectic known as "Chinese script"[4]. Besides the niobium-rich particles, a minor number of very small manganese sulphide inclusions and lead droplets were found. All these phases were only found in the centreline of the cast slab. The results of the spot EDXS analyses from the cast slab are presented in **Table 3** and the spots of the analyses are marked in **Figure 5**. The analyses show that the niobium carbo-nitride particles also contain the mass fraction of Ti approximately 3.7 %, despite there being only 0.005 % of titanium in the steel originating from the steel scrap used. A similar composition of niobium carbo-nitride was reported for Nb-Ti micro-alloyed steels[5].

The solubility of the niobium carbo-nitride with the approximate composition $Nb(C_{0.9}N_{0.1})$ in structural steel is given by the equation[6,7]:

$$\lg\left[(w(\mathrm{Nb})w(\mathrm{C})+\frac{12w(\mathrm{N})}{14}\right]=2{,}26-\frac{6770}{T}$$

with w(Nb), w(C), and w(N) being the mass fractions of the elements in the steel and T being the temperature in K.

Considering the actual contents of niobium, carbon and nitrogen, a solution temperature of 1140 °C was deduced, indicating that the slab soaking temperature was sufficient for a complete solution in austenite of the niobium carbo-nitride with the approximate composition $Nb(C_{0.9}N_{0.1})$. The fact that coarse niobium-rich precipitates were also found in the hot-rolled plate after heating the slabs to 1250 °C indicates that their composition differs from that of the soluble niobium carbo-nitride. The solubility of niobium carbide in austenite is greater than the solubility of niobium nitride[8,9]. It is assumed that the stability of particles in the investigated steel is due to their high content of nitrogen.

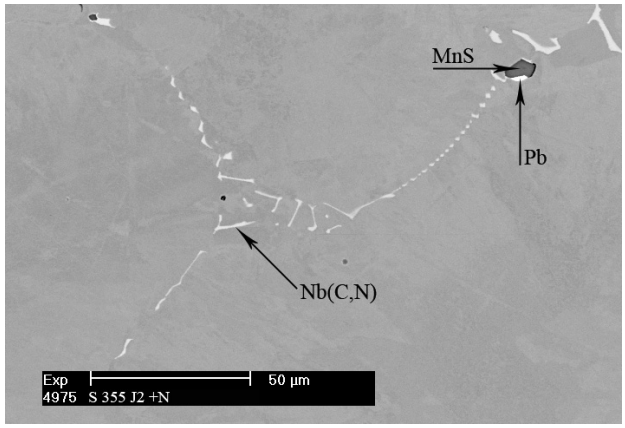

Figure 5: SEM picture of degenerated eutectic in form of "Chinese script" from the sample number 1 of the as-cast slab. The analysed particles are marked with arrows, and the EDXS analyses are presented in **Table 3**
Slika 5: SEM-posnetek spačenega evtektika z obliko "kitajske pisave" iz vzorca številka 1 kontinuirno ulitega slaba. Točke opravljene EDXS-analize prikazujejo puščice, rezultati so podani v **tabeli 3**

The shape and size of the coarse carbo-nitride particles suggest that they are constituents of a degenerated quasi-eutectic Fe-Nb(C,N). The location of the eutectic in the centre of the slab and the composition of the steel suggest that its formation is an improper solidification process related to a high casting temperature, a high slab solidification rate or a deficiency in the secondary slab cooling.

4 CONCLUSIONS

When considering the contents of carbon, nitrogen and niobium in a steel, all the carbo-nitride phase with the approximate composition $Nb(C_{0.9}N_{0.1})$ is in a solid solution in austenite at 1140 °C. Since the slab soaking temperature was 1250 °C, it is evident that the carbo-nitride found in the examined steel does not have the quoted composition and that it has a higher content of nitrogen and correspondingly a higher solution tempera-

ture in austenite. The shape and the size of the niobium-rich particles suggest that they are the constituents of a degenerated eutectic Fe-Nb(CN) that formed because of the improper solidification process of continuous cast slabs.

Acknowledgement

The authors wish to thank Prof. Ladislav Kosec and Mrs. Nika Breskvar (University of Ljubljana) for the SEM and EDXS analyses.

5 REFERENCES

[1] SIST EN 10164:2005: Steel products with improved deformation properties perpendicular to the surface of the product – Technical delivery conditions

[2] F. Vodopivec, M. Gabrovšek, I. Rak, B. Ralić, J. Žvokelj, Železarski zbornik, 12 (**1978**) 1, 1–16

[3] V. K. Heikkinen, R. H. Packwood, Scand. J. Metallurgy, 6 (**1977**), 170-175

[4] F. Haddad, S. E. Amara, R. Kesri, S. Hamar-Thibault, Journal de Physique IV, 122 (**2004**), 35–39

[5] Dae-Hee Woo, Sang-Min Lee, Henri Gaye, Hae-Geon Lee, The formation behaviour of large Nb-Ti carbonitride precipitates during undirectional solidification of Nb-Ti microalloyed steel, International Conference on clean steel 7, Balatonfüred, Hungary, 4-6 June 2007

[6] K. J. Irvine, F. B. Pickering, T. Gladman, Journal of The Iron and Steel Institute, (**1967**), 161–182

[7] A. M. Elwazri, A. Fatehi, J. Calvo, D. Bai, S. Yue, ISIJ International, 48 (**2008**) 1, 107–113

[8] F. Vodopivec, M. Gabrovšek, B. Ralić, Metal Science, 9 (**1975**), 324–326

[9] F. Vodopivec, M. Gabrovšek, B. Ralić, Želez. zbor., 4 (**1976**), 193–198

MATERIALI IN TEHNOLOGIJE

MATERIALS AND TECHNOLOGY

Letnik / Volume 42 2008

ISSN 1580-2949

IMT Ljubljana, Lepi pot 11, 1000 Ljubljana, Slovenija

MATERIALI IN TEHNOLOGIJE / MATERIALS AND TECHNOLOGY

VSEBINA / CONTENTS
LETNIK / VOLUME 42, 2008/1, 2, 3, 4, 5, 6

2008/6

2008/Posebna številka

HEAT TREATMENT

MATERIALI IN TEHNOLOGIJE / MATERIALS AND TECHNOLOGY

AVTORSKO KAZALO / AUTHOR INDEX

LETNIK / VOLUME 42, 2008, A–Ž

MATERIALI IN TEHNOLOGIJE / MATERIALS AND TECHNOLOGY

VSEBINSKO KAZALO / SUBJECT INDEX

LETNIK / VOLUME 41, 2008

Kovinski materiali – Metallic materials

Anorganski materiali – Inorganic materials